Accelerator Physics and the LHC

Ewen .H. Maclean

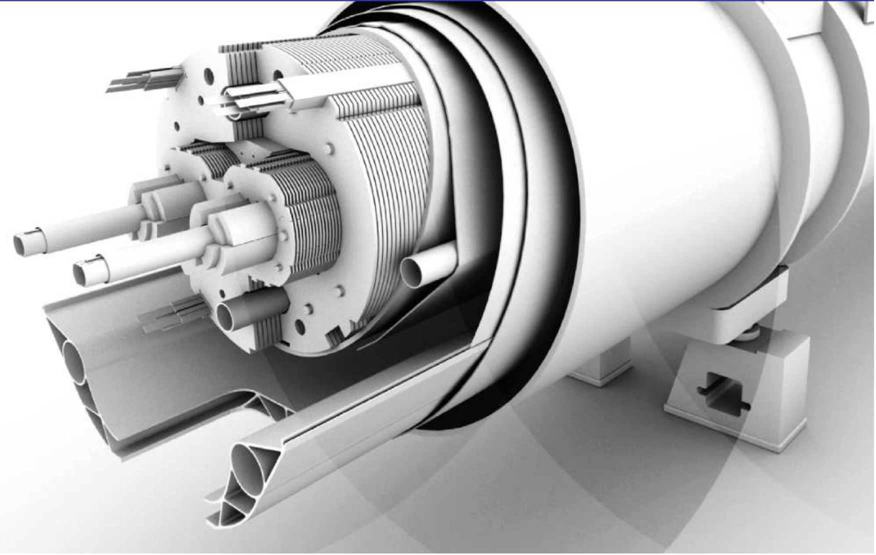

symmetry topics follow +

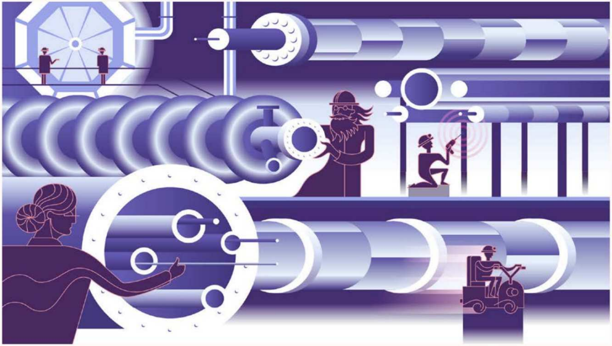

Artwork by Sandbox Studio, Chicago with Ana Kova

The hottest job in physics?

04/26/16 | By Troy Rummler

Accelerator scientists are in demand at labs and beyond.

While the supply of accelerator physicists in the United States has grown modestly over the last decade, it hasn't been able to catch up with demand fueled by industry interest in medical particle accelerators and growing collaborations at the national labs.

~35,000 particle accelerators world-wide

Medicine

physicsworld | Magazine | Latest | People | Impact |

particle therapy

PARTICLE THERAPY | ANALYSIS

Proton therapy on an upward trajectory

16 Feb 2019

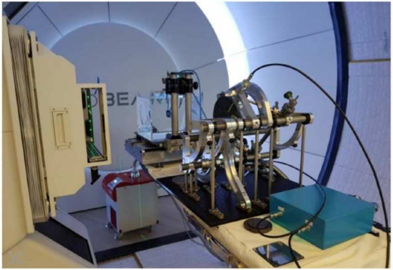

Setting the standard: NPL's portable calorimeter provides a more accurate reference point for proton-beam dosimetry. (Courtesy: NPL)

BBC Sign in News Sport Weather Shop Reel Travel

NEWS

Home | Video | World | UK | Business | Tech | Science | Stories | Entertainment & Arts

Wales | Wales Politics | Wales Business | North West | North East | Mid | South West

Wales cancer patients to get proton beam therapy on NHS

12 December 2018

Share

The centre in Newport will be the second in the UK to offer proton beam therapy on the NHS

Medicine

RESEARCH ARTICLE

RADIATION TOXICITY

Ultrahigh dose-rate FLASH irradiation increases the differential response between normal and tumor tissue in mice

Vincent Favaudon,[1,2*] Laura Caplier,[3†] Virginie Monceau,[4,5‡] Frédéric Pouzoulet,[1,2§] Mano Sayarath,[1,2¶] Charles Fouillade,[1,2] Marie-France Poupon,[1,2‖] Isabel Brito,[6,7] Philippe Hupé,[6,7,8,9] Jean Bourhis,[4,5,10] Janet Hall,[1,2] Jean-Jacques Fontaine,[3] Marie-Catherine Vozenin[4,5,10,11]

In vitro studies suggested that sub-millisecond pulses of radiation elicit less genomic instability than continuous, protracted irradiation at the same total dose. To determine the potential of ultrahigh dose-rate irradiation in radiotherapy, we investigated lung fibrogenesis in C57BL/6J mice exposed either to short pulses (≤500 ms) of radiation delivered at ultrahigh dose rate (≥40 Gy/s, FLASH) or to conventional dose-rate irradiation (≤0.03 Gy/s, CONV) in single doses. The growth of human HBCx-12A and HEp-2 tumor xenografts in nude mice and syngeneic TC-1 Luc^+ orthotopic lung tumors in C57BL/6J mice was monitored under similar radiation conditions. CONV (15 Gy) triggered lung fibrosis associated with activation of the TGF-β (transforming growth factor–β) cascade, whereas no complications developed after doses of FLASH below 20 Gy for more than 36 weeks after irradiation. FLASH irradiation also spared normal smooth muscle and epithelial cells from acute radiation-induced apoptosis, which could be reinduced by administration of systemic TNF-α (tumor necrosis factor–α) before irradiation. In contrast, FLASH was as efficient as CONV in the repression of tumor growth. Together, these results suggest that FLASH radiotherapy might allow complete eradication of lung tumors and reduce the occurrence and severity of early and late complications affecting normal tissue.

INTRODUCTION

The search for procedures to eradicate tumors while sparing normal tissues has long been a challenge for radiation oncologists. Dose fractionation, precision imaging, and chemoradiation, as well as advances in accelerator and computing technologies, have all contributed to increase the therapeutic index of radiotherapy. Stereotactic methodologies, including volumetric-modulated arc therapy (RapidArc, TomoTherapy) and multibeam stereotactic irradiation (CyberKnife) (*1*), may be used to increase the dose delivered to the tumor in a single run but at the cost of a large volume of normal tissue exposed to intermediate doses of radiation. These methods also involve rapid alternation of radiation beams and/or split-dose irradiation of tissues over time scales ranging from seconds to minutes. Such microfractionation might transiently alter the susceptibility of target cells to radiation (*2*). On the other hand, the mean dose rates delivered in flattening filter–free photon beams and proton pencil beam scanning (PBS) facilities (*3*) may be as high as 0.4 and 200 Gy/s, respectively, hence 10 to 10^4 times higher than those produced by conventional radiation sources (*4*) with a time per spot in proton PBS techniques usually below 100 ms (*5*, *6*). Although these procedures might affect the therapeutic outcome (*7*), the effects of such changes in the dose delivery and overall treatment time on tumor control, as well as on early and late normal tissue responses, have not yet been investigated in detail in animal models.

We propose here a radiation methodology in which the dose is given in short pulses at ultrahigh dose rate, based on an experimental linear electron accelerator (LINAC) able to generate 4.5-MeV electrons at a high beam current (table S1 and figs. S1 to S8, Supplementary Materials and Methods), in such a way that large doses of radiation could be delivered in a single beam in less than 500 ms. To investigate the potential of the method, we used the well-established model of lung fibrosis in C57BL/6J mice (*8*–*11*) and assessed the occurrence of fibrosis by histological and immunohistochemical methods after bilateral thorax exposure to continuous, conventional dose-rate (≤0.03 Gy/s, CONV) versus pulsed, ultrahigh dose-rate (≥40 Gy/s, FLASH) irradiation given in a single dose. We used the growth inhibition of tumor xenografts and syngeneic, orthotopic tumors in mice to compare the response of normal tissues and tumors to both irradiation modalities. We show that FLASH irradiation protects the lung from fibrosis and elicits a large decrease in the incidence of apoptosis early in the radiation response at equivalent doses. Cutaneous lesions were also reduced in severity, whereas antitumor efficiency was not modified compared to CONV irradiation. Together, the experimental data demonstrate that FLASH irradiation enhances the differential responses between normal and tumor tissues, suggesting that the method might be advantageous in reducing the complications of radiotherapy without the loss of antitumor efficiency.

[1]Institut Curie, Centre de Recherche, 91405 Orsay, France. [2]INSERM U612, 91405 Orsay, France. [3]Pathology Laboratory, Ecole Nationale Vétérinaire d'Alfort, Université Paris-Est, 94704 Maisons Alfort, France. [4]Université Paris-XI, 91405 Orsay, France. [5]INSERM U1030, Institut Gustave-Roussy, 94805 Villejuif, France. [6]Institut Curie, Centre de Recherche, 75248 Paris 05, France. [7]INSERM U900, 75248 Paris 05, France. [8]Mines ParisTech, 77305 Fontainebleau, France. [9]CNRS, UMR144, 75248 Paris 05, France. [10]Radio-Oncologie/Radiothérapie, Centre Hospitalier Universitaire Vaudois, 1011 Lausanne, Switzerland. [11]INSERM U967, Commissariat à l'Énergie Atomique (CEA), Division des Sciences du Vivant (DSV), Institut de Radiobiologie Cellulaire et Moléculaire (IRCM), 92265 Fontenay aux Roses, France.
*Corresponding author. E-mail: vincent.favaudon@curie.fr
†Present address: BiodOxis, Parc Biocitech, 102 Avenue Gaston-Roussel, 93230 Romainville, France.
‡Present address: CNRS UMR 1166, La Pitié-Salpêtrière Hospital, 75013 Paris, France.
§Present address: Department of Translational Research, Institut Curie-Recherche, Building 101, Centre Universitaire, 91898 Orsay, France.
¶Present address: Institut Curie-Recherche, INSERM U1021/CNRS UMR 3347, 91405 Orsay, France.
‖Present address: XenTech, 4 rue Pierre-Fontaine, 91400 Evry, France.

Radiotherapy and Oncology 124 (2017) 365–369

Contents lists available at ScienceDirect

Radiotherapy and Oncology

journal homepage: www.thegreenjournal.com

ELSEVIER

Flash irradiation

Irradiation in a flash: Unique sparing of memory in mice after whole brain irradiation with dose rates above 100 Gy/s

CrossMark

Pierre Montay-Gruel [a,b,1], Kristoffer Petersson [c,1], Maud Jaccard [c], Gaël Boivin [a], Jean-François Germond [c], Benoit Petit [a], Raphaël Doenlen [d], Vincent Favaudon [b], François Bochud [c], Claude Bailat [c], Jean Bourhis [a,1], Marie-Catherine Vozenin [a,*,1]

[a] *Department of Radiation Oncology/DO/CHUV, Lausanne University Hospital, Switzerland;* [b] *Institut Curie, INSERM U1021/CNRS UMR3347, Université Paris-Saclay, Orsay, France;* [c] *Institute of Radiation Physics (IRA), Lausanne University Hospital; and* [d] *Faculty of Life Sciences, Ecole Polytechnique Fédérale de Lausanne, Switzerland*

A R T I C L E I N F O

Article history:
Received 27 October 2016
Received in revised form 13 April 2017
Accepted 4 May 2017
Available online 22 May 2017

Keywords:
Flash-RT
Whole brain irradiation
Cognition's preservation

A B S T R A C T

This study shows for the first time that normal brain tissue toxicities after WBI can be reduced with increased dose rate. Spatial memory is preserved after WBI with mean dose rates above 100 Gy/s, whereas 10 Gy WBI at a conventional radiotherapy dose rate (0.1 Gy/s) totally impairs spatial memory.

Our recent publications have shown that irradiation at an ultra-high dose rate was able to protect normal tissue from radiation-induced toxicity. When compared to radiotherapy delivered at conventional dose rates (1–4 Gy/min), this so called "Flash" radiotherapy (>40 Gy/s; Flash-RT) was shown to enhance the differential effect between normal tissue and tumor in lung models [1,2] and consequently allowed for dose escalation. The biological interest of Flash-RT seems to rely essentially on a specific, yet undefined, response occurring in normal cells and tissues. We initially hypothesized that the protective effect of Flash was related to the high dose rate delivery, in other words related to the very short time of exposure. In order to further explore Flash-RT and to validate its protective effect on normal tissues, we decided to extend our observation from the lung to other organs. We decided to investigate brain response to Flash-RT as it is a well-defined and robust model in radiobiology [3–5].

When dealing with unexpected biological results, such as the ones previously described with Flash-RT, accurate dosimetry of the delivered irradiation is essential. However, dosimetry at (an ultra-)high dose rate in high dose-per-pulse beams is non-trivial as current radiotherapy dosimetry protocols are not designed for such conditions and because the detectors available for online measurements (i.e. ionization chambers, diodes, and diamond detectors) start to saturate when the dose rate/dose-per-pulse is increased beyond what is used in conventional radiotherapy [6–8]. Therefore, we needed to rely on dosimeters that had been previously validated to function accurately at more extreme irradiation conditions, i.e. mainly passive dosimeters. Among these options, we selected thermo-luminescent dosimeter (TLD) chips because of their small size (3.2 × 3.2 × 0.9 mm^3) so that they could be used for measuring dose in the brain of mice. By positioning the TLD inside the skull of a sacrificed mouse, we were able to validate the dose delivered to the brain during whole brain irradiation (WBI).

Brain injuries after WBI at sub-lethal doses delivered at conventional radiotherapy dose rates are well described [5,9,10]. They include functional alterations, neuronal [11], glial [12,13] and vasculature toxicities [14,15]. Cognitive impairments are the most described functional defects observed in mice and humans following WBI [4,16]. They are caused by an alteration of hippocampal neurogenesis, which can occur as early as one month post 10 Gy single fraction WBI [17]. These cognitive impairments can be evaluated using the "Novel Object Recognition test" [18] on WBI murine models [19]. Therefore, we used this assay to investigate the functional effect of Flash-RT on the normal brain of irradiated mice.

Using a combination of accurate dosimetry measurements and robust biological tests, we first aimed to investigate the potential neuroprotective effect of Flash-RT and indeed found memory preservation in mice after 10 Gy WBI with Flash-RT (delivered in

* Corresponding author at: Laboratoire de Radio-Oncologie, Centre Hospitalier Universitaire Vaudois, Bugnon 46, 1011 Lausanne, Switzerland.
E-mail address: marie-catherine.vozenin@chuv.ch (M.-C. Vozenin).
[1] Equal contribution.

http://dx.doi.org/10.1016/j.radonc.2017.05.003
0167-8140/

Industry & energy

Science & Technology Facilities Council | UK Research and Innovation

Funding | Research | Innovation | Skills | Public engagement | News, events and publications | Abou

Home / News / STFC launches VELA – bringing a new imaging capability for UK industry

STFC launches VELA – bringing a new imaging capability for UK industry

13 March 2015

CERNCOURIER Reporting on international high-energy physics

Physics | Technology | Community | In focus | Magazine

NEWS

GUINEVERE: towards cleaner nuclear energy

27 March 2012

The accelerator used to produce fast neutrons.
Image credit: SCK•CEN. Used by permission.

A particle accelerator has been successfully coupled to a nuclear reactor for the first time at the Belgian Nuclear Research Centre (SCK•CEN). The demonstration model GUINEVERE is now in operation, showing the feasibility of an accelerator-driven system (ADS) for nuclear energy (Mumbai engages ADS for nuclear energy). By using an ADS, the accelerator can be turned off to stop the reactor immediately. This system, known as subcritical, is safer than standard nuclear reactors.

GUINEVERE is a test installation of limited power to fine-tune the operation and control of future subcritical reactors. Unlike conventional reactor systems, it produces fast neutrons that can be used for the transmutation of high-level radioactive waste into less-toxic products with shorter life spans, helping to improve their geological disposal.

Art and History

Anal. Chem. **2008**, *80*, 6436–6442

Visualization of a Lost Painting by Vincent van Gogh Using Synchrotron Radiation Based X-ray Fluorescence Elemental Mapping

Joris Dik,*,† Koen Janssens,‡ Geert Van Der Snickt,‡ Luuk van der Loeff,§ Karen Rickers,‖ and Marine Cotte⊥,⊗

Department of Materials Science, Delft University of Technology, Mekelweg 2, 2628CD Delft, The Netherlands, Centre for Micro- and Trace Analysis, Department of Chemistry, Universiteit Antwerpen, Universiteitsplein 1, 2610 Antwerp, Belgium, Kröller-Müller Museum, Houtkampweg 6, P.O. Box 1, 6730 AA Otterlo, The Netherlands, Deutsches Elektronen-Synchrotron (DESY), Notkestrasse 85, 22603 Hamburg, Germany, Centre of Research and Restoration of the French Museums, UMR-171-CNRS, Palais du Louvre, Porte des Lions, 14 quai François Mitterrand, 75001 Paris, France, and European Synchrotron Radiation Facility BP220, 38043 Grenoble Cedex, France

Vincent van Gogh (1853−1890), one of the founding fathers of modern painting, is best known for his vivid colors, his vibrant painting style, and his short but highly productive career. His productivity is even higher than generally realized, as many of his known paintings cover a previous composition. This is thought to be the case in one-third of his early period paintings. Van Gogh would often reuse the canvas of an abandoned painting and paint a new or modified composition on top. These hidden paintings offer a unique and intimate insight into the genesis of his works. Yet, current museum-based imaging tools are unable to properly visualize many of these hidden images. We present the first-time use of synchrotron radiation based X-ray fluorescence mapping, applied to visualize a woman's head hidden under the work *Patch of Grass* by Van Gogh. We recorded decimeter-scale, X-ray fluorescence intensity maps, reflecting the distribution of specific elements in the paint layers. In doing so we succeeded in visualizing the hidden face with unprecedented detail. In particular, the distribution of Hg and Sb in the red and light tones, respectively, enabled an approximate color reconstruction of the flesh tones. This reconstruction proved to be the missing link for the comparison of the hidden face with Van Gogh's known paintings. Our approach literally opens up new vistas in the nondestructive study of hidden paint layers, which applies to the oeuvre of Van Gogh in particular and to old master paintings in general.

Vincent van Gogh is generally recognized as one of the founding fathers of modern painting.[1] In recent decades his work has undergone extensive art historical and technical study. One striking feature that emerged is Van Gogh's frequent reuse of paintings in order to recycle the canvas.[2,3] The artist would simply paint a new composition on top of an existing work. This is usually attributed to the artist's lifelong economic hardship and the rapid, energetic evolution of his artistic ideas. Visualizing such hidden paintings is of interest to both specialists in the field of Van Gogh and the public alike. Covered paintings in general provide an insight into the making of artworks and the underlying conceptual changes. In the case of Van Gogh, they also present a touchstone for comparison with preparatory drawings and the abundant literary record. The extensive correspondence with his brother Theo van Gogh, an art dealer based in Paris, is full of remarks by Vincent on his work.

Nondestructive imaging of such hidden paint layers is usually realized by means of tube-based X-ray radiation transmission radiography (XRR). The absorption contrast in these images is mostly caused by the heavy metal components of pigments employed, such as lead in lead white or mercury in vermillion. Conventional XRR, however, has a number of important limitations. First of all, the observed X-ray absorbance is a summation of all element-specific absorbances. This implies that the contribution to the overall image contrast due to (low quantities of) weakly absorbing elements will frequently be obscured by heavier elements that are present in higher concentrations. Second, prior to the application of the paint layer, a canvas is usually primed with a homogeneous layer of lead white. This raises the overall background of the absorption image derived from the paint layers. Finally, the polychromatic character of an X-ray tube further reduces the contrast in radiographic images. As a result, conventional XRR imaging of paintings frequently provides only a fragmentary view of their substructure, which can severely hamper the readability of hidden compositions.[4]

* Corresponding author. Phone: +31-15-2789571. E-mail: j.dik@tudelft.nl.
† Delft University of Technology.
‡ Universiteit Antwerpen.
§ Kröller-Müller Museum.
‖ Deutsches Elektronen-Synchrotron (DESY).
⊥ Palais du Louvre.
⊗ European Synchrotron Radiation Facility.

(1) Hulsker, J. *The New Complete Van Gogh: Paintings, Drawings, Sketches*; John Benjamins: Philadelphia, PA, 1996.
(2) Van Heugten, S. *Van Gogh Museum J.* **1995**, 63–85.
(3) Hendriks, E. Van Gogh's Working Practice: A Technical Study. In *New Views on Van Gogh's Development in Antwerp en Paris: An Integrated Art Historical and Technical Study of His Paintings in the Van Gogh Museum*; Hendriks, E., Van Tilborgh, L., Eds.; University of Amsterdam: Amsterdam, The Netherlands, 2006; pp 231−245.
(4) Krug, K.; Dik, J.; Den Leeuw, M.; Whitson, A.; Tortora, J.; Coan, P.; Nemoz, C.; Bravin, A. *Appl. Phys. A: Mater. Sci. Process.* **2006**, *83*, 247–51.

10.1021/ac800965g CCC: $40.75 © 2008 American Chemical Society
Published on Web 07/29/2008

Art and History

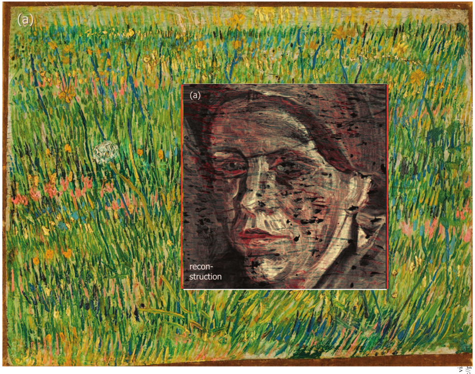

Anal. Chem. **2008**, *80*, 6436–6442

Visualization of a Lost Painting by Vincent van Gogh Using Synchrotron Radiation Based X-ray Fluorescence Elemental Mapping

Joris Dik,*,† Koen Janssens,‡ Geert Van Der Snickt,‡ Luuk van der Loeff,§ Karen Rickers,‖ and Marine Cotte ,⊗

Department of Materials Science, Delft University of Technology, Mekelweg 2, 2628CD Delft, The Netherlands, Centre for Micro- and Trace Analysis, Department of Chemistry, Universiteit Antwerpen, Universiteitsplein 1, 2610 Antwerp, Belgium, Kröller-Müller Museum, Houtkampweg 6, P.O. Box 1, 6730 AA Otterlo, The Netherlands, Deutsches Elektronen-Synchrotron (DESY), Notkestrasse 85, 22603 Hamburg, Germany, Centre of Research and Restoration of the French Museums, UMR-171-CNRS, Palais du Louvre, Porte des Lions, 14 quai François Mitterrand, 75001 Paris, France, and European Synchrotron Radiation Facility BP220, 38043 Grenoble Cedex, France

Vincent van Gogh (1853−1890), one of the founding fathers of modern painting, is best known for his vivid colors, his vibrant painting style, and his short but highly productive career. His productivity is even higher than generally realized, as many of his known paintings cover a previous composition. This is thought to be the case in one-third of his early period paintings. Van Gogh would often reuse the canvas of an abandoned painting and paint a new or modified composition on top. These hidden paintings offer a unique and intimate insight into the genesis of his works. Yet, current museum-based imaging tools are unable to properly visualize many of these hidden images. We present the first-time use of synchrotron radiation based X-ray fluorescence mapping, applied to visualize a woman's head hidden under the work *Patch of Grass* by Van Gogh. We recorded decimeter-scale, X-ray fluorescence intensity maps, reflecting the distribution of specific elements in the paint layers. In doing so we succeeded in visualizing the hidden face with unprecedented detail. In particular, the distribution of Hg and Sb in the red and light tones, respectively, enabled an approximate color reconstruction of the flesh tones. This reconstruction proved to be the missing link for the comparison of the hidden face with Van Gogh's known paintings. Our approach literally opens up new vistas in the nondestructive study of hidden paint layers, which applies to the oeuvre of Van Gogh in particular and to old master paintings in general.

Vincent van Gogh is generally recognized as one of the founding fathers of modern painting.[1] In recent decades his work has undergone extensive art historical and technical study. One striking feature that emerged is Van Gogh's frequent reuse of paintings in order to recycle the canvas.[2,3] The artist would simply paint a new composition on top of an existing work. This is usually attributed to the artist's lifelong economic hardship and the rapid, energetic evolution of his artistic ideas. Visualizing such hidden paintings is of interest to both specialists in the field of Van Gogh and the public alike. Covered paintings in general provide an insight into the making of artworks and the underlying conceptual changes. In the case of Van Gogh, they also present a touchstone for comparison with preparatory drawings and the abundant literary record. The extensive correspondence with his brother Theo van Gogh, an art dealer based in Paris, is full of remarks by Vincent on his work.

Nondestructive imaging of such hidden paint layers is usually realized by means of tube-based X-ray radiation transmission radiography (XRR). The absorption contrast in these images is mostly caused by the heavy metal components of pigments employed, such as lead in lead white or mercury in vermillion. Conventional XRR, however, has a number of important limitations. First of all, the observed X-ray absorbance is a summation of all element-specific absorbances. This implies that the contribution to the overall image contrast due to (low quantities of) weakly absorbing elements will frequently be obscured by heavier elements that are present in higher concentrations. Second, prior to the application of the paint layer, a canvas is usually primed with a homogeneous layer of lead white. This raises the overall background of the absorption image derived from the paint layers. Finally, the polychromatic character of an X-ray tube further reduces the contrast in radiographic images. As a result, conventional XRR imaging of paintings frequently provides only a fragmentary view of their substructure, which can severely hamper the readability of hidden compositions.[4]

* Corresponding author. Phone: +31-15-2789571. E-mail: j.dik@tudelft.nl.
† Delft University of Technology.
‡ Universiteit Antwerpen.
§ Kröller-Müller Museum.
‖ Deutsches Elektronen-Synchrotron (DESY).
 Palais du Louvre.
⊗ European Synchrotron Radiation Facility.

(1) Hulsker, J. *The New Complete Van Gogh: Paintings, Drawings, Sketches*; John Benjamins: Philadelphia, PA, 1996.
(2) Van Heugten, S. *Van Gogh Museum J.* **1995**, 63–85.
(3) Hendriks, E. Van Gogh's Working Practice: A Technical Study. In *New Views on Van Gogh's Development in Antwerp en Paris: An Integrated Art Historical and Technical Study of His Paintings in the Van Gogh Museum*; Hendriks, E., Van Tilborgh, L., Eds.; University of Amsterdam: Amsterdam, The Netherlands, 2006; pp 231−245.
(4) Krug, K.; Dik, J.; Den Leeuw, M.; Whitson, A.; Tortora, J.; Coan, P.; Nemoz, C.; Bravin, A. *Appl. Phys. A: Mater. Sci. Process.* **2006**, *83*, 247–51.

10.1021/ac800965g CCC: $40.75 2008 American Chemical Society
Published on Web 07/29/2008

Light Sources

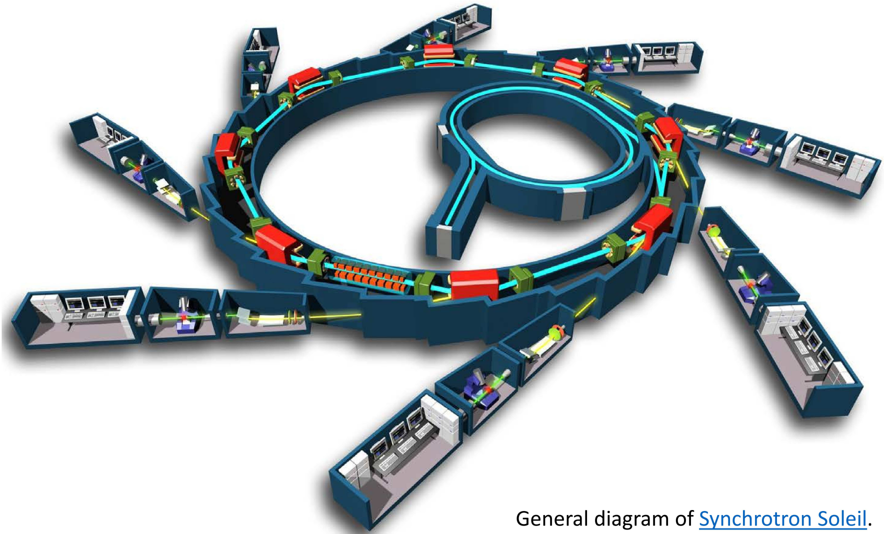

General diagram of Synchrotron Soleil.

Light Sources

Facilitate many types of research:

- Life science
- Chemistry
- Engineering
- Earth science
- Environmental science
- Life science
- Physics/material science
- Cultural heritage
- Forensics
- Food science
- Oceanography
- …

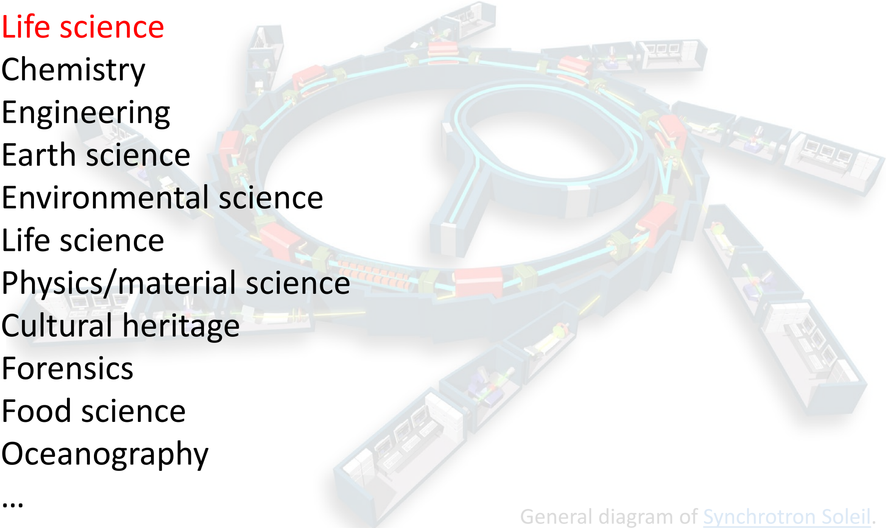

General diagram of Synchrotron Soleil.

Light Sources

Facilitate many types of research:

- Life science

https://www.helmholtz-berlin.de/forschung/unsere-forschung/photonenforschung/corona-forschung_en.html

Research on SARS-CoV-2 at BESSY II

At synchrotron light sources like BESSY II, research is currently gaining crucial insights into combating the SARS-CoV2 virus. The results are helping to contain the spread and fight the disease more effectively.

For corona research, BESSY II has provided access via a fast-track method even during the strictest lockdown phases. Immediately after the genome of the novel coronavirus SARS-CoV2 was sequenced in early 2020, the first measurements of viral proteins started at BESSY II.

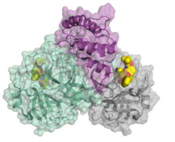

Schematic picture of the coronavirus protease.
(© H. Tabermann / HZB)

- **A first major success at the beginning of 2020** was the decoding of the three-dimensional structure of the main protease of the SARS-CoV2 virus, which was already achieved at BESSY II in February 2020. This protein is elementary in the life cycle of the coronavirus because it is involved in the reproduction of the viruses. Knowledge of its 3D structure helps in the search for suitable active substances that dock onto the protein and hinder its function. Because without information about the target protein, the search for an active agent is like looking for a needle in a haystack. Structure-based drug discovery" helps to identify the best candidates for active substances from the multitude of possible substances. > Read more here (news piece)
- **The BMBF is currently funding the two projects "CTS-COV-2" and "STOP CORONA"** at the two light sources PETRA III and BESSY II. In both projects, the main protease of the virus, which was decoded at BESSY II, was selected as the target for a drug.
  - In the STOP-CORONA project, which began as a collaboration between the Helmholtz-Zentrum Berlin (HZB), the University of Lübeck and the University of Würzburg, the aim is to use small organic substances, so-called fragments, to identify active surfaces of the main viral protease. For this fragment screening, the HZB has two libraries available F2X-Entry with 96 substances and F2X-Universal with 1103 substances.
    In a first step, crystals of the main protease were tested against the F2X-Entry library. From the binders obtained, a more strongly binding subsequent substance could be identified by optimisation. This substance is currently in binding studies and will be further optimised.
    These results provide important insights for drug discovery against SARS-CoV-2, as drugs are still urgently needed to get COVID19 under control. However, Corona research at synchrotrons is not limited to X-ray structure analysis.

RESEARCH

CORONAVIRUS

Crystal structure of SARS-CoV-2 main protease provides a basis for design of improved α-ketoamide inhibitors

Linlin Zhang[1,2], Daizong Lin[1,3], Xinyuanyuan Sun[1,2], Ute Curth[4], Christian Drosten[5], Lucie Sauerhering[6,7], Stephan Becker[6,7], Katharina Rox[8,9], Rolf Hilgenfeld[1,2]*

The coronavirus disease 2019 (COVID-19) pandemic caused by severe acute respiratory syndrome–coronavirus 2 (SARS-CoV-2) is a global health emergency. An attractive drug target among coronaviruses is the main protease (M^{pro}, also called $3CL^{pro}$) because of its essential role in processing the polyproteins that are translated from the viral RNA. We report the x-ray structures of the unliganded SARS-CoV-2 M^{pro} and its complex with an α-ketoamide inhibitor. This was derived from a previously designed inhibitor but with the P3-P2 amide bond incorporated into a pyridone ring to enhance the half-life of the compound in plasma. On the basis of the unliganded structure, we developed the lead compound into a potent inhibitor of the SARS-CoV-2 M^{pro}. The pharmacokinetic characterization of the optimized inhibitor reveals a pronounced lung tropism and suitability for administration by the inhalative route.

In December 2019, a new coronavirus caused an outbreak of pulmonary disease in the city of Wuhan, the capital of Hubei province in China, and has since spread globally (*1*, *2*). The virus has been named severe acute respiratory syndrome–coronavirus 2 (SARS-CoV-2) (*3*) because the RNA genome is about 82% identical to that of the SARS coronavirus (SARS-CoV); both viruses belong to clade b of the genus *Betacoronavirus* (*1*, *2*). The disease caused by SARS-CoV-2 is called coronavirus disease 2019 (COVID-19). Whereas at the beginning of the outbreak, cases were connected to the Huanan seafood and animal market in Wuhan, efficient human-to-human transmission led to exponential growth in the number of cases. On 11 March 2020, the World Health Organization (WHO) declared the outbreak a pandemic. As of 9 April, there were >1,500,000 cumulative cases globally, with a ~5.9% case fatality rate.

One of the best-characterized drug targets among coronaviruses is the main protease (M^{pro}, also called $3CL^{pro}$) (*4*). Along with the papain-like protease(s), this enzyme is essential for processing the polyproteins that are translated from the viral RNA (*5*). The M^{pro} operates at no fewer than 11 cleavage sites on the large polyprotein 1ab (replicase 1ab, ~790 kDa); the recognition sequence at most sites is Leu-Gln↓(Ser, Ala, Gly) (↓ marks the cleavage site). Inhibiting the activity of this enzyme would block viral replication. Because no human proteases with a similar cleavage specificity are known, such inhibitors are unlikely to be toxic.

Previously, we designed and synthesized peptidomimetic α-ketoamides as broad-spectrum inhibitors of the main proteases of betacoronaviruses and alphacoronaviruses as well as the 3C proteases of enteroviruses (*6*). The best of these compounds (**11r**; Fig. 1) showed an half-maximal effective concentration (EC_{50}) of 400 pM against Middle East respiratory syndrome–coronavirus (MERS-CoV) in Huh7 cells as well as low-μM EC_{50} values against SARS-CoV and a whole range of enteroviruses in various cell lines, although the antiviral activity seemed to depend to a great extent on the cell type used in the experiments (*6*). To improve the half-life of the compound in plasma, we modified **11r** by hiding the P3-P2 amide bond within a pyridone ring (Fig. 1, green ovals) in the expectation that this might prevent cellular proteases from accessing this bond and cleaving it. Further, to increase the solubility of the compound in plasma and to reduce its binding to plasma proteins, we replaced the hydrophobic cinnamoyl moiety by the somewhat less hydrophobic Boc group (Fig. 1, red ovals) to give **13a** (see scheme S1 for synthesis).

To examine whether the introduced pyridone ring is compatible with the three-dimensional structure of the target, we determined the crystal structure, at 1.75 Å resolution, of the M^{pro} of SARS-CoV-2 (Fig. 2). The three-dimensional structure is highly similar to that of the SARS-CoV M^{pro}, as expected from the 96% sequence identity (see fig. S8); the root mean square deviation between the two free-enzyme structures is 0.53 Å for all Cα positions [comparison between SARS-CoV-2 M^{pro} structure and SARS-CoV M^{pro}, PDB entry 2BX4 (*7*)]. The chymotrypsin-like and picornavirus 3C protease–like domains I and II (residues 10 to 99 and 100 to 182, respectively) are six-stranded antiparallel β barrels that harbor the substrate-binding site between them. Domain III (residues 198 to 303), a globular cluster of five helices, is involved in regulating the dimerization of the M^{pro}, mainly through a salt-bridge interaction between Glu^{290} of one protomer and Arg^{4} of the other (*8*). The tight dimer formed

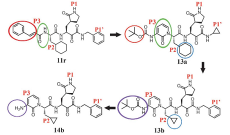

Fig. 1. Chemical structures of α-ketoamide inhibitors 11r, 13a, 13b, and 14b. Colored ovals and circles highlight the modifications from one development step to the next (see text).

[1]Institute of Biochemistry, Center for Structural and Cell Biology in Medicine, University of Lübeck, 23562 Lübeck, Germany. [2]German Center for Infection Research (DZIF), Hamburg-Lübeck-Borstel-Riems Site, University of Lübeck, 23562 Lübeck, Germany. [3]Changchun Discovery Sciences Ltd., 789 Shunda Road, Changchun, Jilin 130012, China. [4]Institute for Biophysical Chemistry, Hannover Medical School, 30625 Hannover, Germany. [5]Institute of Virology, Charité Universitätsmedizin Berlin, 10117 Berlin, Germany. [6]Institute of Virology, University of Marburg, 35043 Marburg, Germany. [7]German Center for Infection Research (DZIF), Marburg-Gießen-Langen Site, University of Marburg, 35043 Marburg, Germany. [8]Department of Chemical Biology, Helmholtz Center for Infection Research (HZI), 38124 Braunschweig, Germany. [9]German Center for Infection Research (DZIF), Hannover-Braunschweig Site, Helmholtz Center for Infection Research, 38124 Braunschweig, Germany.
*Corresponding author. Email: rolf.hilgenfeld@uni-luebeck.de

Accelerator research

CERN Accelerating science

ABOUT NEWS SCIEN

News › News › Topic: Accelerators

Voir en français

CLEAR prospects for accelerator research

A new user facility, the CERN Linear Electron Accelerator for Research (CLEAR), hosts accelerator research and development projects

1 NOVEMBER, 2017 | By Matthew Chalmers

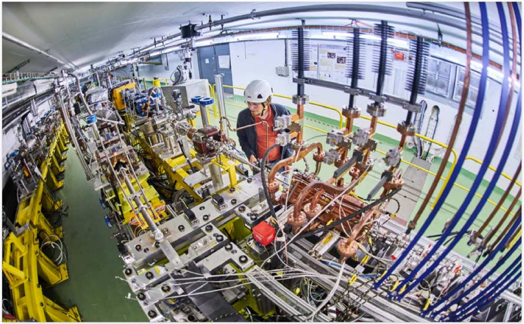

The CERN Linear Electron Accelerator for Research (CLEAR) will enhance and complement the existing accelerator R&D programme at CERN. (Image: Julien Ordan/CERN)

Accelerator research

CERN Accelerating science

CERN

ABOUT NEWS SCIEN

Fermilab

Home | About | Science | Jobs | Contact | Phone Book

Newsroom | DUNE at LBNF | Come visit us | Resources for

News

Newsroom

- News and features
- Press releases
- Fermilab in the news
- Fact sheets and brochures
- DUNE at LBNF newsroom
- Photo, video and graphics galleries
- Search photo, video and graphics
- Social media
- Press release sign-up
- Subscribe to Fermilab Frontiers
- Internship in science writing
- Contact

Fermilab news Search

Useful links

- Symmetry magazine
- Interactions

Fermilab's newest accelerator delivers first results

August 14, 2019 | Bailey Bedford

Share Tweet Email

Fermilab's newest particle accelerator is small but mighty. The Integrable Optics Test Accelerator, designed to be versatile and flexible, is enabling researchers to push the frontiers of accelerator science.

Instead of smashing beams together to study subatomic particles like most high-energy physics research accelerators, IOTA is dedicated to exploring and improving the particle beams themselves.

IOTA researchers say they are excited by the observation of single-electron beams near the speed of light and the first results on decreasing beam instabilities. They are eager to use their single-electron technique to probe aspects of quantum science and see future breakthroughs in accelerator science.

"The scientists who designed the accelerator are also the scientists that use it," said Vladimir Shiltsev, a Fermilab distinguished scientist and one of the founders of IOTA. "It's an opportunity to get great insight into the physics of beams at relatively small cost."

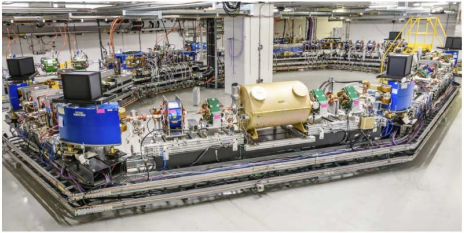

Scientists using the 40-meter-circumference Integrable Optics Test Accelerator saw their first results from IOTA this summer. Photo: Giulio Stancari

accelerator

ccelerator for Research (CLEAR), hosts

s

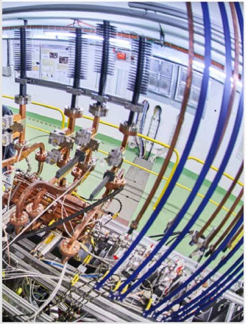

nplement the existing accelerator R&D programme at CERN. (Image:

Accelerator research

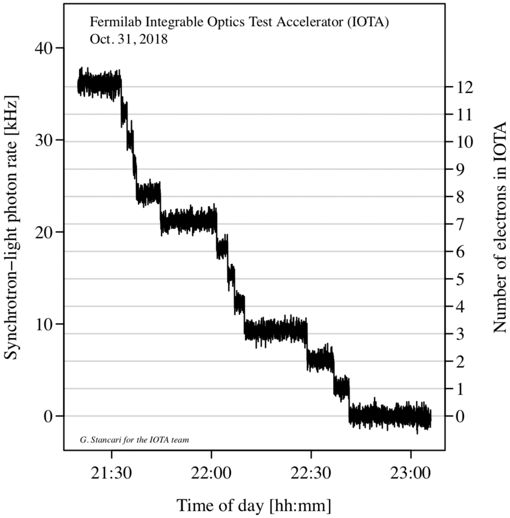

https://news.fnal.gov/2018/11/single-electron-beam-observed-in-iota-for-the-first-time/

10th Int. Particle Accelerator Conf. IPAC2019, Melbourne, Australia JACoW Publishing
ISBN: 978-3-95450-208-0 doi:10.18429/JACoW-IPAC2019-MOPRB089

EXPERIMENTAL STUDY OF A SINGLE ELECTRON IN A STORAGE RING VIA UNDULATOR RADIATION

S. Nagaitsev*,[1], G. Stancari, A. Romanov, Fermilab, Batavia, USA
A. Arodzero, A. Murokh, M. Ruelas, RadiaBeam Technologies, Santa Monica, USA
I. Lobach, The University of Chicago, Chicago, USA
T. Shaftan, BNL, Upton, USA
[1]also at the University of Chicago, Chicago, USA

Abstract

A single electron orbiting around a ring and emitting single quanta at the rate of about one event per hundred turns could produce a wealth of information about physical processes in large traps (i.e. storage rings) for charged particles. It should be noted that Paul and Penning traps in the 1980s led to the Nobel prize for studying state and motion of single quantum particles, and just recently the Penning trap technique has enabled the measurement of a single proton magnetic moment with an unprecedented precision of 10 decimal places. The information from the storage ring traps could also be used for characterization of a quantum system as well as the "trap" itself, i.e. measuring properties of the storage ring lattice and electron interaction with the laser fields. Although, the interest in single electron quantum processes today is mostly academic in nature, the diagnostics and methodology developed for single electron radiation studies could find subsequent applications in a variety of applied disciplines in quantum technology, including quantum communications and quantum computing.

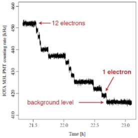

Figure 2: A measured photo-multiplier signal from a synchrotron radiation monitor after the bend magnet. One can clearly see finite jumps in the average proton count rate level as the number of trapped electrons becomes small, until a single electron is left in the IOTA storage ring.

INTRODUCTION

PHYSICAL REVIEW ACCELERATORS AND BEAMS **23,** 054701 (2020)

Towards storage rings as quantum computers

K. A. Brown* and T. Roser
Brookhaven National Laboratory, Upton, New York 11973-5000, USA

(Received 28 February 2020; accepted 4 May 2020; published 13 May 2020)

We explore the possible use of particle beam storage rings as quantum computers. More precisely, we consider creating an ion trap system, in which the same computational basis states can be defined as in a modern ion trap system, but in which the ions have a constant velocity and are rotating in a circular trap. The basic structures that we explore are classical and ultracold crystalline beams. What we propose is a novel method that uses the ion trap quantum computer concept, but puts the ions into a rotating frame of reference. The benefits of this approach are discussed.

DOI: 10.1103/PhysRevAccelBeams.23.054701

I. INTRODUCTION

A particle accelerator storage ring is an apparatus that stores charged particle beams. The beams, if not cooled, can have very high temperatures and can be treated as classical thermodynamic ensembles of particles confined to some volume. When stored, either as bunches of particles or debunched into a uniform longitudinal (temporal) distribution, the ensemble is in steady state and has constant entropy. In general, such a beam has no specific structure and should act like an ideal gas. However, the particles are necessarily charged and can interact with each other through intrabeam collisions and other phenomena. These processes can cause beam heating, increasing the entropy. In addition, these particle distributions do contain information encoded into the behavior of the beams as they traverse the electromagnetic optics that keep them confined within the storage ring [1–4].

$$\epsilon_u = 4\pi(\langle u^2\rangle\langle u'^2\rangle - \langle uu'\rangle^2)^{\frac{1}{2}}, \quad (1)$$

where ϵ_u is the horizonal or vertical beam emittance. We will call the transverse beam temperature the temperature associated with the transverse emittance. Longitudinally, the temperature, T, is a function of the momentum spread [8],

$$\frac{1}{2}k_B T = \frac{1}{2}m(\delta v)^2, \quad (2)$$

where δv is the spread in velocity of the ions in the beam. k_B is Boltzmann's constant. In more practical units, temperatures for ion beams can be expressed as,

$$T_{\parallel}[K] = \frac{2}{k_B}\left(\frac{\delta p}{p_0}\right)E_0[\mathrm{eV}] \quad (3)$$

High energy physics

Fixed target e.g. SHIP @ CERN SPS

- Simpler design/implementation $\rightarrow$ **cost!**
- Potential for very high intensity beams & large numbers of collissions

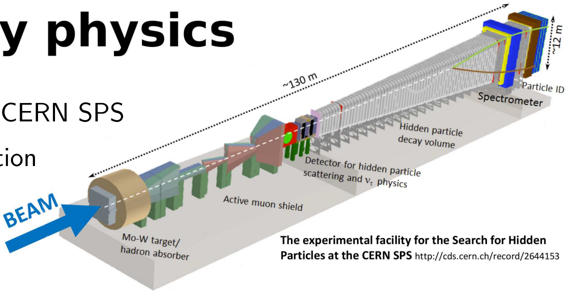

The experimental facility for the Search for Hidden Particles at the CERN SPS http://cds.cern.ch/record/2644153

Collider e.g. LHC @ CERN

- More complex design + many extra challenges
- **LAB frame = CM frame** $\rightarrow$ maximum energy available for new particle creation

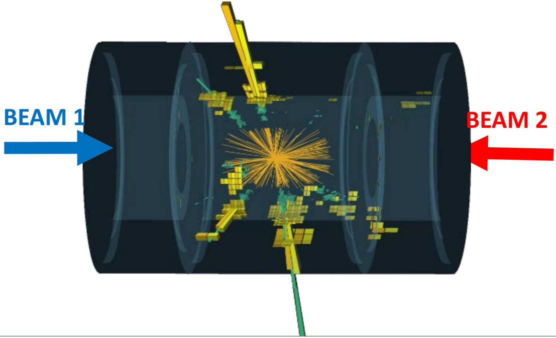

Key Points

- **Accelerators aren't just for HEP**
- **advantages / disadvantages of a beam collider vs fixed target experiment**

- *Of 114 times a Nobel Prize in physics has been awarded $\approx$ 25 involved direct use of a particle accelerator!*
- *A further 20 Nobel Prizes across Physics/Chemistry/Medicine have been awarded for research using X-rays!*
- https://www.epfl.ch/labs/lpap/wp-content/uploads/2018/10/AcceleratorsNobelPrizes.pdf

Accelerators for HEP

300

Address of the President, Sir Ernest Rutherford, O.M., at the Anniversary Meeting, November 30, 1927.

At this Anniversary Meeting we are naturally conscious of the losses suffered by our Society during the year. These include thirteen of our Fellows and three Foreign Members. We have also to record the loss of one of our Fellows under Statute 12, Edward Cecil Guinness, Earl of Iveagh, elected 1906.

Sir William Augustus Tilden passed away on December 11, 1926, in his 85th year. He was appointed Professor of Chemistry and Metallurgy in the Mason College, Birmingham, in 1880, and in 1894 became Professor of Chemistry in the Royal College of Science: he retained this latter position until his retire-

...

the α-particle has sufficient energy to penetrate deeply into the nucleus and to cause its disintegration manifested by the liberation of swift protons.

It would be of great scientific interest if it were possible in laboratory experiments to have a supply of electrons and atoms of matter in general, of which the individual energy of motion is greater even than that of the α-particle. This would open up an extraordinarily interesting field of investigation which could not fail to give us information of great value, not only on the constitution and stability of atomic nuclei but in many other directions.

It has long been my ambition to have available for study a copious supply of atoms and electrons which have an individual energy far transcending that of the α and β-particles from radioactive bodies. I am hopeful that I may yet have my wish fulfilled, but it is obvious that many experimental difficulties will have to be surmounted before this can be realised, even on a laboratory scale.

We shall now consider briefly the present situation with regard to the production of intense magnetic fields. Electro-magnets are ordinarily employed for this purpose and the magnetic fields obtainable are in the main limited

https://royalsocietypublishing.org/doi/pdf/10.1098/rspa.1928.0001

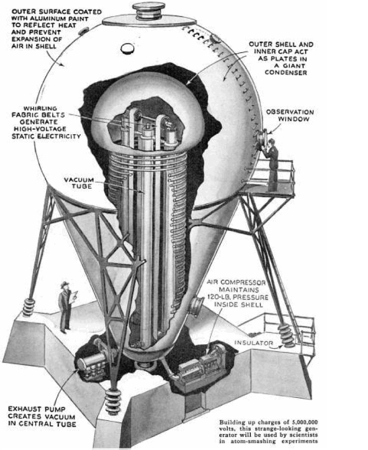

Westinghouse Atom Smasher, 5MeV
1937 – 1958, Pennsylvania, USA

For historical development of particle accelerators see, e.g.

P.J. Bryant, *A brief history and review of accelerators*, CERN Accelerator School: 5th General Accelerator Physics Course, Jyväskylä, Finland, Sep 1992 https://cds.cern.ch/record/261062/

Accelerators for HEP

- **CERN accelerator complex**

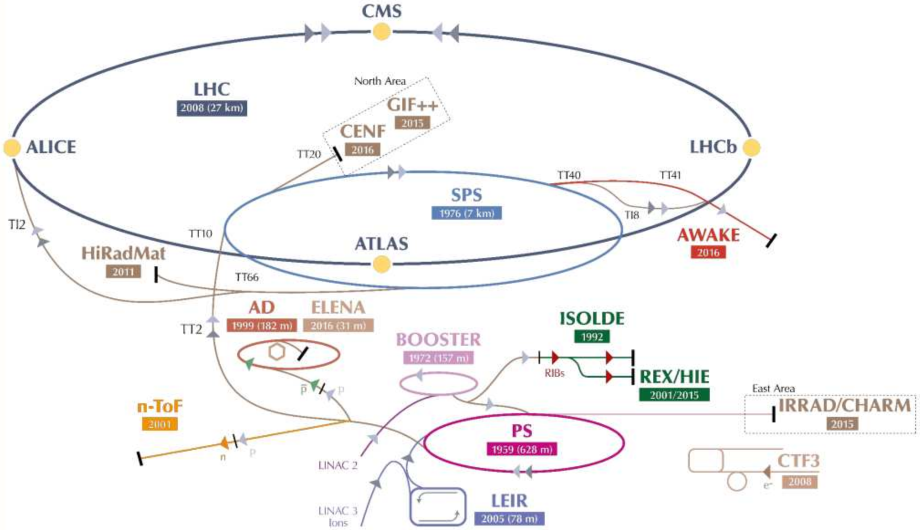

Accelerators for HEP

LHC injector chain

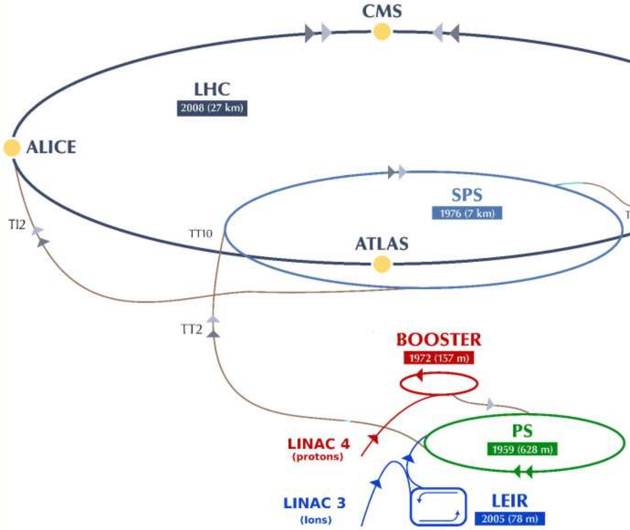

E_k (extraction)	post-LIU ($\geq$ 2020)
Linac 4 (H^-)	160 MeV
PSB (H^+)	2.0 GeV
PS	25 GeV
SPS	449 GeV
LHC	$\geq$ 6.8 TeV

Accelerators for HEP

Linear Accelerator → 'Linac'

Colloquially 'Linac' can refer both to a general Linear Accelerator facility or to a specific accelerating structure

- **Single pass accelerator**

→ beam goes through once

→ facility not always straight, e.g. SLC

- **Energy depends on length**

For HEP 2 main applications:

- **Low energy hadrons**
- **High energy e^- or e^+ collider**
  - e.g. Stanford Linear Collider (1987-98, $3\,\mathrm{km}/0.09\mathrm{TeV}$)
  - e.g. next-gen lepton colliders: ILC ($50\,\mathrm{km}$ / $1\mathrm{TeV}$)
  - e.g. next-gen lepton colliders: CLIC ($50\,\mathrm{km}$ / $3\mathrm{TeV}$)

Accelerators for HEP

Synchrotron

→ *'circular accelerator'*, *'collider ring'* (doesn't actually need to be a circle)

→ e.g. **LHC**, LEP, Tevatron, RHIC, HERA, SPS, PS, ISR...

- **Repeated passage around the accelerator ring → great for HEP!**
  → re-use accelerating structures
  → collide same beams over & over

- **During acceleration guiding magnetic fields increase to keep the beam on the same ($\sim$) orbit**

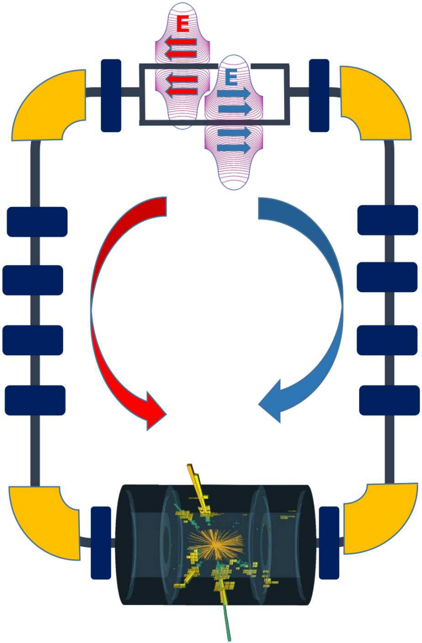

Acceleration

$$\vec{F} = q(\vec{E} + \vec{v} \times \vec{B})$$

$$\Delta W = \int_{s_1}^{s_2} \boldsymbol{F}.\mathrm{d}\boldsymbol{s} = \int_{s_1}^{s_2} q\vec{E}.\mathrm{d}\vec{s}$$

- To accelerate charged particle do work via Lorentz force
- Magnetic field does no work $\vec{s}\ .\ (\frac{\mathrm{d}\vec{s}}{\mathrm{d}t} \times \vec{B}) = 0$

$$\vec{E} = -\nabla\phi - \frac{\partial\vec{A}}{\partial t}$$

Electrostatic accelerators

- **Acceleration via high DC voltage**

RF

- **Acceleration via time-varying fields**
- ***`radiofrequency technology'***

Electrostatic accelerators

e.g. Cockcroft-Walton (left), Van-de-Graff, …

- **Limited by DC-breakdown voltage**
- **Can't be used for repeated acceleration around a closed loop (**e.g. in a synchrotron)

$$\oint \nabla\phi . \mathrm{d}\vec{\boldsymbol{s}} = 0$$

- **Critical element in the design of particle sources**

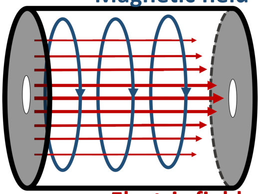

RF Cavities

- Basis of all modern high-energy accelerators
- Conducting cavity or waveguide enforces boundary conditions which have solution with an accelerating mode

There are many varieties of RF-cavity:

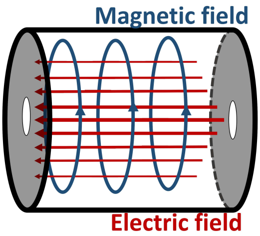

RF Cavities

- Basis of all modern high-energy accelerators
- Conducting cavity or waveguide enforces boundary conditions which have solution with an accelerating mode

There are many varieties of RF-cavity:

e.g. travelling wave structures

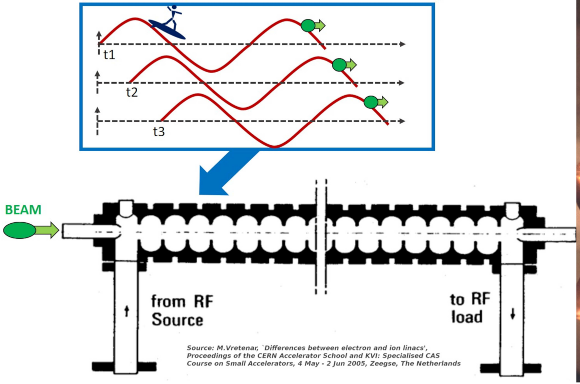

Source: M.Vretenar, `Differences between electron and ion linacs', Proceedings of the CERN Accelerator School and KVI: Specialised CAS Course on Small Accelerators, 4 May - 2 Jun 2005, Zeegse, The Netherlands

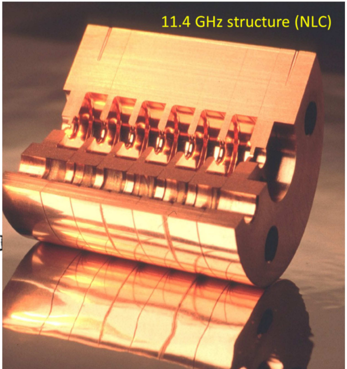

Source: E.Jensen, `RF Cavity Design', Proceedings of the CAS-CERN Accelerator School: Advanced Accelerator Physics, Trondheim, Norway, 19-29 August 2013, CERN-2014-009

RF Cavities

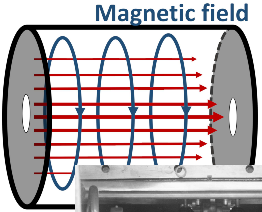

There are many varieties of RF-cavity:

e.g. standing wave drift tube Alvarez structure

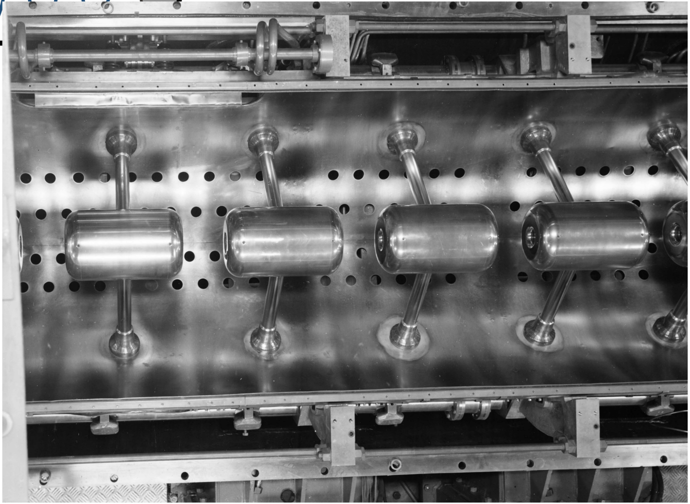

RF Cavities

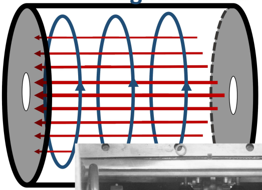

There are many varieties of RF-cavity:

e.g. standing wave drift tube Alvarez structure

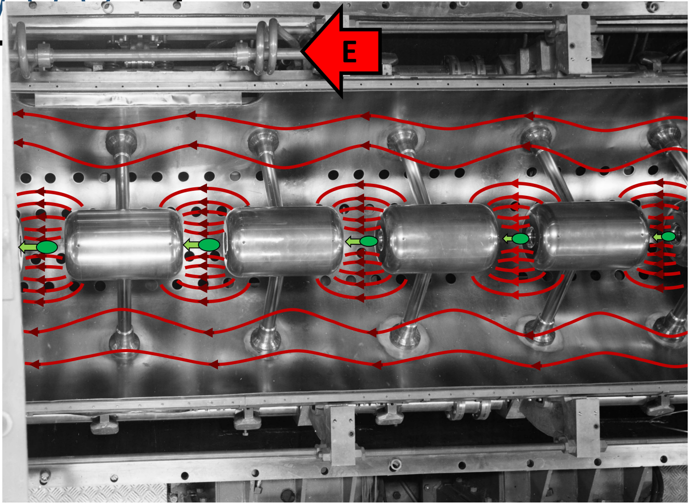

RF Cavities

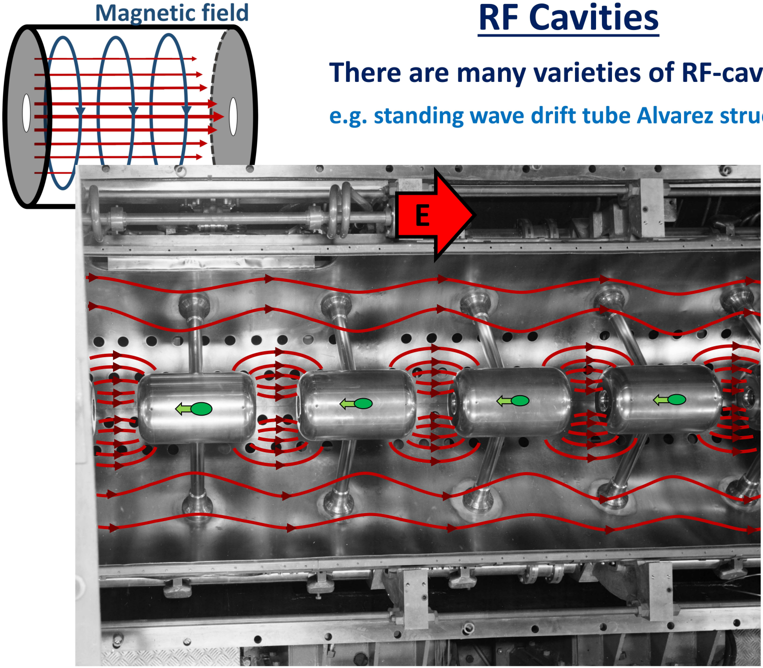

There are many varieties of RF-cavity:

e.g. standing wave drift tube Alvarez structure

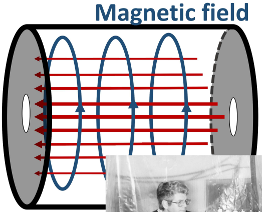

RF Cavities

There are many varieties of RF-cavity:

e.g. standing wave drift tube Alvarez structure

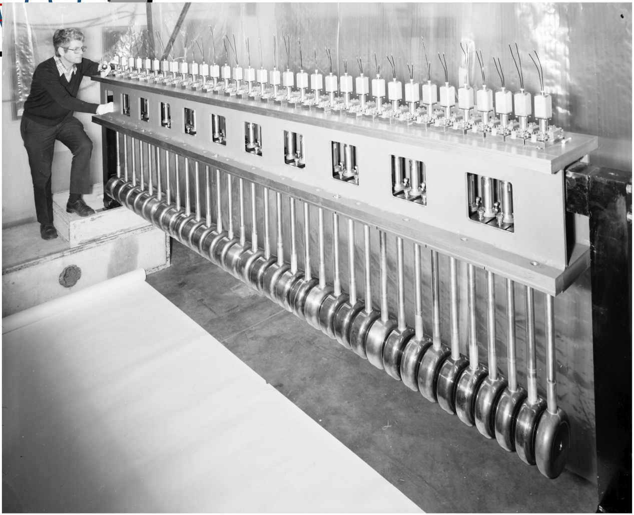

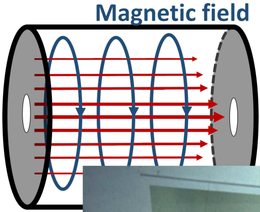

RF Cavities

There are many varieties of RF-cavity:

e.g. superconducting elliptical cavities (LEP)

RF Cavities

There are many varieties of RF-cavity:

e.g. superconducting elliptical cavity (LHC)

- RF frequency is harmonic of revolution frequency

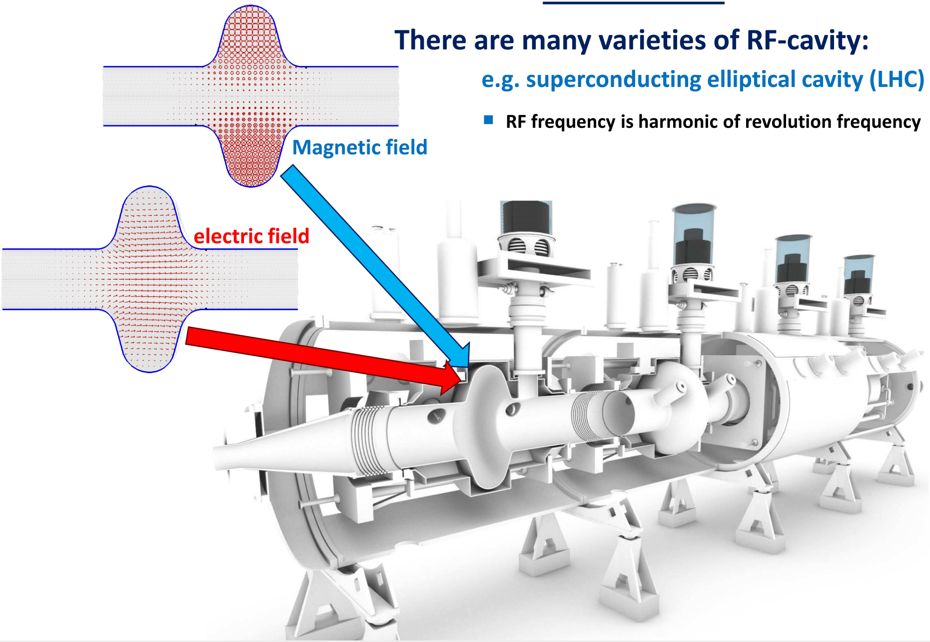

Particles come in bunches!

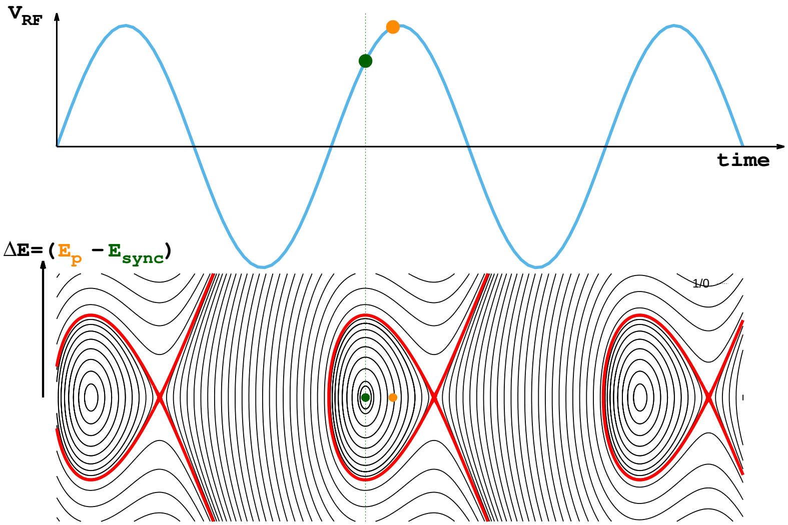

Picutre valid for low-energy particles (below transition energy). For high energy particles (above transition) picture can be reversed if higher-energy particles take longer to travel around the ring due to relativistic saturation of particle velocity and dependence of path length on particle momentum.

Particles come in bunches!

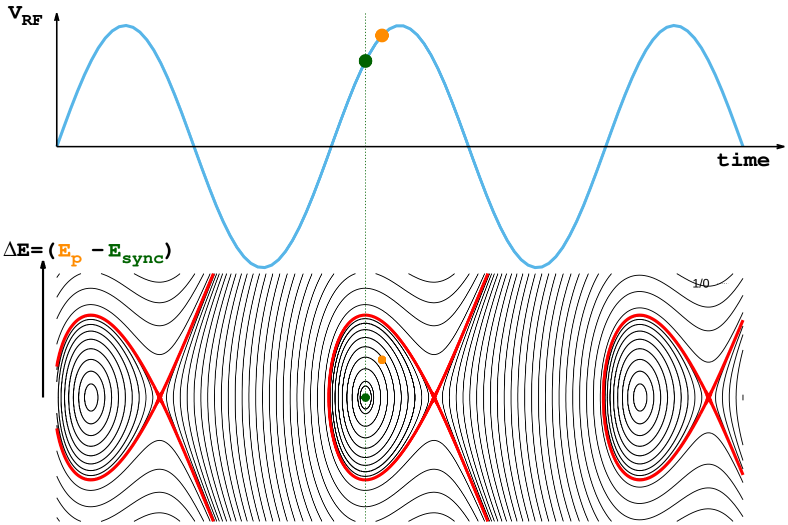

Picutre valid for low-energy particles (below transition energy). For high energy particles (above transition) picture can be reversed if higher-energy particles take longer to travel around the ring due to relativistic saturation of particle velocity and dependence of path length on particle momentum.

Particles come in bunches!

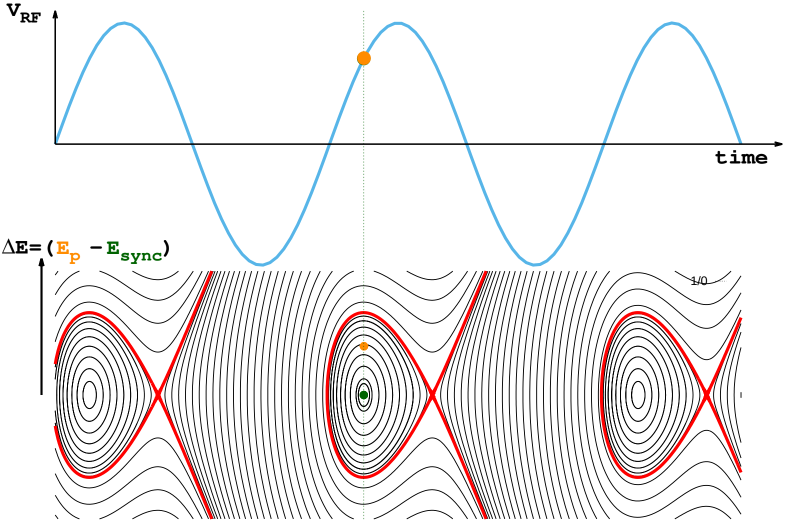

Picutre valid for low-energy particles (below transition energy). For high energy particles (above transition) picture can be reversed if higher-energy particles take longer to travel around the ring due to relativistic saturation of particle velocity and dependence of path length on particle momentum.

Particles come in bunches!

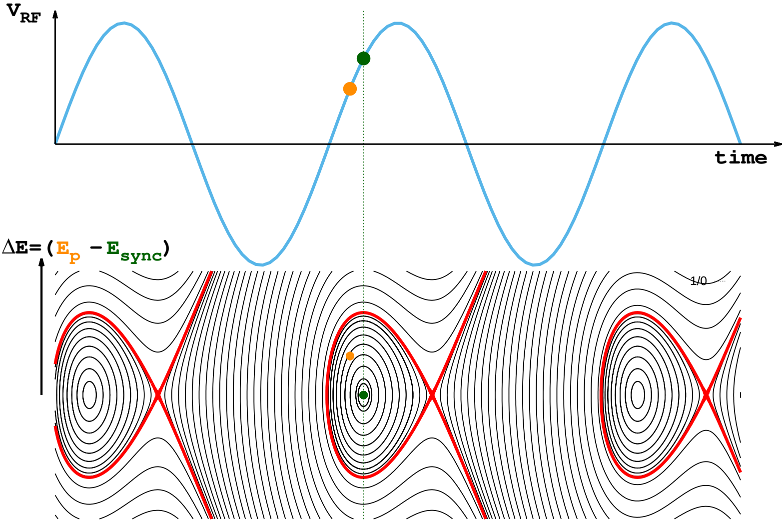

Picutre valid for low-energy particles (below transition energy). For high energy particles (above transition) picture can be reversed if higher-energy particles take longer to travel around the ring due to relativistic saturation of particle velocity and dependence of path length on particle momentum.

Particles come in bunches!

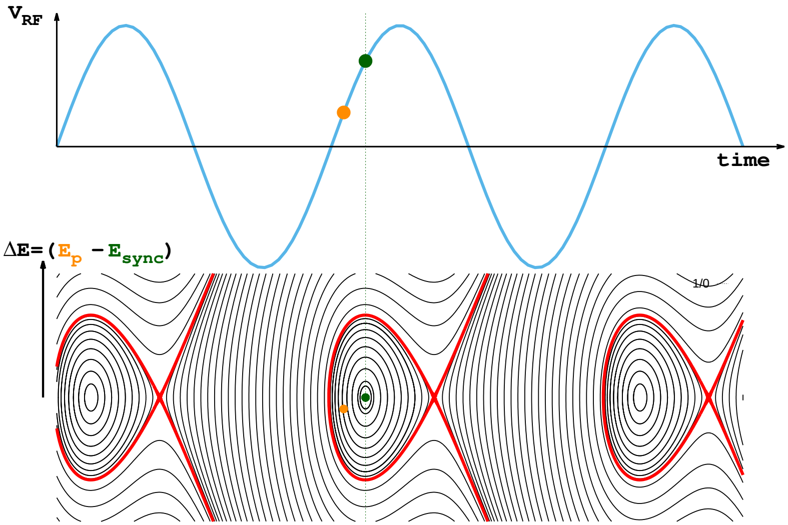

Picutre valid for low-energy particles (below transition energy). For high energy particles (above transition) picture can be reversed if higher-energy particles take longer to travel around the ring due to relativistic saturation of particle velocity and dependence of path length on particle momentum.

Particles come in bunches!

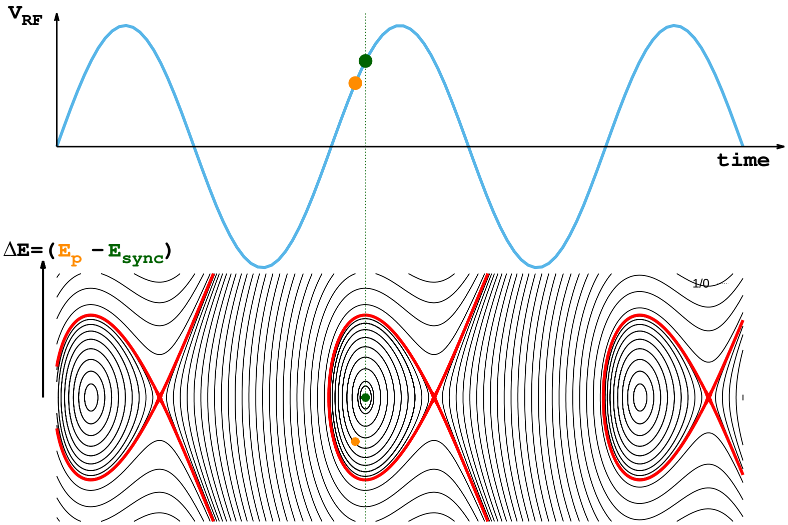

Picutre valid for low-energy particles (below transition energy). For high energy particles (above transition) picture can be reversed if higher-energy particles take longer to travel around the ring due to relativistic saturation of particle velocity and dependence of path length on particle momentum.

Particles come in bunches!

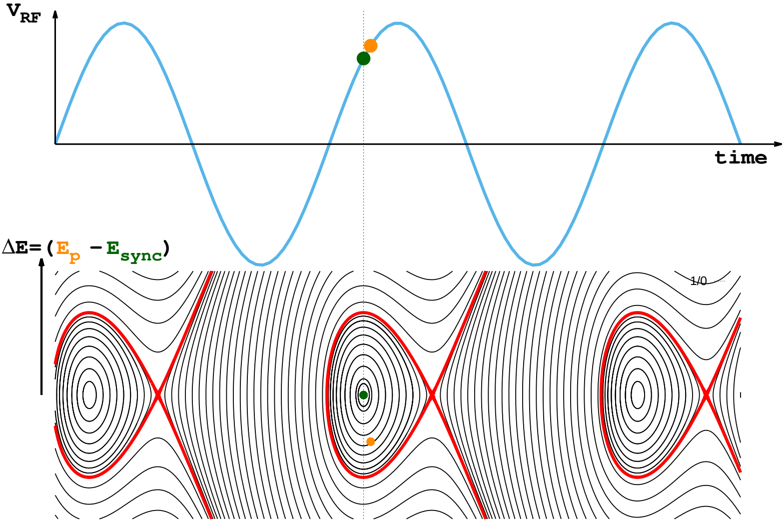

Picutre valid for low-energy particles (below transition energy). For high energy particles (above transition) picture can be reversed if higher-energy particles take longer to travel around the ring due to relativistic saturation of particle velocity and dependence of path length on particle momentum.

Particles come in bunches!

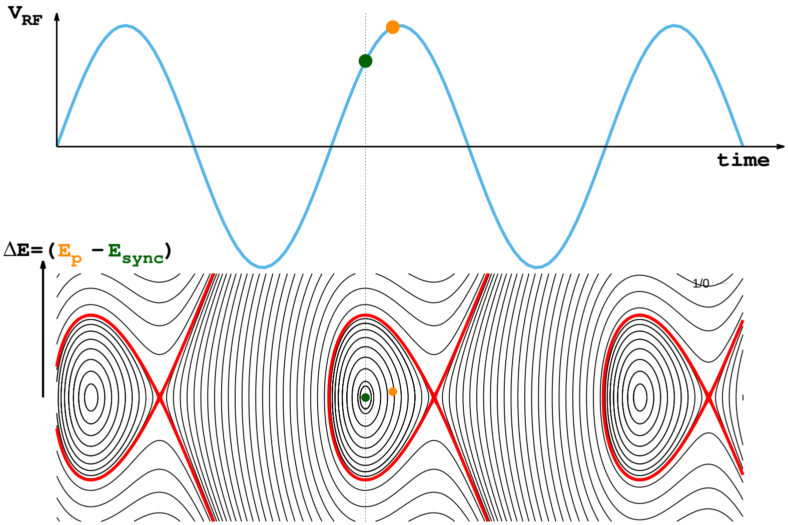

Picutre valid for low-energy particles (below transition energy). For high energy particles (above transition) picture can be reversed if higher-energy particles take longer to travel around the ring due to relativistic saturation of particle velocity and dependence of path length on particle momentum.

But what about the moon?

Credit: NASA/Goddard Space Flight Center/Arizona State University

Tidal deformation of earths crust changes the LHC circumference

→ **If uncorrected this causes a drift in the beam energy**

Effect of terrestrial tides on the LEP beam energy

L. Arnaudon et al. CERN SL/94-07 http://cds.cern.ch/record/260368

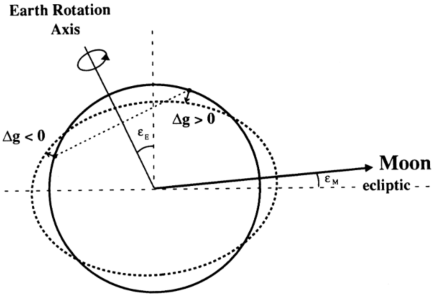

Timeseries Chart between 2016-11-13 04:55:51.338 and 2016-11-13 18:55:51.338 (LOCAL_TIME)

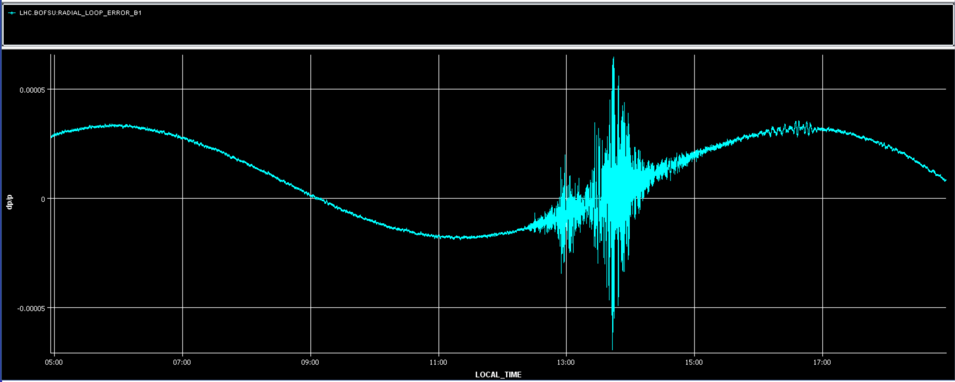

Bending

$$\vec{F} = \mathrm{q}(\vec{E} + \vec{v} \times \vec{B})$$

- Use Lorentz force to bend bunches around the synchrotron ring
- Use dipole magnets

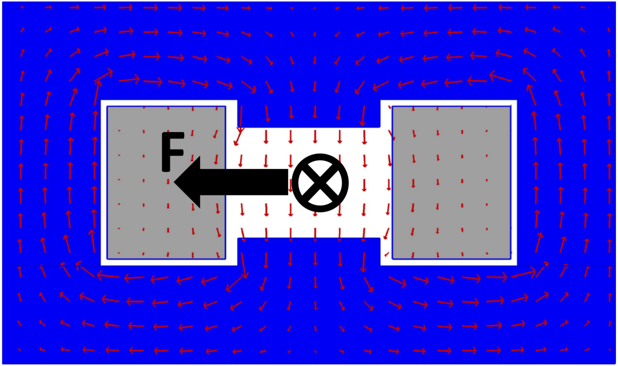

- **Conventional dipole field defined by core**
- **Conventional dipoles limited to $\sim 2\,\mathrm{T}$ by saturation of core**

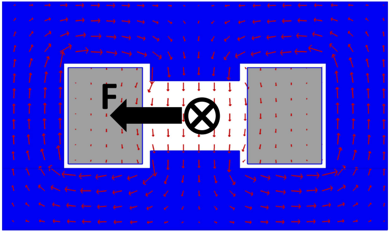

- $> 2\,\mathrm{T}$ **need very large current** $\rightarrow$ **superconductors!!!!**
- **Field defined by coil geometry** $\rightarrow$ $I \propto \cos\Theta$

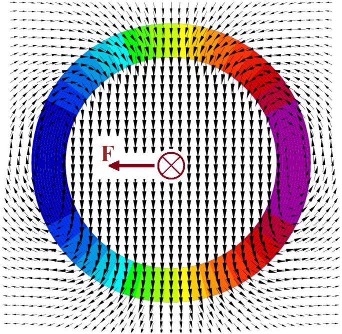

For discussion of magnet design: **S.Russenschuck**, **Design of accelerator magnets**, CERN accelerator school, Loutraki, Greece, Oct' 2000 https://cds.cern.ch/record/865932

- **Conventional dipole field defined by core**
- **Conventional dipoles limited to $\sim 2\,\mathrm{T}$ by saturation of core**

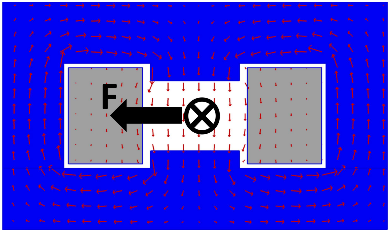

- $> 2\,\mathrm{T}$ **need very large current** $\rightarrow$ **superconductors!!!!**
- **Field defined by coil geometry** $\rightarrow$ $I \underset{\sim}{\propto} \cos\Theta$

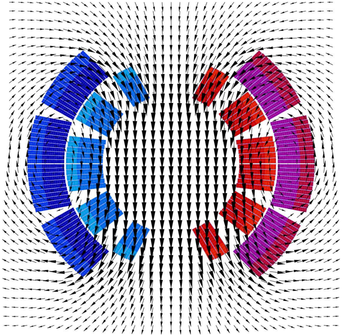

For discussion of magnet design: **S.Russenschuck**, **Design of accelerator magnets**, CERN accelerator school, Loutraki, Greece, Oct' 2000 https://cds.cern.ch/record/865932

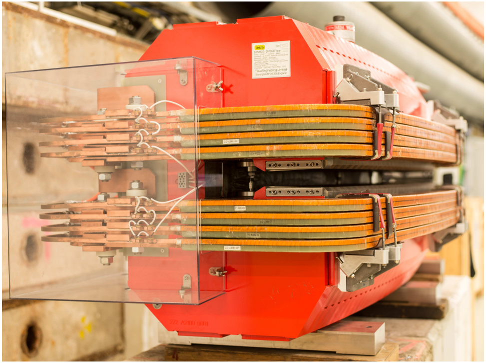

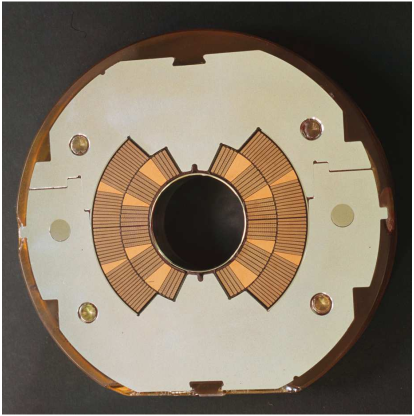

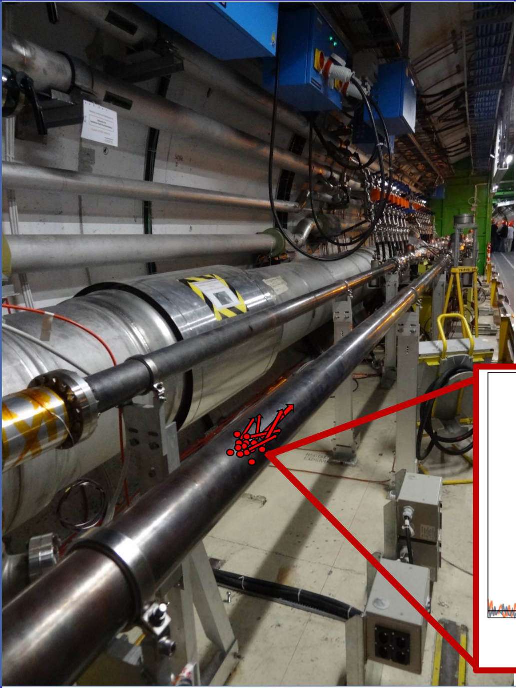

- **Beams typically contained inside `beam-pipe' at high vacuum**
- **Particle bunches have finite size and angular divergence**
- **Individual particles follow slightly different trajectories around the synchrotron**
- **To contain the particles in the synchrotron also need to focus particles back towards the center of the beam pipe**

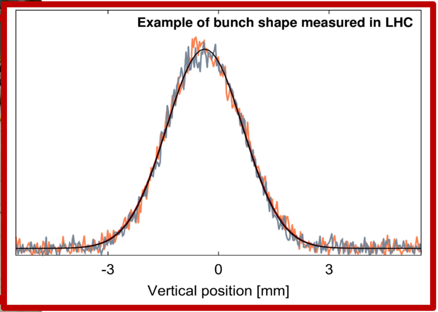

Focusing

- **Use quadrupole fields to focus particle beams**
  - $\rightarrow F \propto$ displacement from center
  - $\rightarrow I \propto \cos 2\Theta$

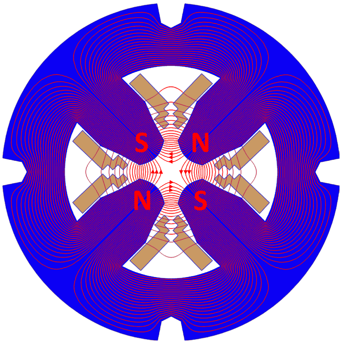

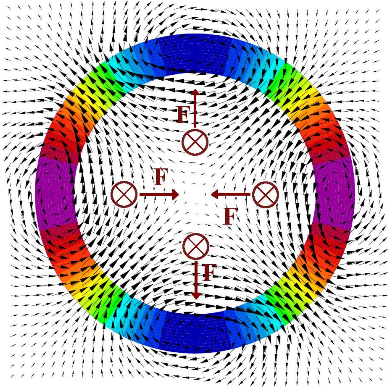

For discussion of magnet design: **S.Russenschuck**, **Design of accelerator magnets**, CERN accelerator school, Loutraki, Greece, Oct' 2000 https://cds.cern.ch/record/865932

Focusing

- **Use quadrupole fields to focus particle beams**

  $\rightarrow$ $F \propto$ displacement from center

  $\rightarrow$ $I \underset{\sim}{\propto} \cos 2\Theta$

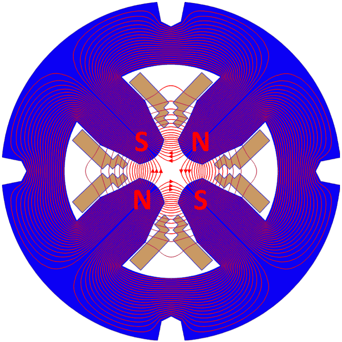

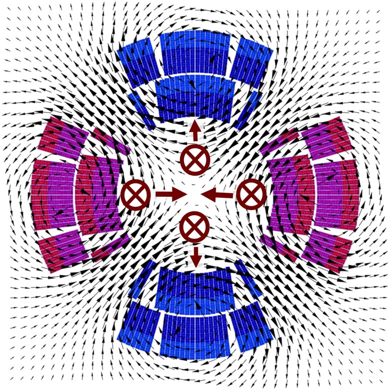

For discussion of magnet design: **S.Russenschuck**, **Design of accelerator magnets**, CERN accelerator school, Loutraki, Greece, Oct' 2000 https://cds.cern.ch/record/865932

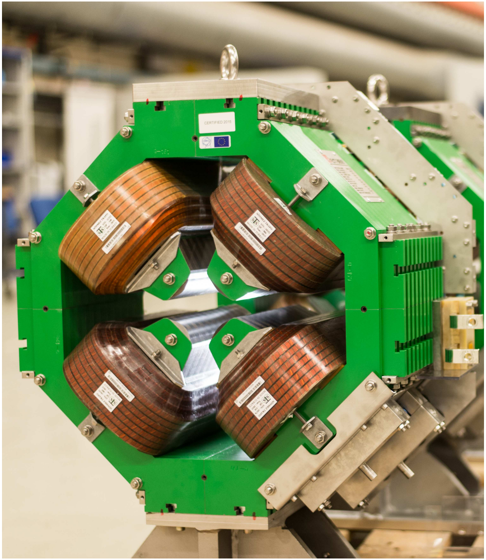

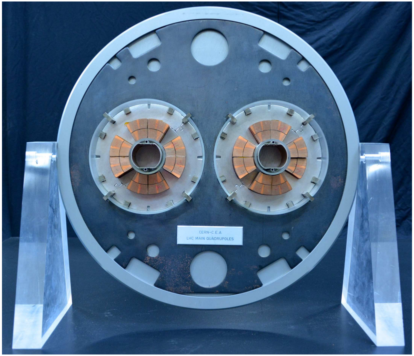
CERN-C.E.A
LHC MAIN QUADRUPOLES

Focusing

- **Single quadrupole can focus in either H or V. Not both.**
- **Use alternating lattice of focusing/defocusing quads**

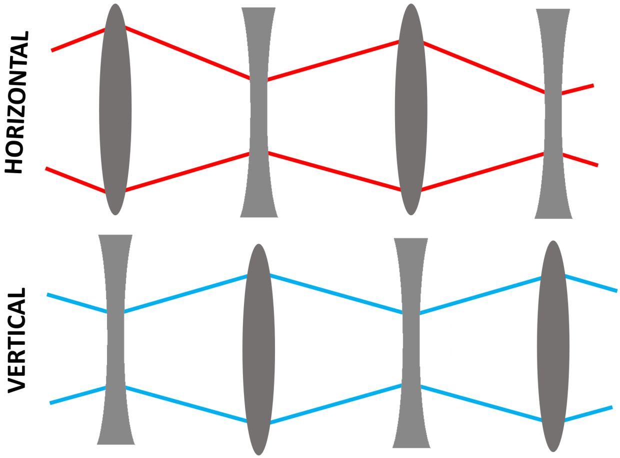

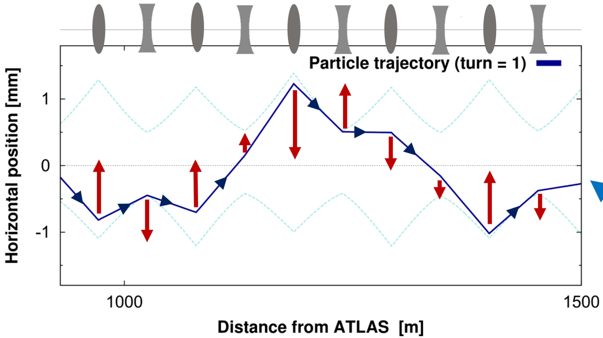

central (closed) orbit defined by dipole magnets

Individual particles oscillate about central (closed) orbit according to quadrupole placement and strength

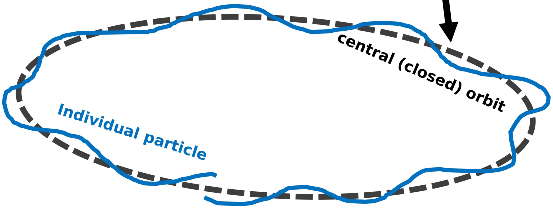

- Number of times a particle oscillates about the closed orbit in 1 turn is the **TUNE** ($Q_{x,y}$) of the accelerator
- One of the most important properties of any accelerator
- In the LHC $Q_{x,y} \approx (62.31\,,\ 60.32)$

Accelerators can also use a variety of higher-order multipole magnets to control various aspects of linear & nonlinear beam dynamics

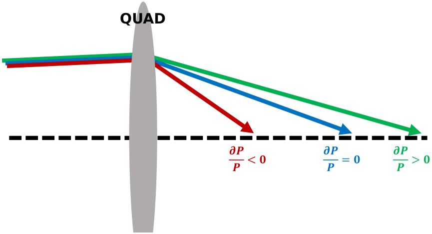

- Quadrupoles focus low & high momentum particles differently
- **CHROMATICITY:** $Q' = \partial Q / \partial(\frac{\delta P}{P_0})$
- Momentum dependent focusing causes **tune-spread** within the bunch

- **Chromaticity** controlled with **SEXTUPOLES** →
- 2n-pole field defined by complex potential:

$$\Psi_n = \left(\frac{\partial^{n-1}B_x}{\partial y^{n-1}} + i\frac{\partial^{n-1}B_x}{\partial x^{n-1}}\right)\frac{(x+iy)^n}{n!}$$

$$\Psi_n = (B_n + iA_n)\frac{(x+iy)^n}{n}$$

- octupoles, decapoles, dodecapoles have all been used in particle accelerators

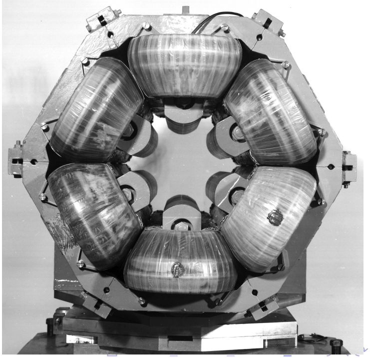

Accelerators for HEP

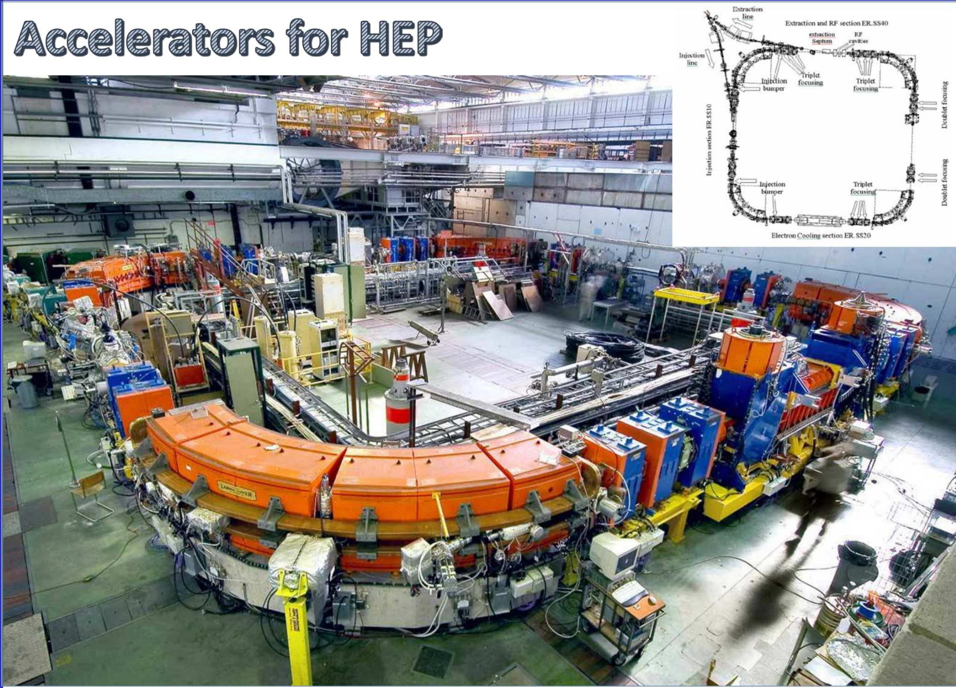

Key Points

- The LHC injector chain
- What is a synchrotron?
- What is the Tune ($Q_{x,y}$)?
- How do we accelerate?
  $\rightarrow$ Particles come in bunches
- Dipoles and quadrupoles to bend/focus
- Nonlinear multipole magnets can also be used, e.g. sextupoles for chromaticity correction

The Large Hadron Collider (LHC)

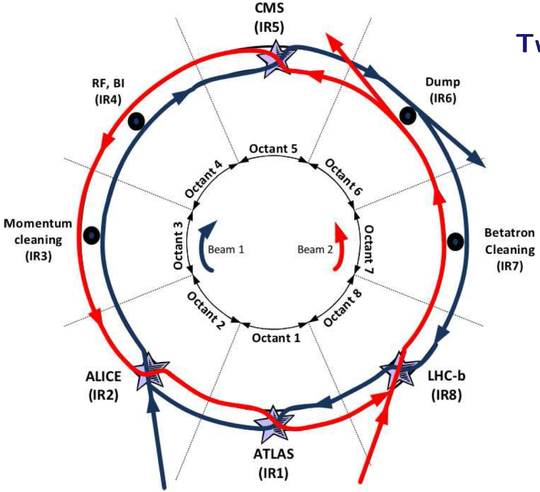

Twin-ring synchrotron collider

- **Collides** p, Pb, Xe, O
- **2 counter-rotating beams**
- **Curvilinear coordinate system**

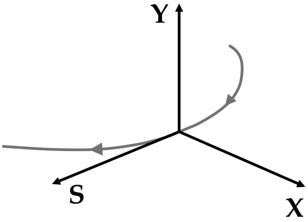

- **8 straight insertion regions** (IRs) **& 8 bending Arcs** *'A12 → A81'*

Arcs utilize superconducting dual bore main dipoles

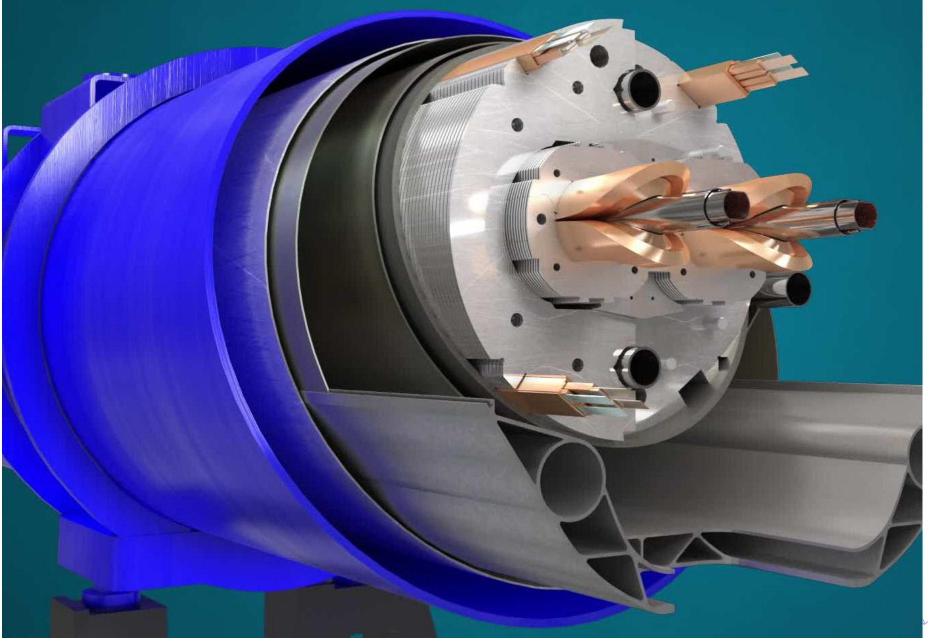

Arcs utilize superconducting $\approx 8\,\mathrm{T}$ dual bore dipoles

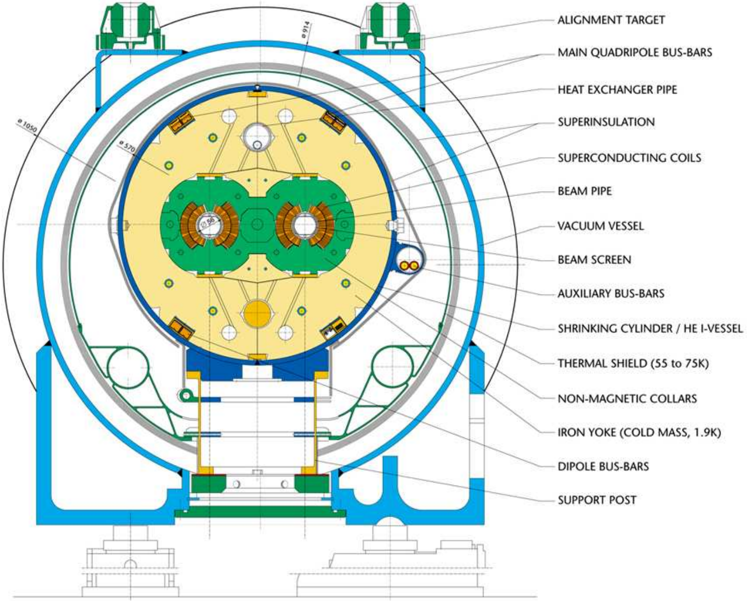

Arcs utilize superconducting $\approx 8\,\mathrm{T}$ dual bore dipoles

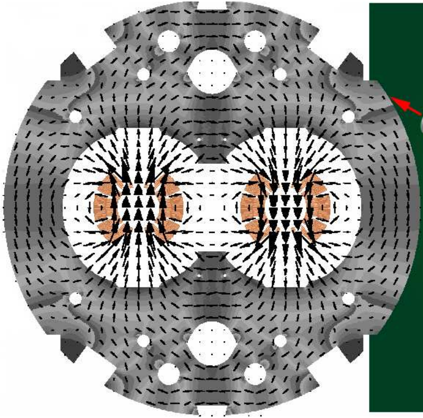

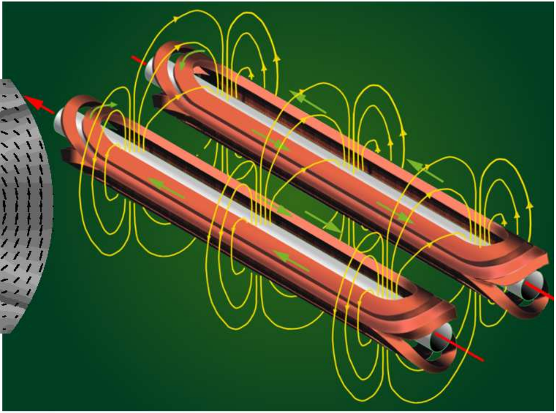

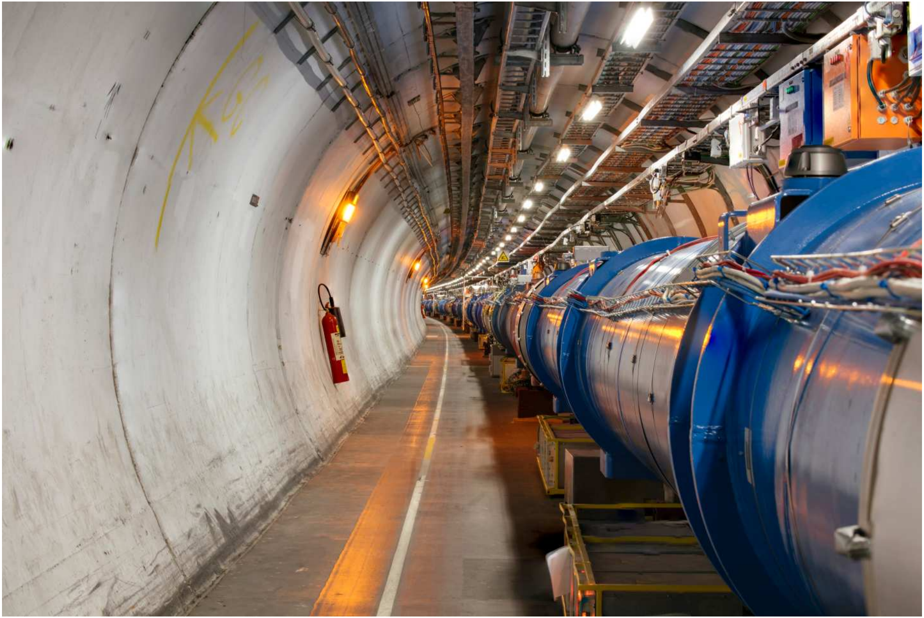

Arcs have repeating pattern ('lattice') of magnets

23 repeating ‘cells’ per Arc

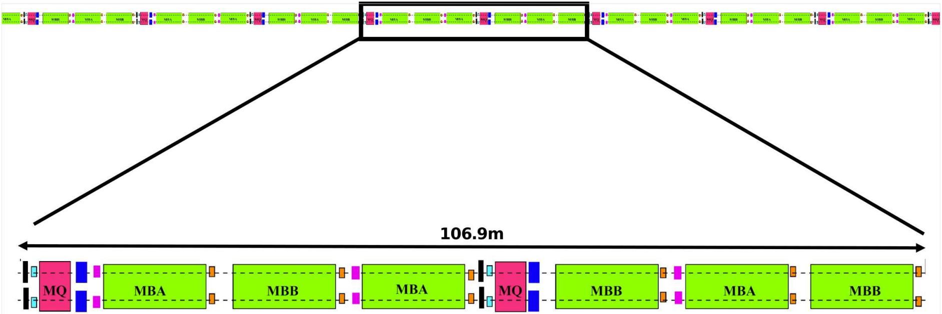

Magnets powered in series (arc-by-arc or families)

23 repeating ‘cells’ per Arc

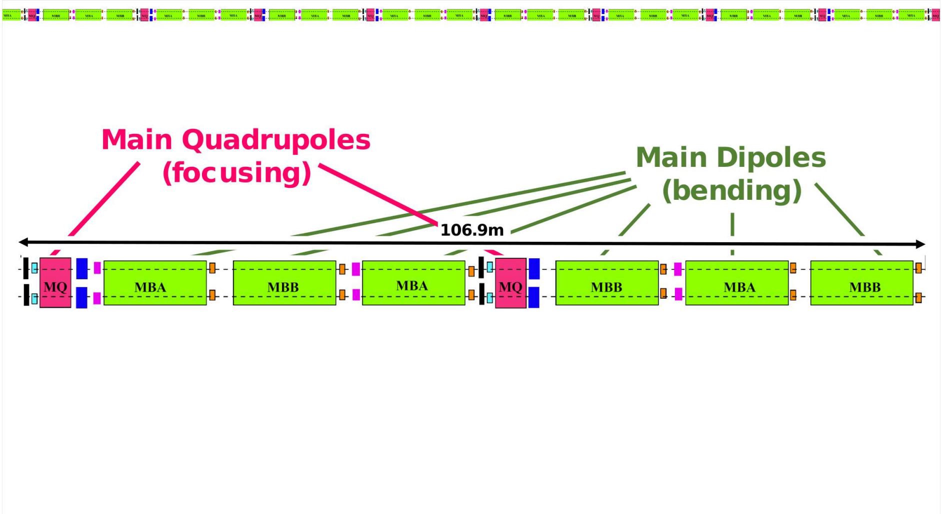

Most space occpied by dipoles and main quadrupoles

23 repeating 'cells' per Arc

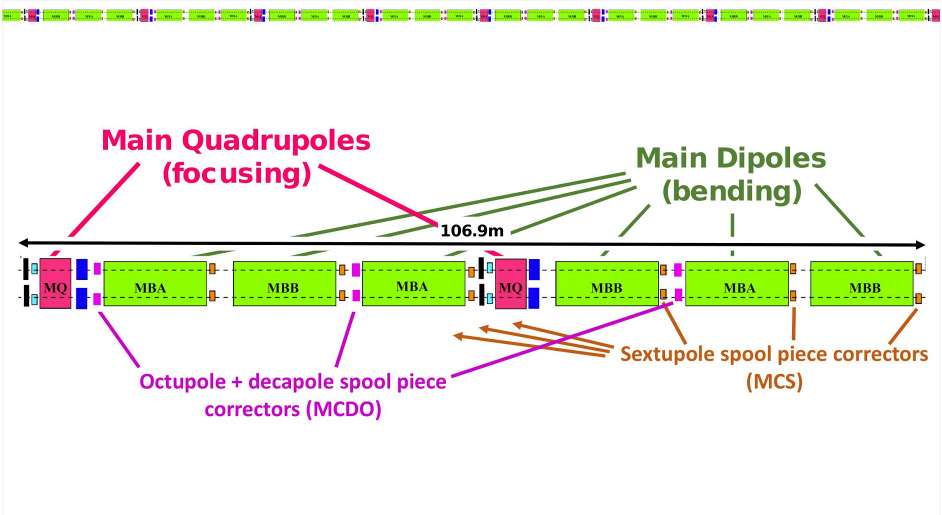

Higher order magnets correct field imperfections in main dipoles

23 repeating ‘cells’ per Arc

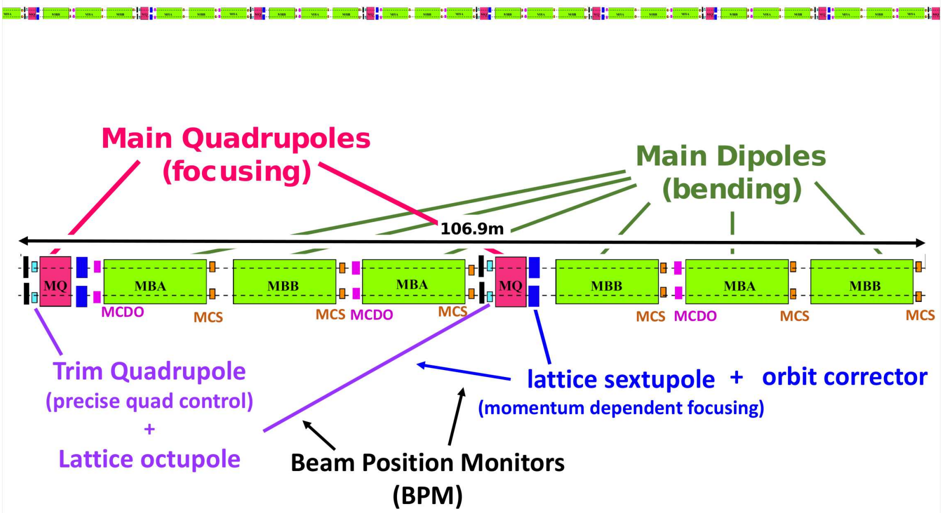

Need room for beam instrumentation & magnet connections

The Large Hadron Collider (LHC)

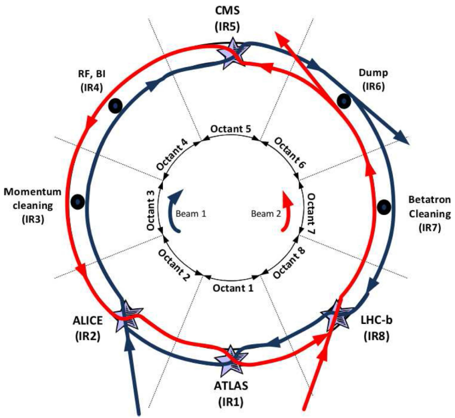

8 insertions:

- **IR2:** LHC B1 injection + HEP (ALICE)
- **IR8:** LHC B2 injection + HEP (LHCb)

- **IR1:** HEP (ATLAS)
- **IR5:** HEP (CMS)

- **IR3:** COLLIMATION (momentum)
- **IR7:** COLLIMATION (transverse)

- **IR4:** Acceleration + instrumentation

- **IR6:** LHC B1+B2 BEAM DUMP

Structure of a HEP insertion:

→ e.g. **Insertion Region 1 (IR1)** hosting the ATLAS experiment

→ Beams collide at the **Interaction Point (IP1)**

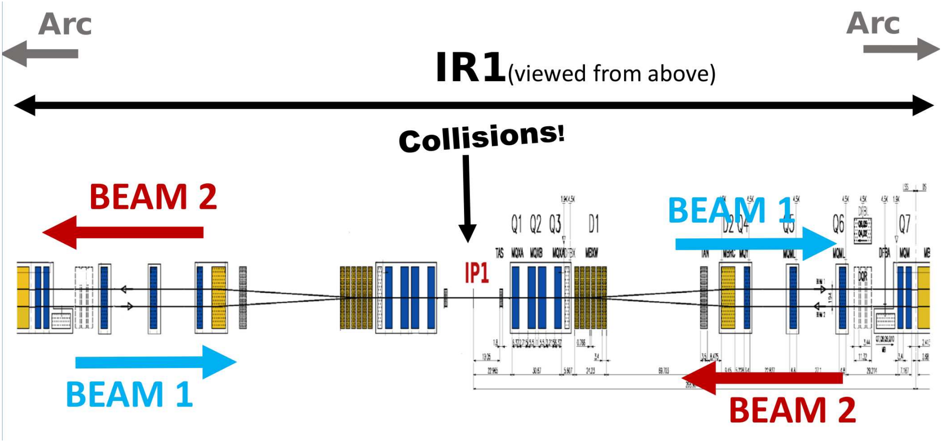

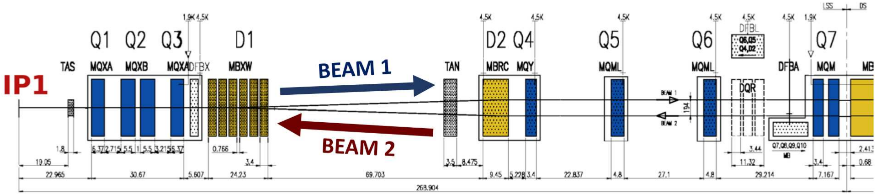

Right side of IR1, viewed from above

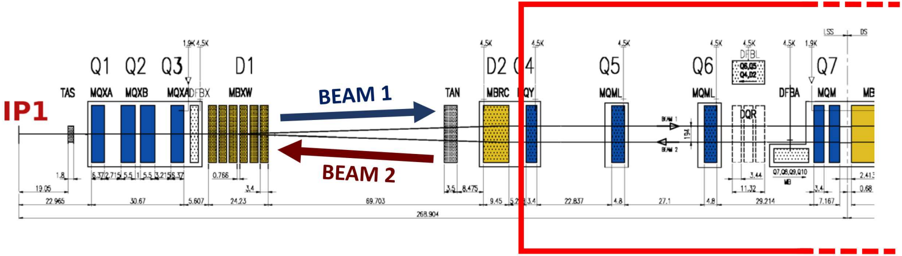

Matching section

(individually powered quads control transition from arc)

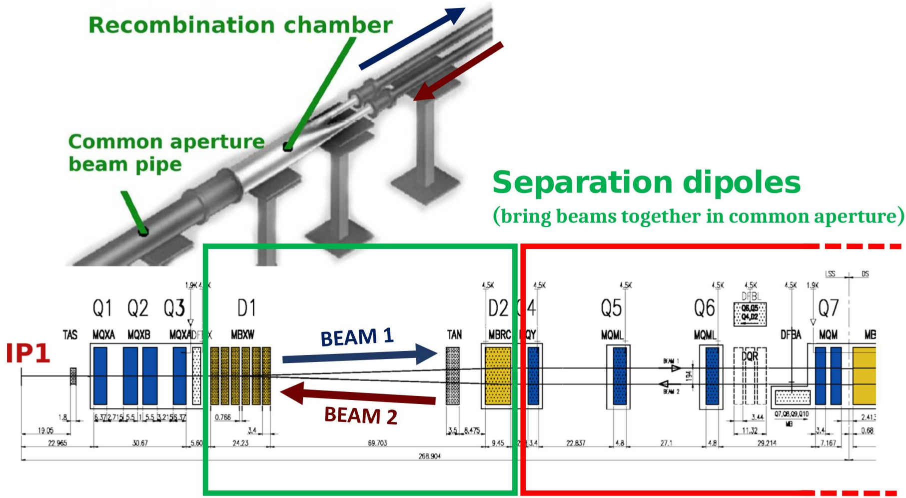

Matching section

(individually powered quads control transition from arc)

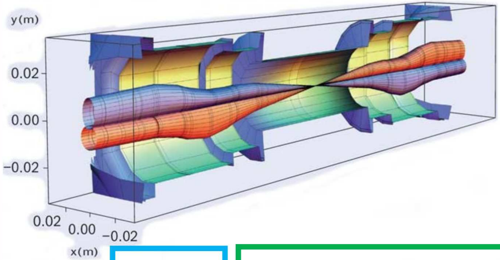

Separation dipoles

(bring beams together in common aperture)

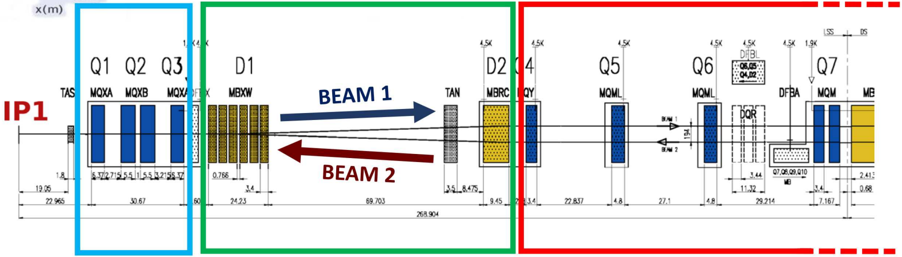

Quadrupole triplets

Squeeze beam from ~1mm in Arc to ~10um at IP

Matching section

(individually powered quads control transition from arc)

Also corrector magnets

(coupling, sextupole, octupole, dodecapole)

The Large Hadron Collider (LHC)

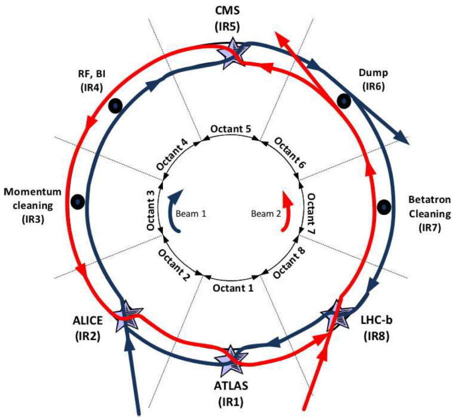

8 insertions:

- **IR2:** LHC B1 injection + HEP (ALICE)
- **IR8:** LHC B2 injection + HEP (LHCb)

- **IR1:** HEP (ATLAS)
- **IR5:** HEP (CMS)

- **IR3:** COLLIMATION (momentum)
- **IR7:** COLLIMATION (transverse)

- **IR4:** Acceleration + instrumentation

- **IR6:** LHC B1+B2 BEAM DUMP

- **IR design varies with function**

e.g. IR4 (BI/RF)

(right side viewed from above)

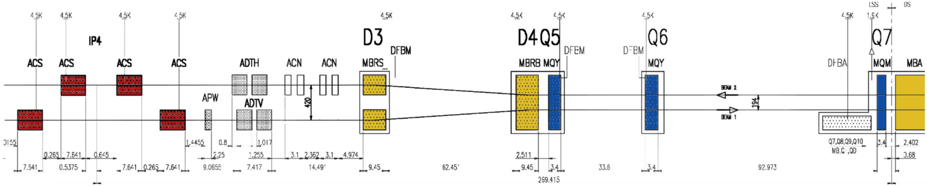

- **IR design varies with function**

e.g. IR4 (BI/RF)

(right side viewed from above)

Matching section

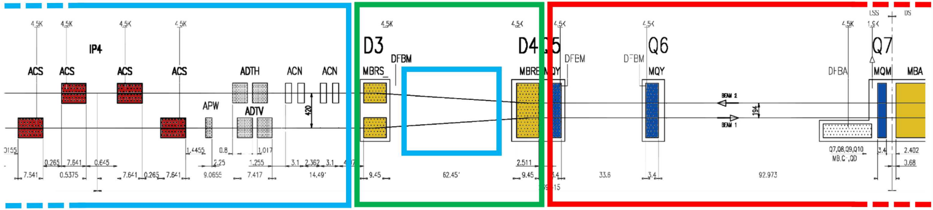

Accelerating cavities & Beam instrumentation

Dipoles (increase beam separation to give space for accelerating cavities)

- **IR design varies with function**

e.g. IR4 (BI/RF)

(right side viewed from above)

Matching section

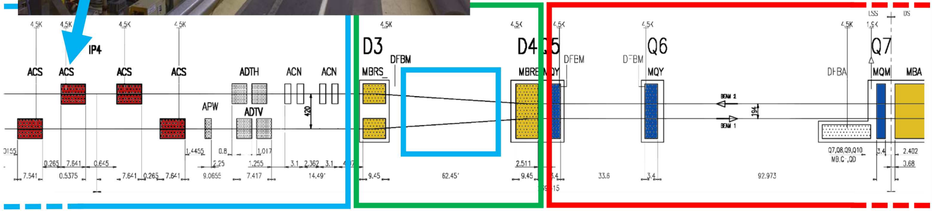

Accelerating cavities & Beam instrumentation

Dipoles (increase beam separation to give space for accelerating cavities)

Day to day operation of the CERN accelerators handled by the operations group, from the CERN Control Center (CCC)

LHC page 1: machine status & OP comments

https://op-webtools.web.cern.ch/vistar/vistars.php

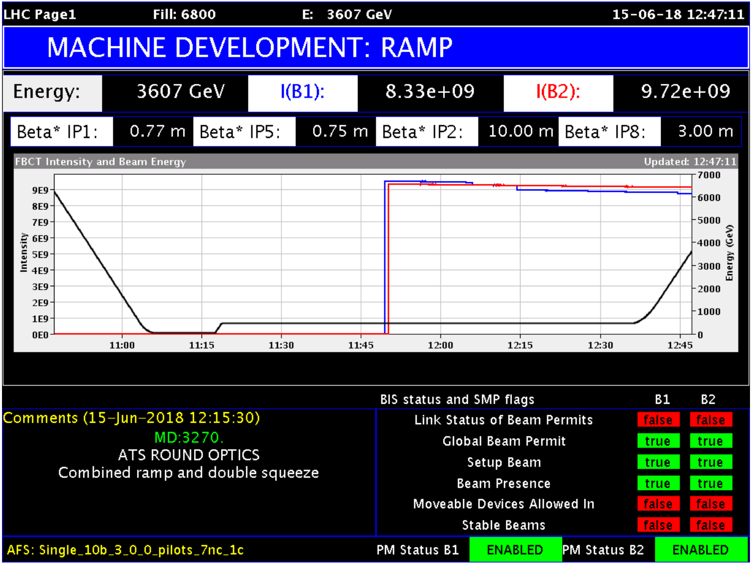

For general questions about LHC one commonly used resource is the LHC Design Report

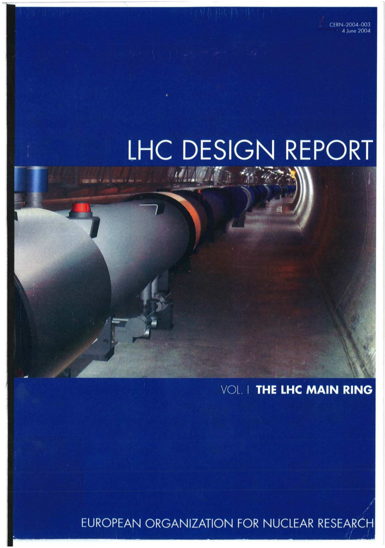

LHC Design Report, v.1 : the LHC Main Ring

http://cds.cern.ch/record/782076/

LHC Design Report, v.2 : the LHC Infrastructure and General Services

http://cds.cern.ch/record/815187

LHC Design Report, v.3 : the LHC Injector Chain http://cds.cern.ch/record/823808

BE CAREFUL: some parameters may be out of date

$\rightarrow$ **LHC has already exceeded its design performance in many ways!**

Key Points

- **Coordinate scheme for accelerators**
- **Overall structure of LHC**

  → 8 Arcs - this is where the beams are bent around the ring

  → 8 IRs - various functions
- **Repeating lattice in the arcs → the LHC arc cell**

  → can't fill the arc completely with dipoles!

  → also quadrupoles for focusing, sextupoles for momentum-dependent focussing & chromaticity, nonlinear magnets for correcting field errors, instrumentation...
- **Typical layout of an insertion region**

What do particle physicists care about??

Energy

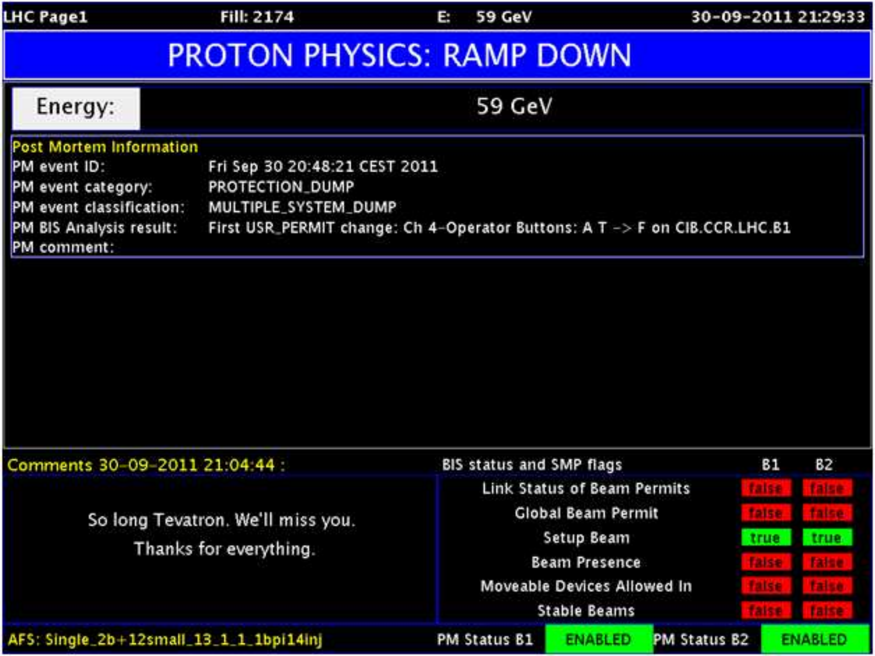
LHC Page1
Fill: 2174
E: 59 GeV
30-09-2011 21:29:33
PROTON PHYSICS: RAMP DOWN
Energy:
59 GeV
Post Mortem Information
PM event ID: Fri Sep 30 20:48:21 CEST 2011
PM event category: PROTECTION_DUMP
PM event classification: MULTIPLE_SYSTEM_DUMP
PM BIS Analysis result: First USR_PERMIT change: Ch 4-Operator Buttons: A T -> F on CIB.CCR.LHC.B1
PM comment:
Comments 30-09-2011 21:04:44 :
So long Tevatron. We'll miss you.
Thanks for everything.
BIS status and SMP flags
B1
B2
Link Status of Beam Permits false false
Global Beam Permit false false
Setup Beam true true
Beam Presence false false
Moveable Devices Allowed In false false
Stable Beams false false
AFS: Single_2b+12small_13_1_1_1bpi14inj
PM Status B1 ENABLED
PM Status B2 ENABLED

From 2001 Snowmass AQccelerator R&D report,
Part I : Executive Summaries, eConf C010630, SLAC-R-599
http://www.slac.stanford.edu/econf/C010630/papers/MT1001.PDF

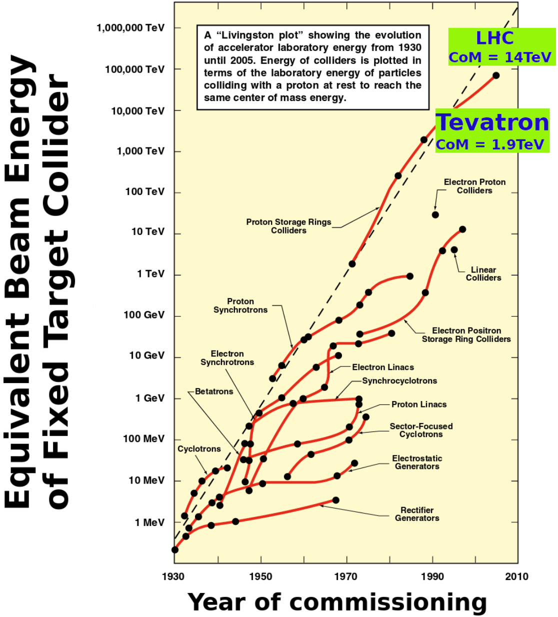

Limiting factor for circular e^+ / e^- accelerators:

→ particles emit **synchrotron radiation** as they are bent around ring

$$\Delta E/\text{turn} \propto \frac{(\beta_{rel}\gamma_{rel})^4}{\rho}$$

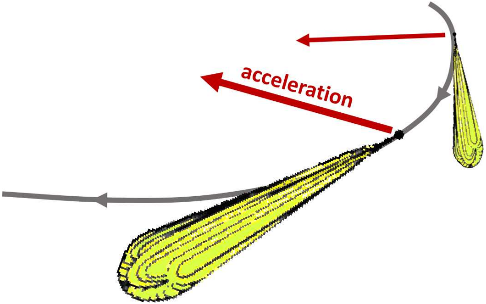

- **LEP** (e) **energy loss:** $\sim 3\,\text{GeV}/\text{turn}$ (@ $101\,\text{GeV}$)
- **LHC** (p) **energy loss:** $\sim 5\,\text{keV}/\text{turn}$ (@ $6.5\,\text{TeV}$)

Limiting factor for circular hadron collider:

$\rightarrow$ need sufficient dipole field strength to bend beams around the ring

$\rightarrow$ **High Energy = high magnetic rigidity**

$$F_{Lorentz} = F_{centrip}$$

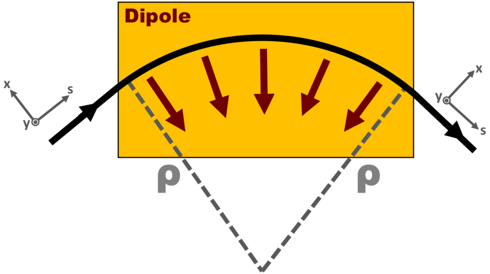

- consider pure dipole fields
- $(p_x, p_y) << p_s$

Limiting factor for circular hadron collider:

→ need sufficient dipole field strength to bend beams around the ring

→ **High Energy = high magnetic rigidity**

$$F_{Lorentz} = F_{centrip}$$

$$qvB = \frac{\gamma m_{rest} v^2}{\rho} = \frac{pv}{\rho}$$

$$B\rho = \frac{p}{q}$$

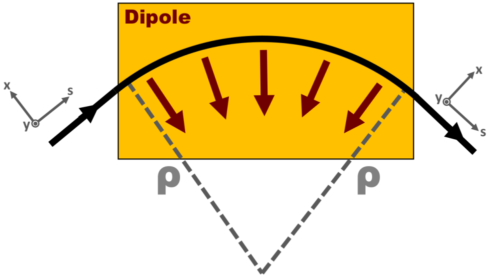

Limiting factor for circular hadron collider:

$\rightarrow$ need sufficient dipole field strength to bend beams around the ring

$\rightarrow$ **High Energy = high magnetic rigidity**

$$B\rho \ \ [\mathrm{Tm}] = \frac{p \ \ [\mathrm{kgms}^{-1}]}{q \ \ [\mathrm{C}]}$$

$$B\rho \ \ [\mathrm{Tm}] = \frac{10}{2.998} p \ [GeV/c]$$

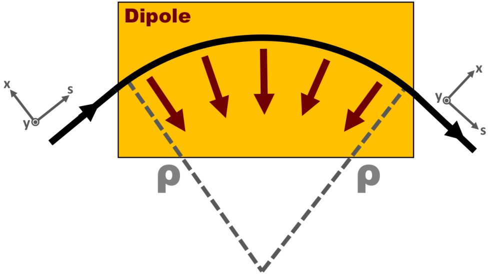

$B\rho$ is 'magnetic rigidity': defines the maximum energy you can reach for a given dipole field in a given tunnel geometry

The Future of laboratory based HEP?

$$\Delta E/\mathrm{turn} \propto \frac{(\beta_{rel}\gamma_{rel})^4}{\rho}$$

$$B\rho \ \ [\mathrm{Tm}] = \frac{10}{2.998}\, p \ \ [GeV/c]$$

- **linear e/e colliders (ILC/CLIC)**
- $100\,\mathrm{km}$ **e/e collider ring (FCC-ee,CEPC)**
- **New magnets in LHC tunnel (HE-LHC)**
- $100\,\mathrm{km}$ **hadron collider (FCC-hh,SppC)**
- **Something new?**

In practice LHC still not reached its design energy!

→ **main dipole designed for** $8.327\,\mathrm{T} \implies 7.0\,\mathrm{TeV/beam}$ **(protons)**

→ **"Report of the Task Force on the Incident of 19th September 2008 at the LHC", CERN-LHC-PROJECT-Report-1168** https://cds.cern.ch/record/1168025/

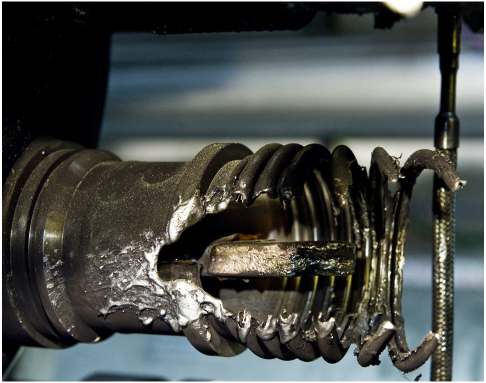

"The dipole bus bar at the location of the arc was vaporized, as well as the M3 line bellows around it, thus breaking open the helium enclosure..."

"The force was applied to the external support jacks, displacing the cryomagnets from them and in some cases, rupturing their ground anchors or the concrete in the tunnel floor."

To ensure machine protection the LHC operated at lower energy during Run1 until hardware consolidation performed during the first long-shutdown

SC-magnets must be trained to reach higher fields/currents

Time needed for training also influenced choice of LHC energy in Run2 and Run3

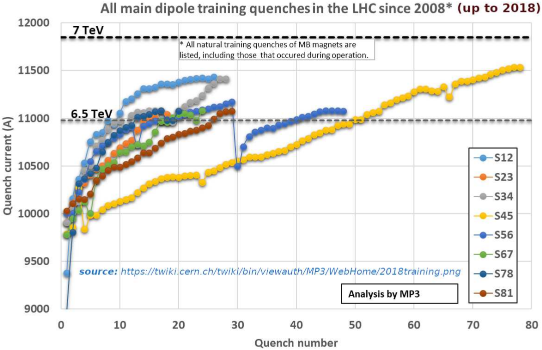

Year	mode	Beam energy [TeV]	pp-CoM [TeV]
2010-2011	pp	3.5	7.0
2012	pp	4.0	8.0
2015-2018	pp	6.5	13.0
≥2022	pp	≥6.8?	≥13.6?

Ultimate energy of LHC is still unclear!

"New High Luminosity LHC Baseline and Performance at Ultimate Energy"

CERN-ACC-2018-069

WATCH OUT: HEP normally discuss CoM → ABP may use alternative definition of energy! e.g. energy/nucleon or beam energy (E*Z/A)

Key Points

- **Different limitations on beam-energy for $e^{\pm}$ and hadron accelerators**
- **What is magnetic rigidity & where does it come from?** $\rightarrow$ the future of colliders?
- **Accelerator physicists don't always talk about CoM - watch out!**

What do particle physicists care about???

→ How much data (how many collisions) are generated?

Luminosity

Event rate for a HEP interaction:

$$R = L \times \sigma$$

- R: *Event Rate* $[\mathrm{s}^{-1}]$
- σ: *Cross Section* $[\mathrm{barn} = 10^{-24}\mathrm{cm}^2]$
  property of the HEP interaction
- L: *Luminosity* **[inverse barn / s]**
  property of the collider

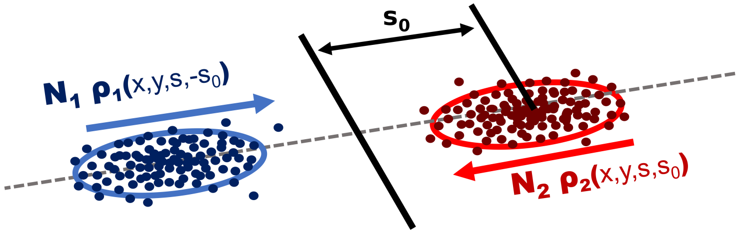

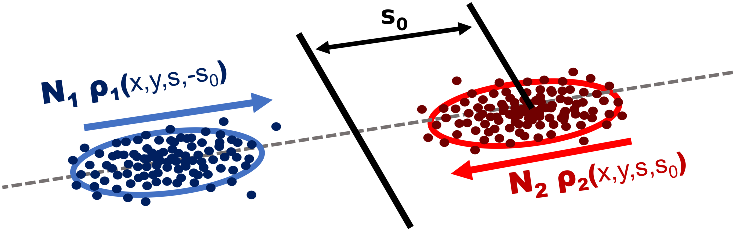

$$L = f\sqrt{(\bar{v}_1-\bar{v}_2)^2-(\bar{v}_1\times\bar{v}_2)^2\ /\ c^2}\ N_1 N_2 \iiiint_{-\infty}^{+\infty} \rho_1(x,y,s,-s_0)\rho_2(x,y,s,s_0)\,\mathrm{d}x\,\mathrm{d}y\,\mathrm{d}s\,\mathrm{d}s_0$$

For detailed discussion of Luminosity relations:

W.Herr & B.Muratori, *Concept of Luminosity*, CERN Accelerator School, Zeuthen, Germany, 15 - 26 Sep 2003

Toshio Suzuki, *General Formulas of Luminosity for Various Types of Colliding Beam Machines*, KEK-76-3, (1976)

M.A. Furman, *The Møller Luminosity Factor*, LBNL-53553,CBP Note-543, September 24, 2003

C.Møller, *General properties of the characteristic matrix in the theory of elementary particles I*,
K. Danske Vidensk. Selsk. Mat.-Fys. Medd. 23, 1 (1945) http://gymarkiv.sdu.dk/MFM/kdvs/mfm 2020-29/mfm-23-1.pdf

with some approximation:

$$L = \frac{\left(f_{rev} n_{coll}\right) \ N_1 N_2}{2\pi\sqrt{\left(\sigma_{x,1}^2 + \sigma_{x,2}^2\right)}\sqrt{\left(\sigma_{y,1}^2 + \sigma_{y,2}^2\right)}}$$

Assume:

- **uncorrellated gaussian bunch profiles in x,y,s**
- **head-on colinear collission of equal/opposite velocity beams**
- **equal bunch lengths** $\sigma_{s,1} \approx \sigma_{s,2}$
- **revolution frequency of 2 beams are in sync**
- n_{coll} **colliding bunches are all described by similar** $N_{1,2}, \sigma$

$$L = \frac{\left(f_{rev}\, n_{coll}\right)\ N_1 N_2}{2\pi\sqrt{\left(\sigma_{x,1}^2 + \sigma_{x,2}^2\right)}\sqrt{\left(\sigma_{y,1}^2 + \sigma_{y,2}^2\right)}}$$

- n_{coll}: **Number of colliding bunches**

How many bunches can we fit in the LHC?

- **LHC revolution frequency** $\approx 11.245\,\mathrm{kHz}$

  $\rightarrow$ **revolution period** $\approx 89\,\mu s$

- **Minimum separation of bunches defined by RF system of the injector chain**

  $\rightarrow$ 25 ns bunch spacing

soooo... $\approx$ 3560 bunches?

NO!

Also need time to dump / inject beams

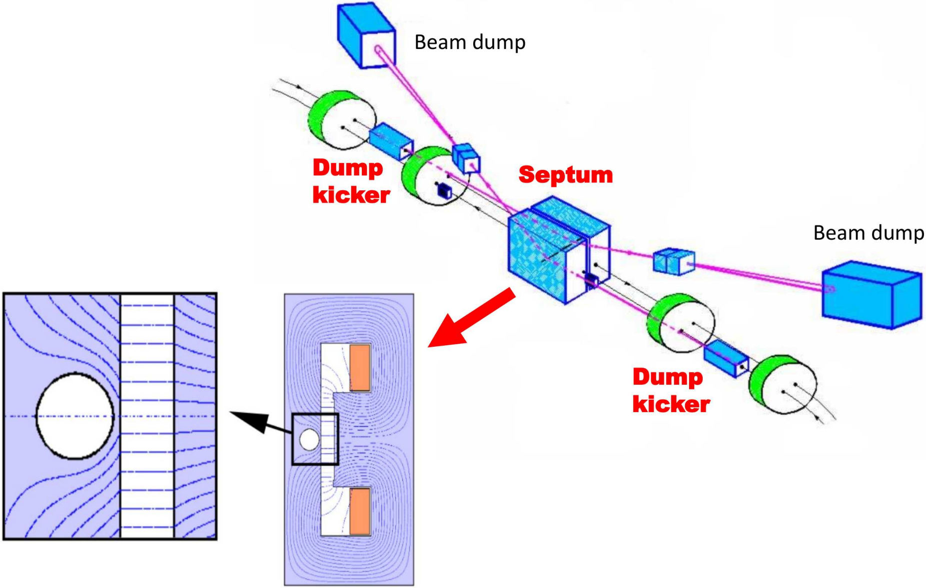

Also need time to dump / inject beams

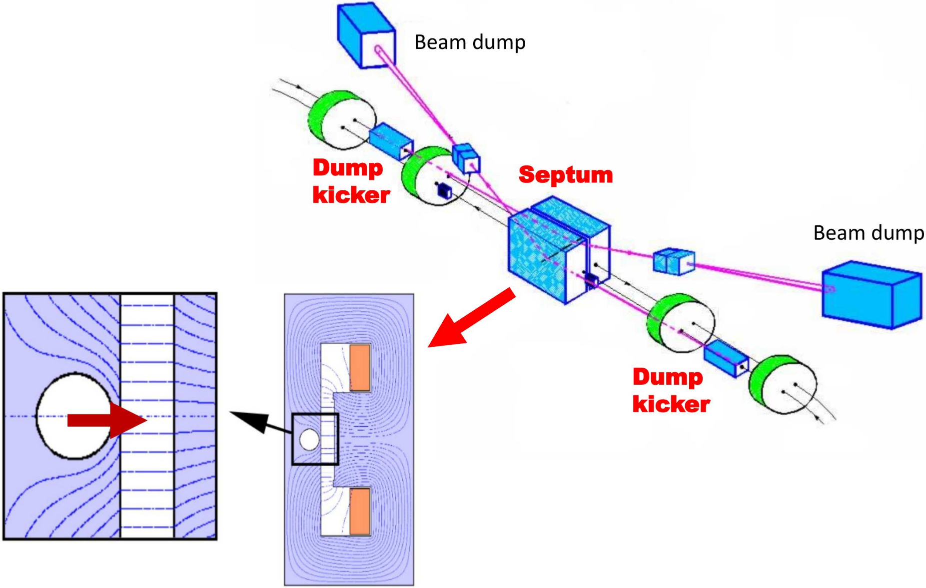

Also need time to dump / inject beams

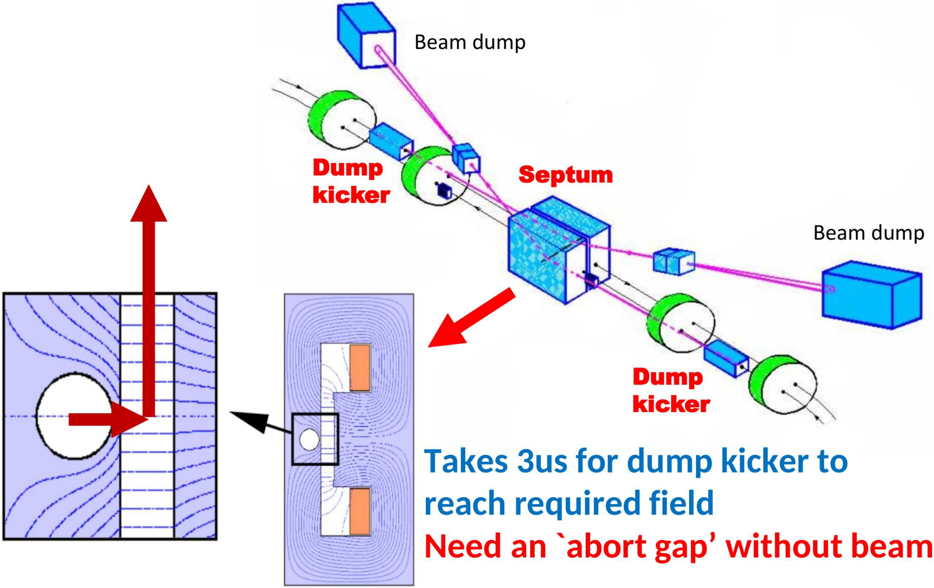

Takes 3us for dump kicker to reach required field

Need an `abort gap' without beam

Also need time to dump / inject beams

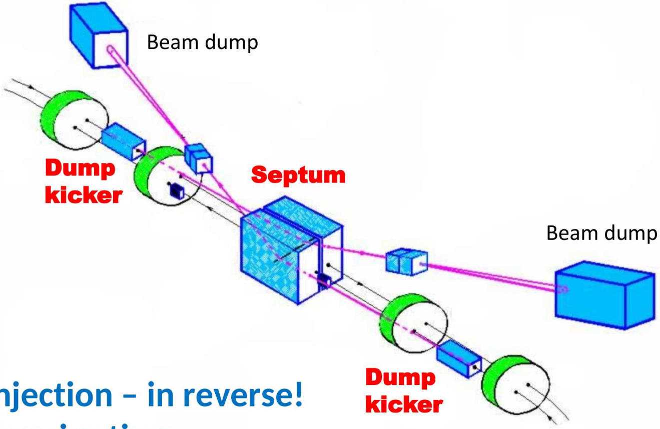

Similar issue at injection – in reverse!
1us injection kicker rise time

Not practical to inject bunches one at a time!

Increase luminosity by colliding trains

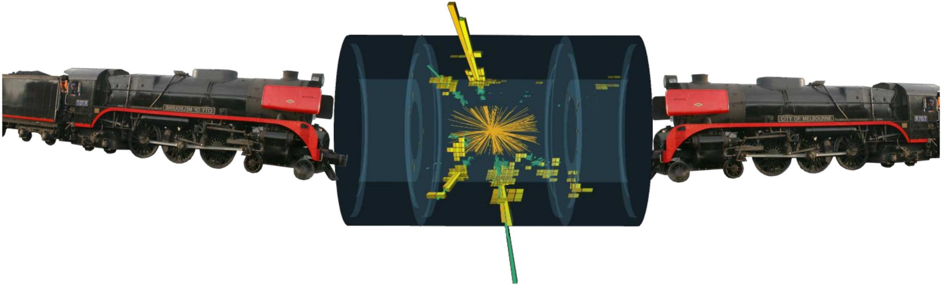

Increase luminosity by colliding trains

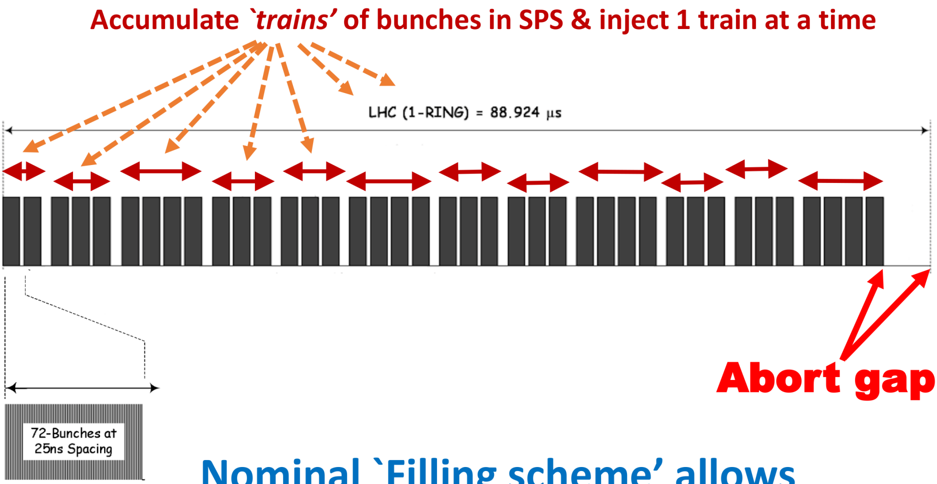

Nominal `Filling scheme' allows 2808 bunches in each ring

In practice many different types of filling scheme are used in the LHC and it may not be desirable to operate with the nominal scheme

Good example of this is `electron cloud'

- seed electron generated by e.g. photoemission / gas ionization
- electron accelerated by field of the beam hits chamber wall
- liberates more secondary electrons
- creates an avalanche of electrons in the beam pipe

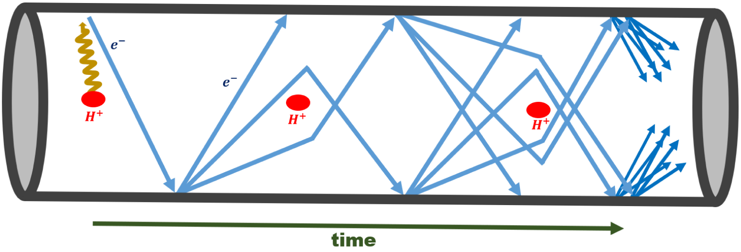

Formation of electron cloud can be suppressed by leaving gaps in the bunch trains:

➡ During parts of Run2 LHC used a special `8b4e' filling scheme (micro-trains of 8 bunches followed by 4 empty slots)

For more details about electron cloud see:
G. Rumolo and G. Iadarola, *Electron Clouds*, CERN Yellow Reports: School Proceedings, Vol. 3/2017, CERN-2017-006-SP
https://doi.org/10.23730/CYRSP-2017-003

8b4e filling scheme was a significant factor in limiting the impact of UFO's on LHC Run2!

UFO = *Unidentified Falling Object*

J.M. Jiménez et. al, *Observations, analysis and mitigation of recurrent LHC beam dumps caused by fast losses in arc half-cell 16L2*, MOPMF053, IPAC2018, https://doi.org/10.18429/JACoW-IPAC2018-MOPMF053

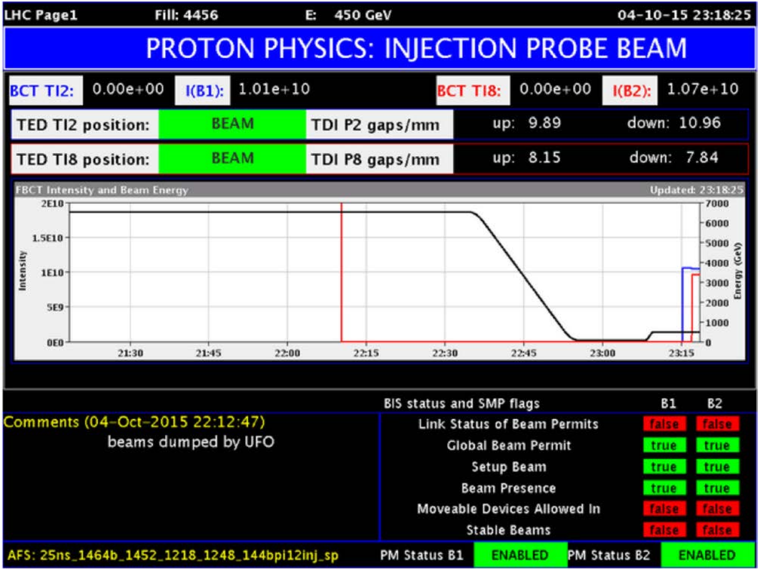

Introduce ‘*crossing angle*’ to prevent parasitic collisions either side of the IP

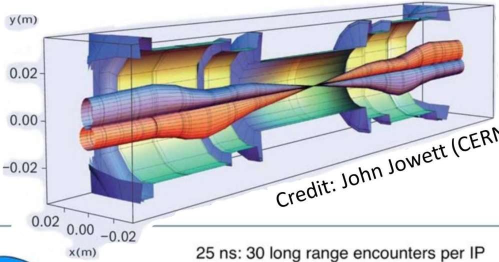

Credit: John Jowett (CERN)

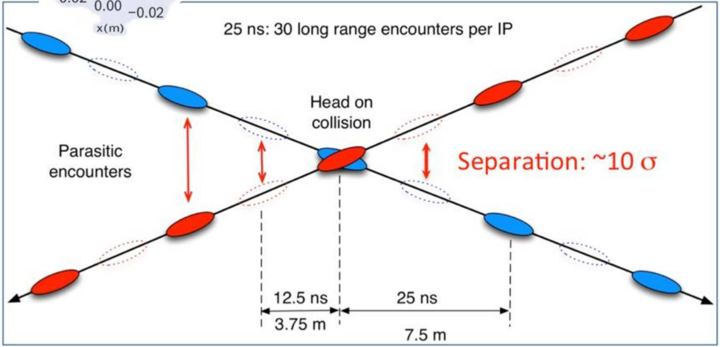

Credit: Mike Lamont (CERN)

Crossing angles reduce the luminosity

$$\boldsymbol{L} = \frac{\left(f_{rev}\, n_{coll}\right)\ N_1 N_2}{2\pi\sqrt{\left(\sigma_{x,1}^2 + \sigma_{x,2}^2\right)}\sqrt{\left(\sigma_{y,1}^2 + \sigma_{y,2}^2\right)}} \times S$$

- **Exact value of S depends on operating conditions**
- **Very approximately $S \approx 0.8$**

$$L = \frac{(f_{rev} n_{coll})\ N_1 N_2}{2\pi \sqrt{(\sigma_{x,1}^2 + \sigma_{x,2}^2)} \sqrt{(\sigma_{y,1}^2 + \sigma_{y,2}^2)}}$$

Beamsize:

$$\sigma_{x,y} = \sqrt{\beta_{x,y}(s)\ \epsilon_{x,y}}$$

- $\beta(s)$: *'beta-function'* [m]
  - → **Property of the magnetic lattice**
  - → **varies around the ring**
- ϵ: *'emittance'* [μm]
  - → **Property of the particle bunch**
  - → **Invariant around the ring**

$$\sigma_{x,y}(s) = \sqrt{\beta_{x,y}(s)\ \epsilon_{x,y}}$$

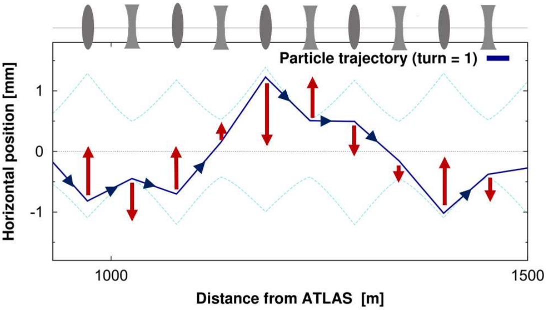

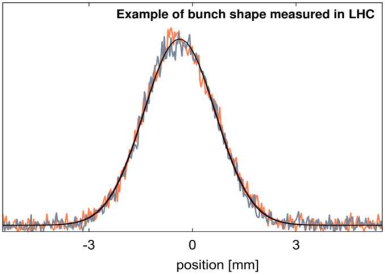

Particle motion about central closed-orbit described by **Hill's equation:**

- linear restoring force from quadrupoles is a function of location around the ring
- restoring force is periodic to at least the accelerator circumference

$$\frac{\mathrm{d}^2 x}{\mathrm{d}s^2} - K(s)x = 0 \qquad\qquad x = \sqrt{2J_x\beta_x(s)}\cos\left(\phi_x(s) + \phi_0\right)$$

β-function describes envelope of particle oscillations

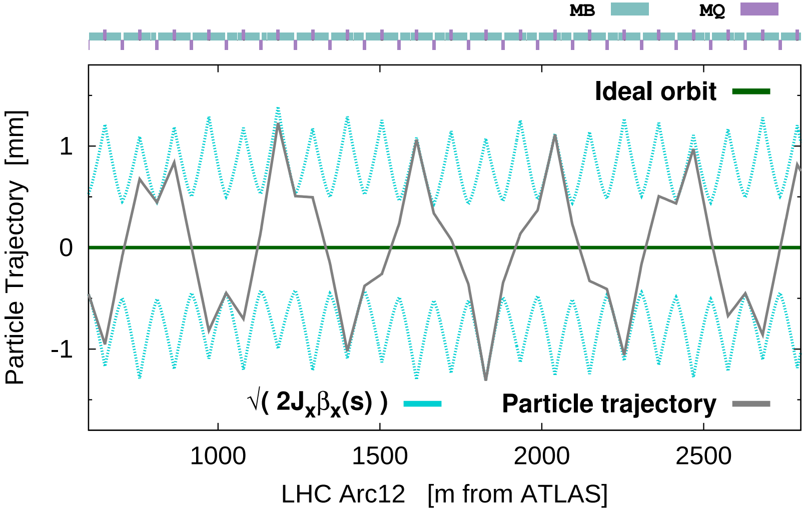

β-function describes envelope of particle oscillations

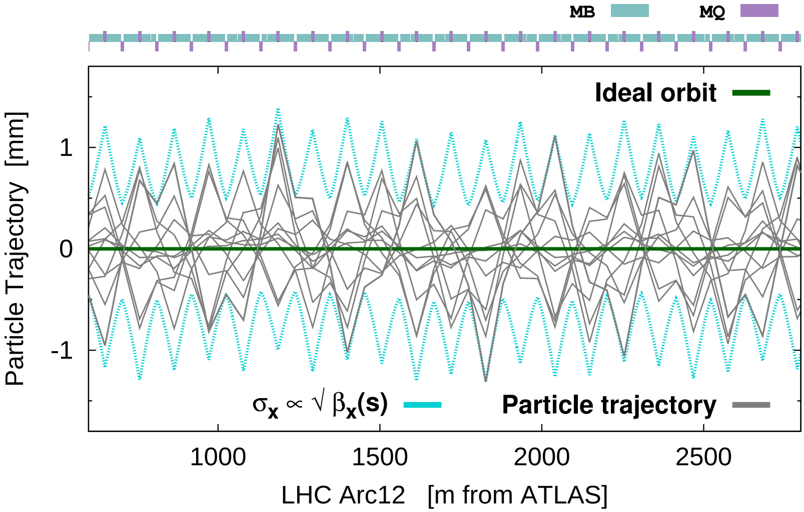

β-function describes envelope of particle oscillations

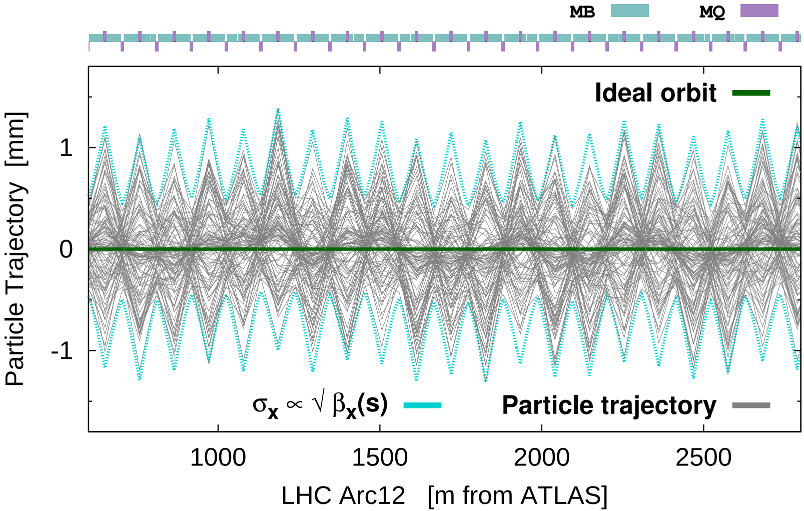

β-function describes envelope of particle oscillations

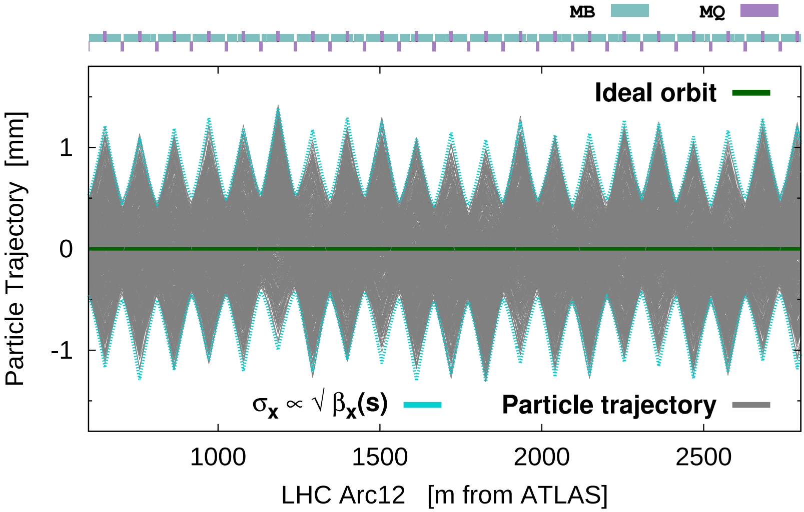

Triplet quadrupoles in experimental IRs squeeze $\beta_{x,y}$

$\rightarrow \beta^* =$ minimum β in the IR $\approx 25\,\mathrm{cm}$

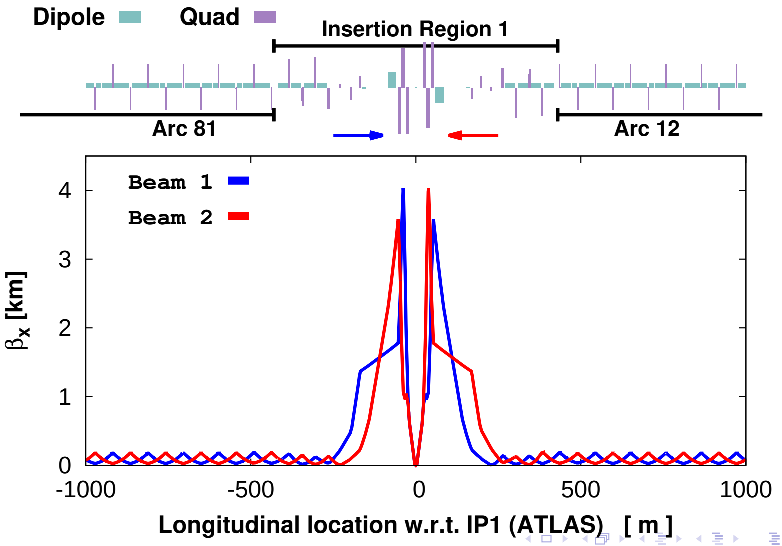

What about the real world?

→ **Linear & nonlinear magnetic errors can introduce substantial perturbations to the optics/beam-size**

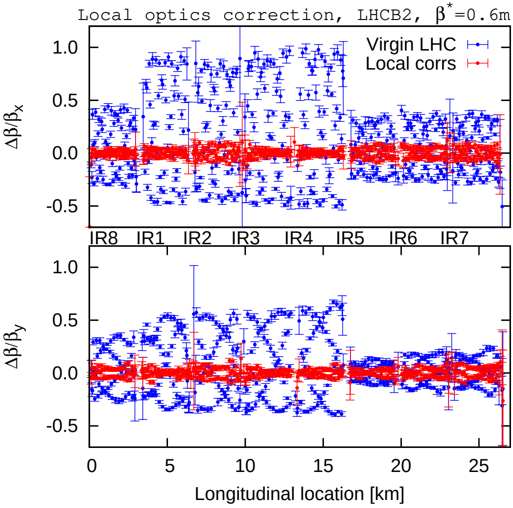

Characterize optics quality by 'beta-beating'

$$\frac{\Delta\beta}{\beta} = \frac{\beta_{meas} - \beta_{nominal}}{\beta_{nominal}}$$

Beam-based correction of LHC optics is essential to operation

$$\sigma_{x,y}(s) = \sqrt{\beta_{x,y}(s)\ \epsilon_{x,y}}$$

Characterise particle trajectory by position (x) and angle ($x' = \frac{dx}{ds}$)

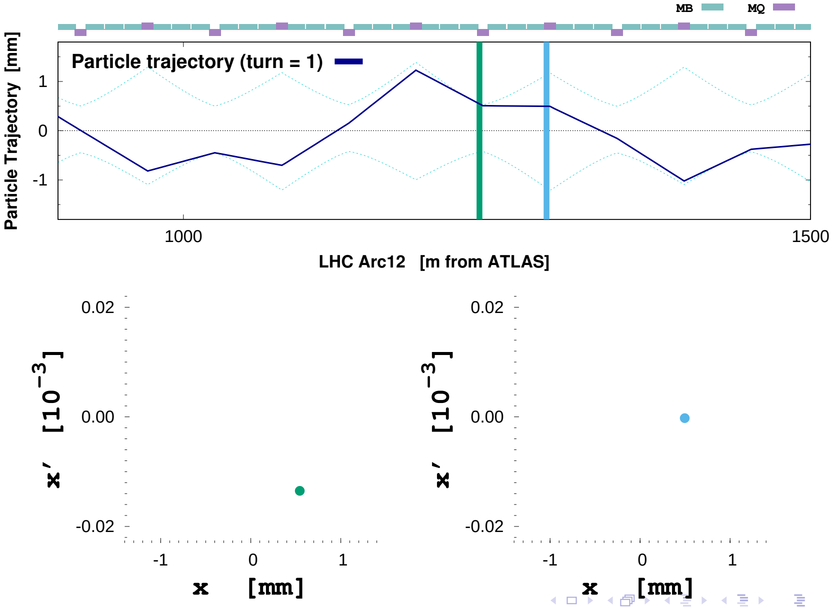

Characterise particle trajectory by position (x) and angle ($x' = \frac{dx}{ds}$)

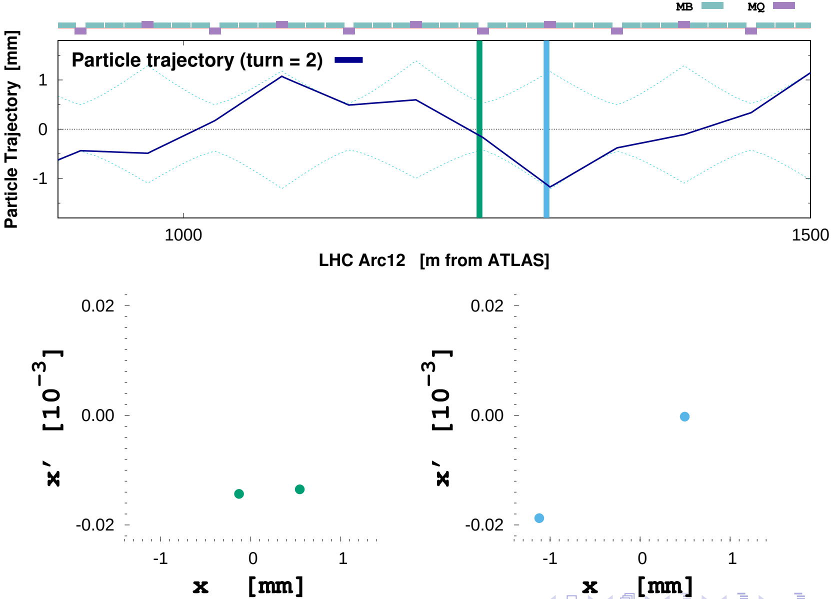

Characterise particle trajectory by position (x) and angle ($x' = \frac{dx}{ds}$)

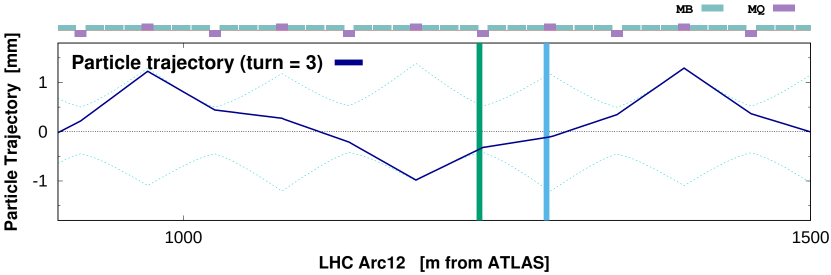

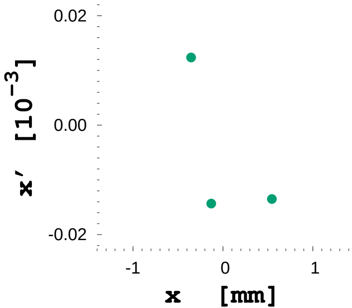

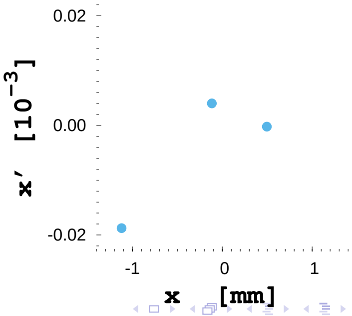

Characterise particle trajectory by position (x) and angle ($x' = \frac{dx}{ds}$)

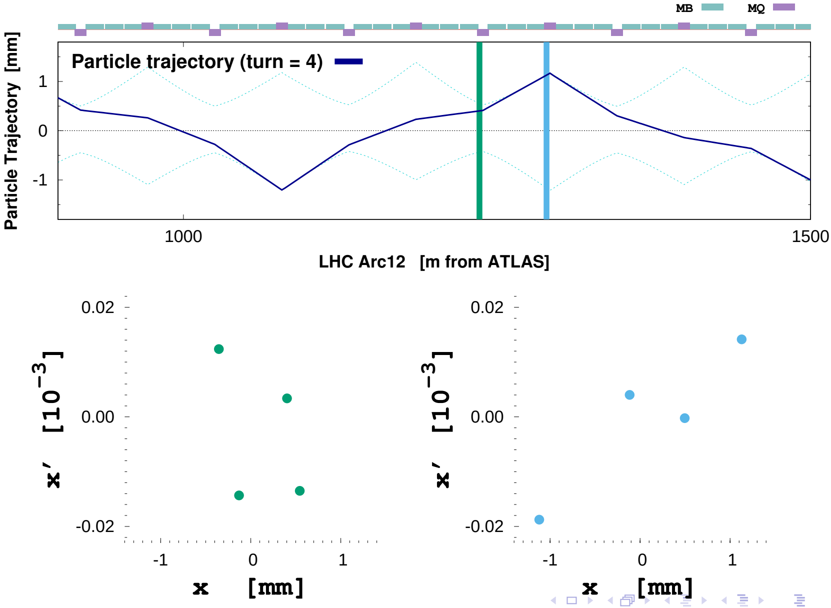

Characterise particle trajectory by position (x) and angle ($x' = \frac{\mathrm{d}x}{\mathrm{d}s}$)

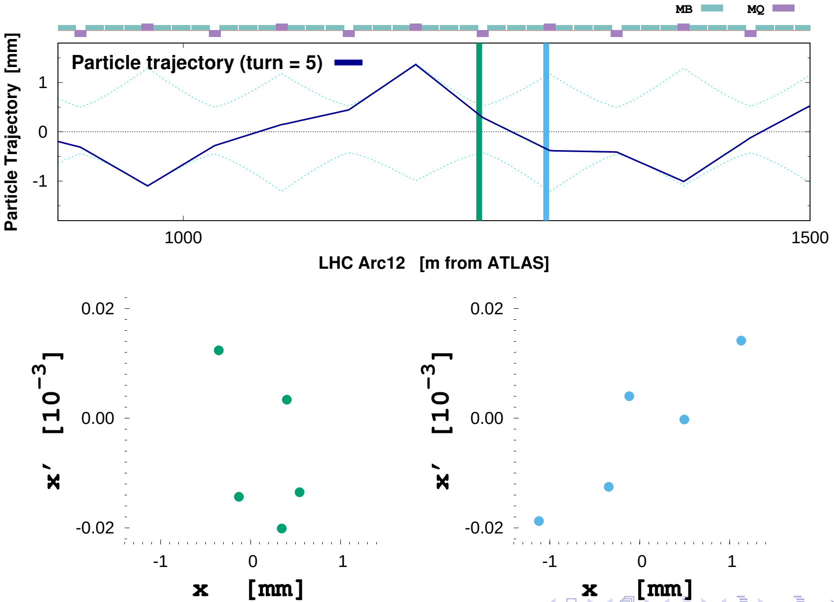

Characterise particle trajectory by position (x) and angle ($x' = \frac{dx}{ds}$)

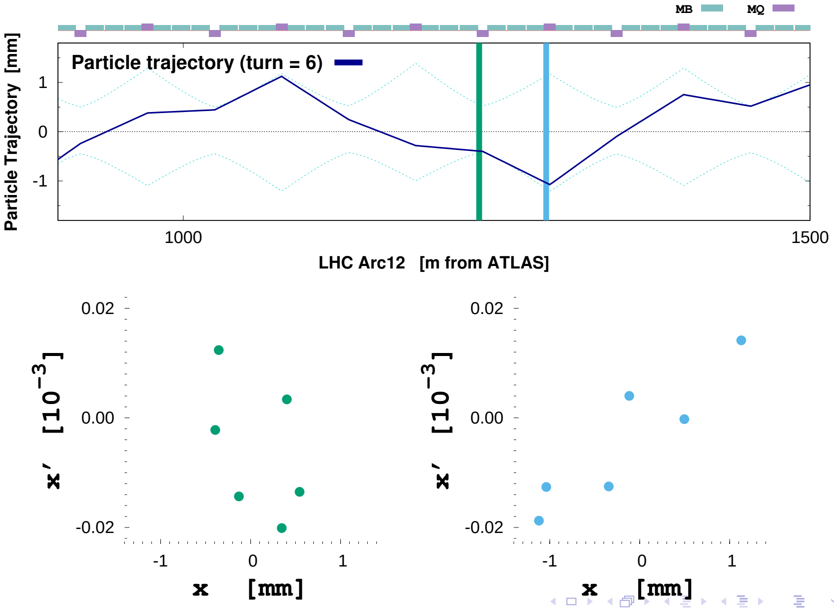

Characterise particle trajectory by position (x) and angle ($x' = \frac{\mathrm{d}x}{\mathrm{d}s}$)

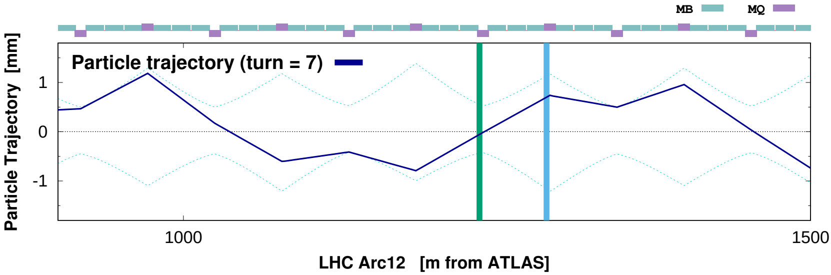

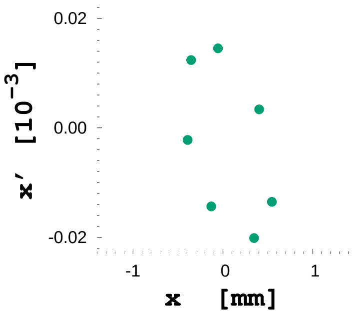

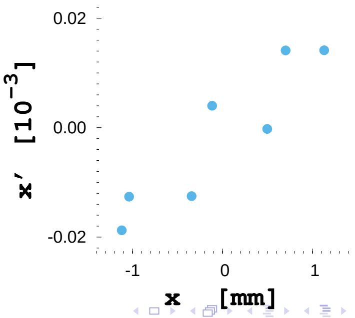

Characterise particle trajectory by position (x) and angle ($x' = \frac{dx}{ds}$)

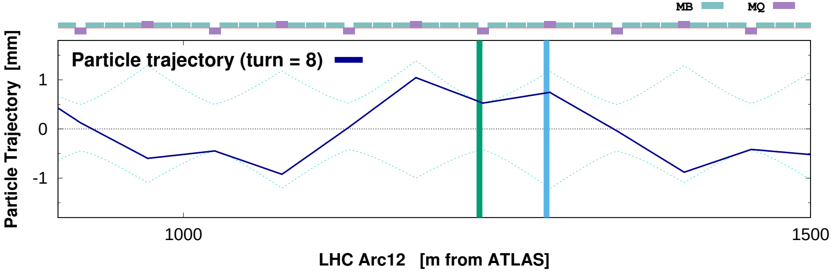

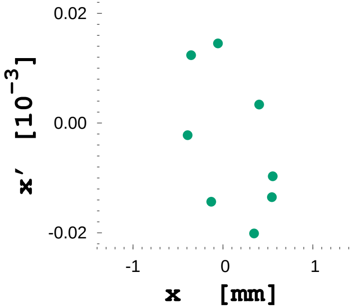

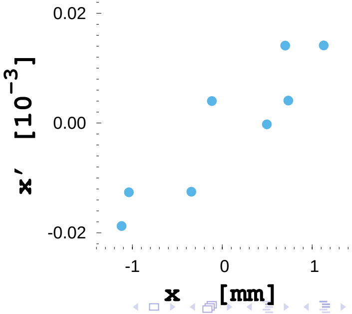

Characterise particle trajectory by position (x) and angle ($x' = \frac{\mathrm{d}x}{\mathrm{d}s}$)

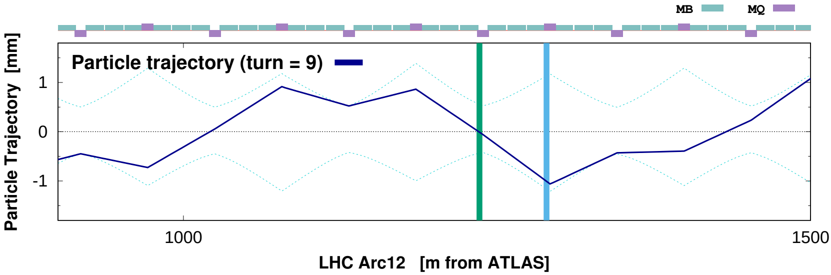

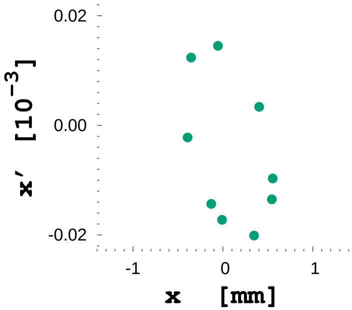

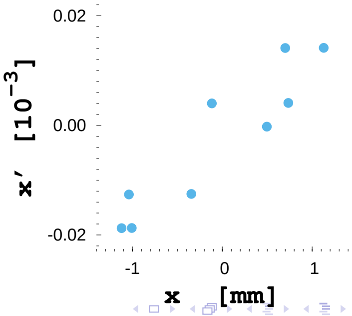

Characterise particle trajectory by position (x) and angle ($x' = \frac{\mathrm{d}x}{\mathrm{d}s}$)

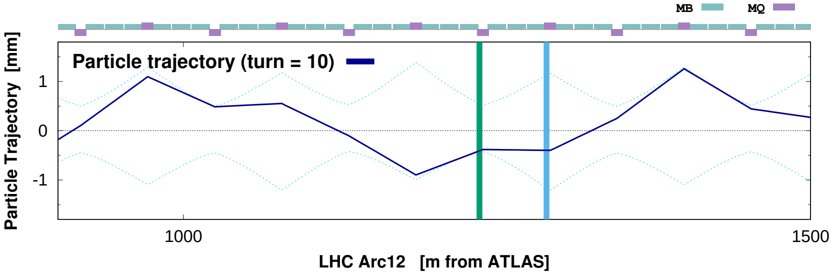

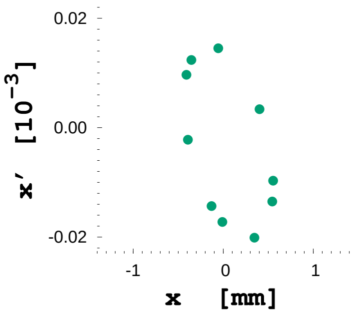

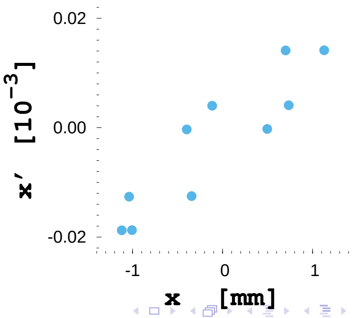

Particles trace out elliptical paths in (x,x') phase space

- shape changes around the ring
- **Area of ellipse is invariant** (for constant energy)

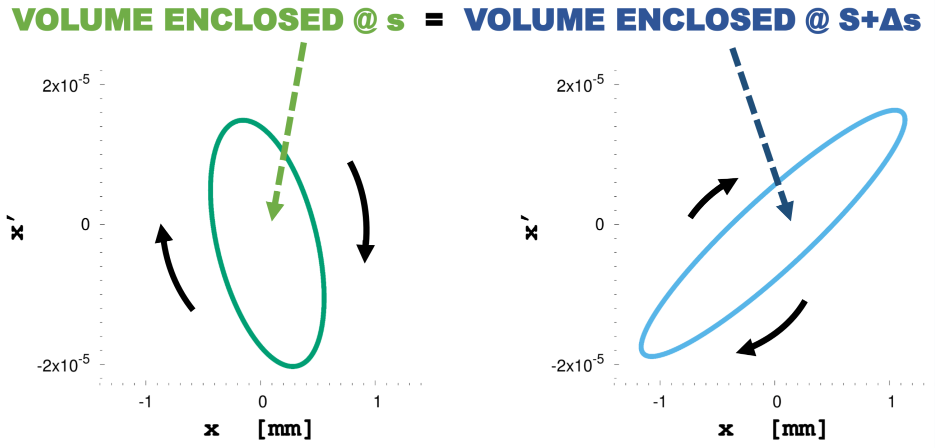

Particles trace out elliptical paths in (x,x') phase space

- in practice have many particles
- all follow similar elliptical trajectories (linear approximation)

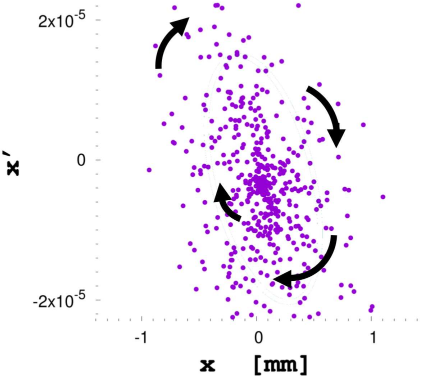

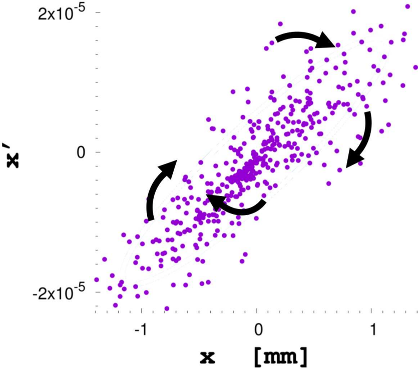

Particles trace out elliptical paths in (x,x') phase space

- '**beam emittance**' is area/π of elipse enclosing 1σ of the particles in the bunch

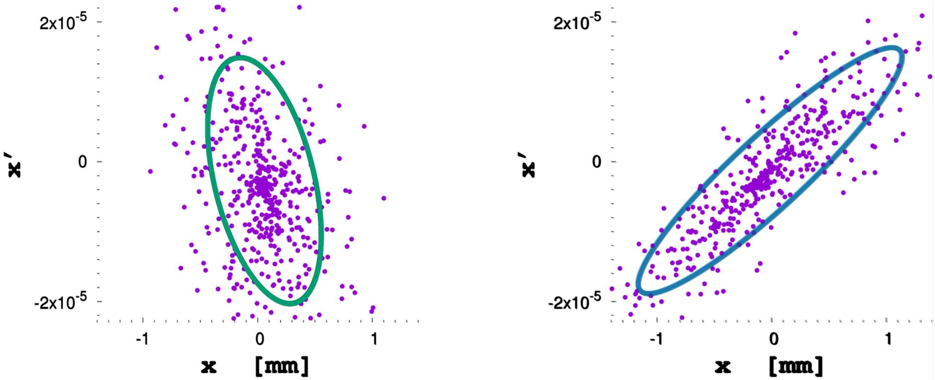

Emittance conserved provided particle's energy is constant

Acceleration

Define *'normalized emittance'* which is invariant with the beam energy

$$\epsilon^* = \beta_{rel}\gamma_{rel}\epsilon$$

In practice many effects can change or dilute emittance

- **Injection errors**
- **Synchrotron radiation**
- **IntraBeam Scattering**
- **Emittance evolution in LHC still not fully understood!**

More accurate beam-size description considers coupled 4D-phase-space

$$\Sigma_x^2 = \beta_{11}\epsilon_1 + \beta_{12}\epsilon_2$$
$$\Sigma_y^2 = \beta_{21}\epsilon_1 + \beta_{22}\epsilon_2$$

Betatron motion with coupling of horizontal and vertical degrees of freedom V.A.Lebedev, S.A.Bogacz FERMILAB-PUB-10-383-AD

Plot courtesy T.H.B. Persson (CERN)

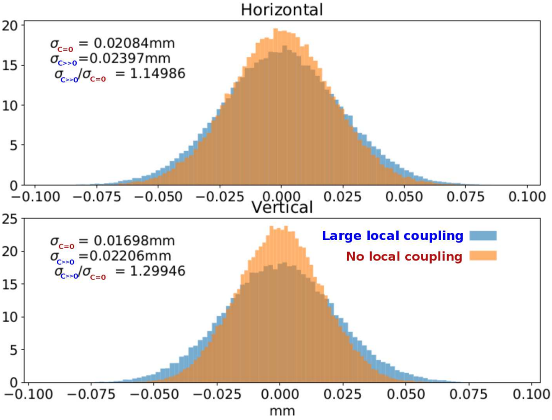

Poor local coupling correction in IR2 during 2018 Pb/Pb run caused 50 % reduction to Luminosity delivered to ALICE until diagnosed & corrected

$$\boldsymbol{L} = \frac{\left(f_{rev} n_{coll}\right) \; N_1 N_2}{2\pi\sqrt{\left(\sigma_{x,1}^2 + \sigma_{x,2}^2\right)}\sqrt{\left(\sigma_{y,1}^2 + \sigma_{y,2}^2\right)}}$$

- $N_{1,2}$: **Number of particles per bunch**

- **Accumulate bunch trains in the LHC ring at 450GeV**
- **Accelerate to 6.5TeV**
- **Bring bunches into collision & store for several hours**
- **Dump / Repeat**

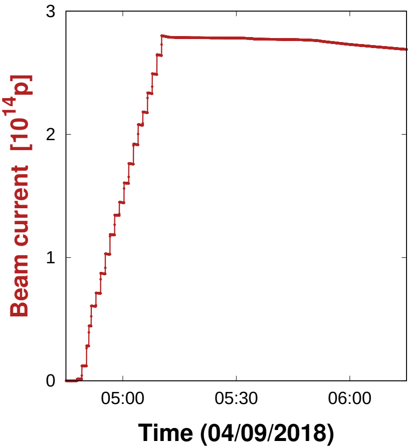

- **Beam intensity decays during a fill**
- **Show a corresponding reduction in instantaneous luminosity**
- **Bulk of decay (LHC ideal conditions) is losses of particles which are colliding at the IPs 'burnoff'**

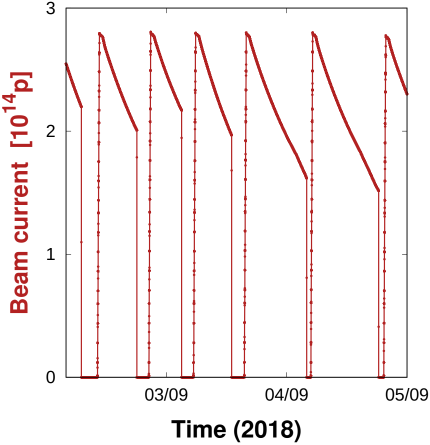

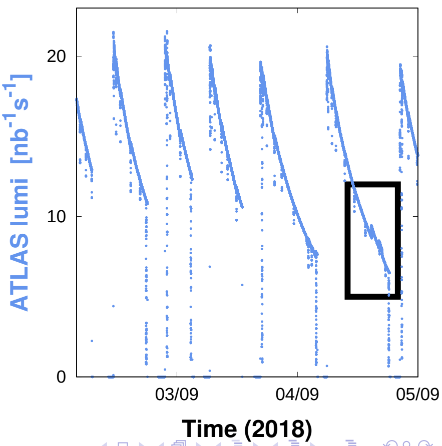

- **Can try to maintain luminosity while $N_{1,2}$ decays by changing other accelerator parameters which influence luminosity**
- **'Luminosity levelling'** $\rightarrow$ e.g. β^*-levelling

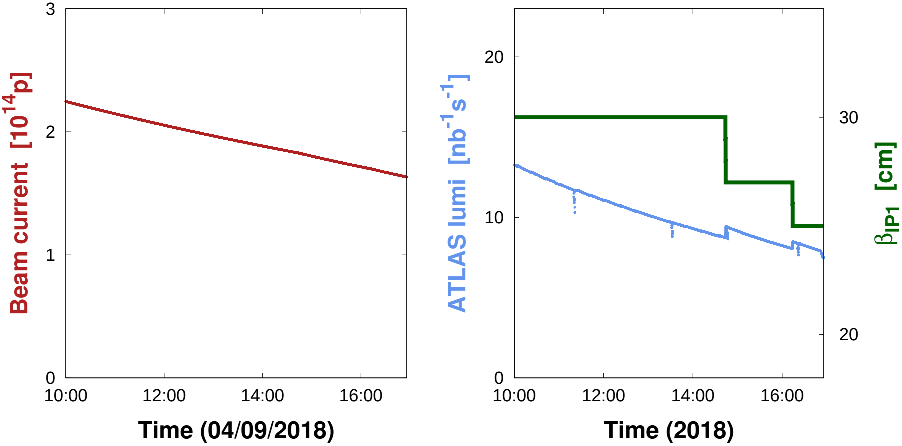

- **Can try to maintain luminosity while $N_{1,2}$ decays by changing other accelerator parameters which influence luminosity**
- **'Luminosity levelling'** $\rightarrow$ e.g. crossing-angle levelling

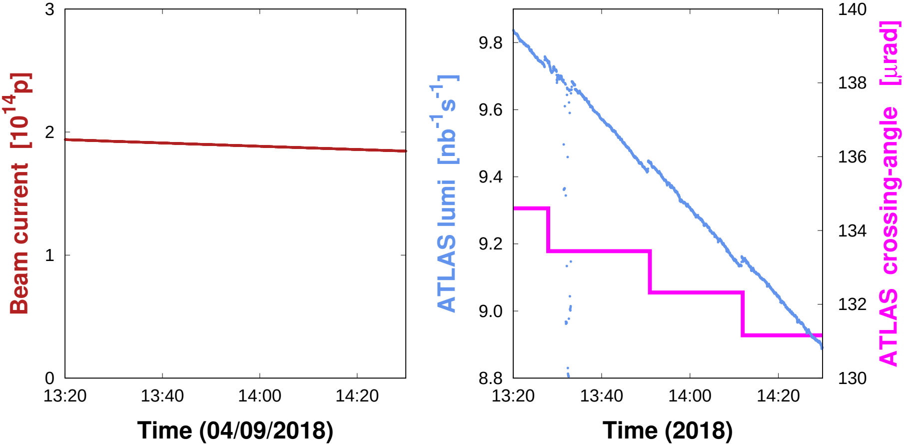

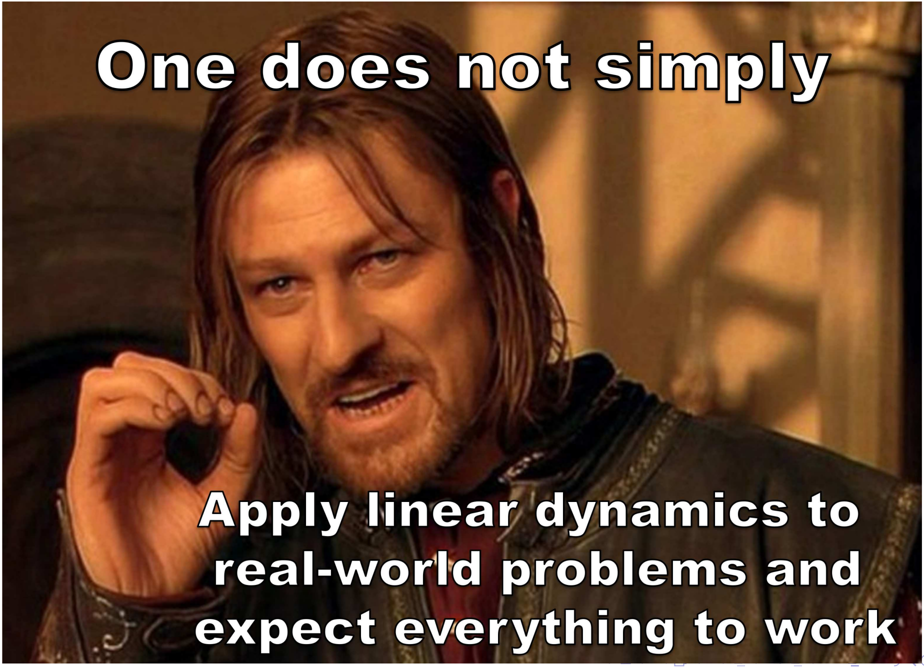
One does not simply
Apply linear dynamics to
real-world problems and
expect everything to work

Large amplitude particles' motion can become chaotic & unstable → 'Dynamic aperture'

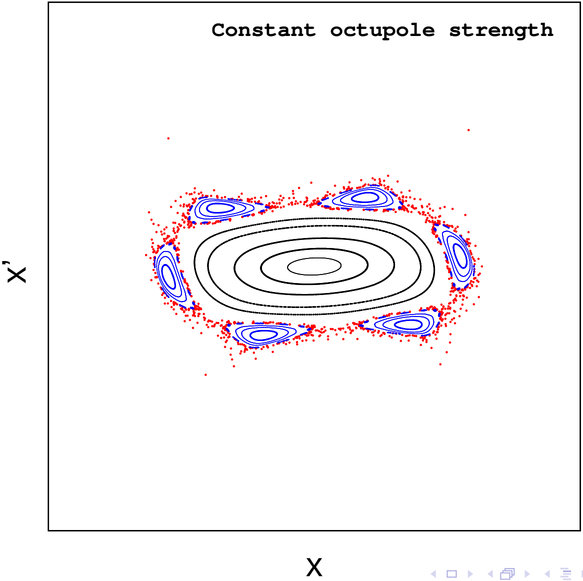

The more nonlinear the beam dynamics becomes the smaller the dynamic aperture

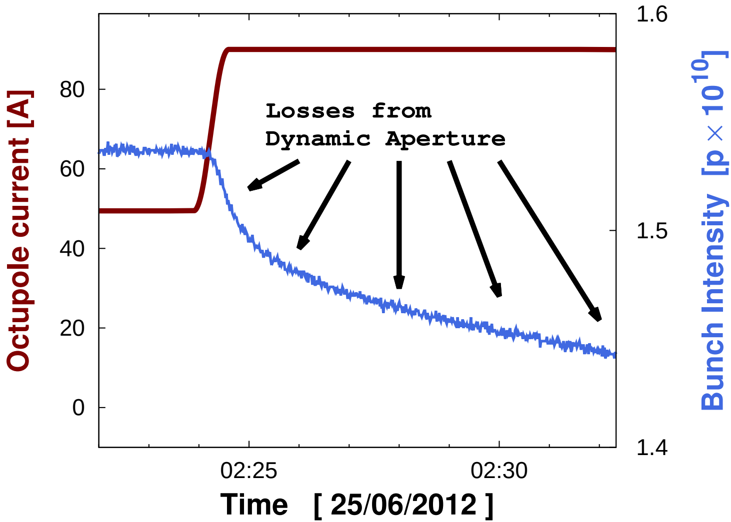

Use sextupole, octupole, decapole & dodecapole magnets to correct nonlinear dynamics in LHC & HL-LHC

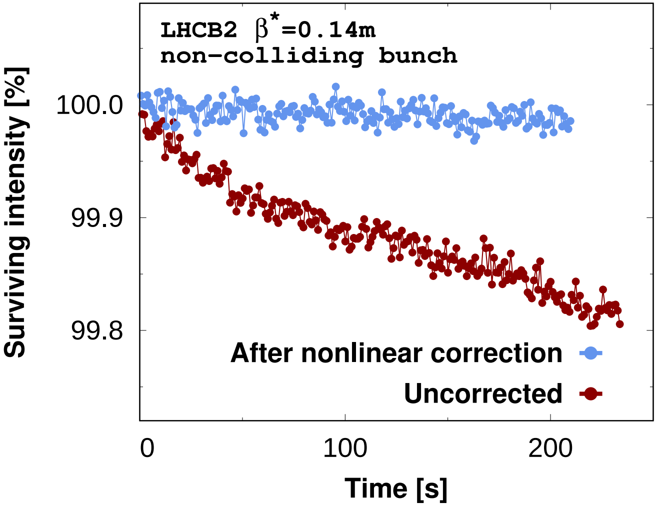

Beams themselves can introduce large nonlinearities into the dynamics e.g.

Beam-Beam

- Force exerted on a particle by the fields of bunches in the other beam
- **A major limitation to LHC performance**

W. Herr and T. Pieloni, `Beam-Beam effects'
CERN Accelerator School

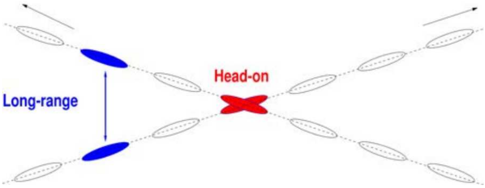

Collective effects have a big influence on LHC performance!

'Intensity Limitations in Particle Beams' CERN Accelerator School, 2-11 Nov 2015, Geneva, Switzerland https://cds.cern.ch/record/865932

Key Points

- **What is luminosity?**
- **What are its main dependencies?**
- **There are many real world complications which affect the luminosity!**

Event rate for a HEP interaction:

$$R = L \times \sigma$$

- R: *Event Rate* $[\mathrm{s}^{-1}]$
- σ: *Cross Section* $[\mathrm{barn} = 10^{-34}\mathrm{cm}^2]$
  property of the HEP interaction
- L: *Luminosity* **[inverse barn / s]**
  property of the collider

Total number of interactions defined by the Integrated Luminosity [inverse femto-barn]

$$N = \left(\int L(t)\mathrm{d}t\right) \times \sigma$$

Integrated Luminosity is key figure of merit for collider like LHC

→ significant factor is how much time spent on luminosity production

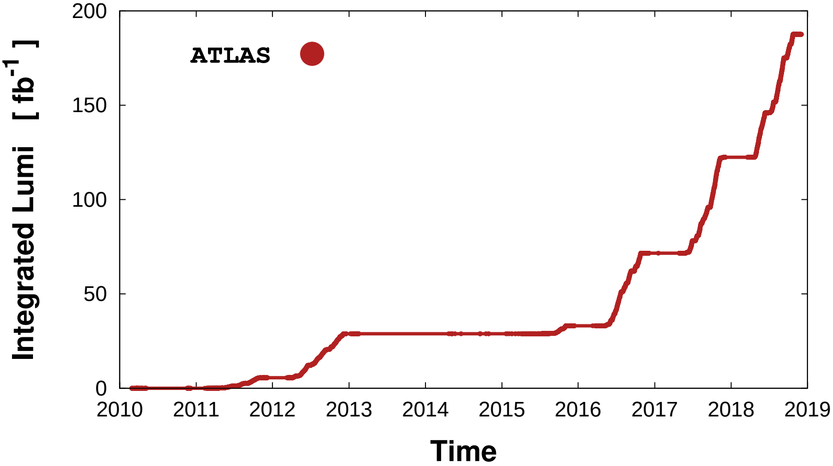

https://lhc-statistics.web.cern.ch/LHC-Statistics/

Approximate schedule for LHC lifetime (accurate up to 2021)

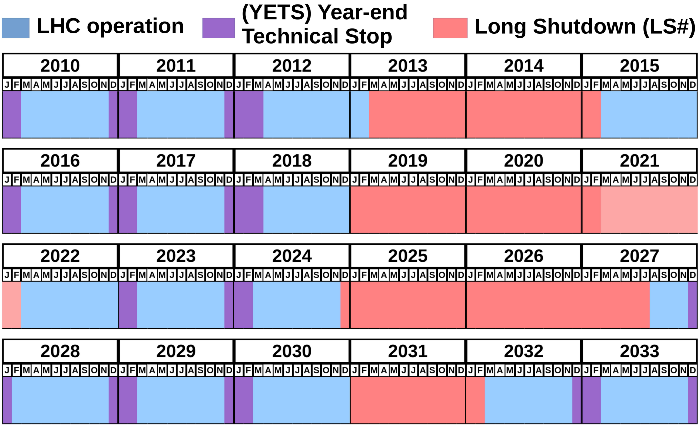

- LHC operation is interspersed with regular **shutdown** periods for maintenance and upgrades

LHC schedule over 1 year (2017)

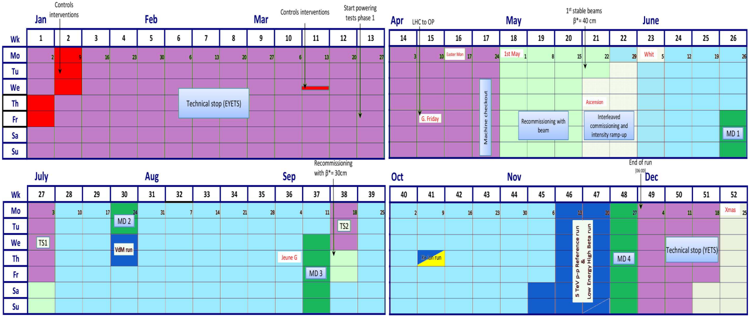

Many types of activities during 1 year of LHC operation

- **Technical Stop (YETS + regular breaks)**
- **Accelerator commissioning**
- **Accelerator physics/technology studies**
- **Luminosity production proton-proton and special runs**

LHC is an extremely complicated system

- Even small technical problems add up over 1 year
- Statistics for LHC availabitity/faults monitored by *availability working group*, e.g. 2017:

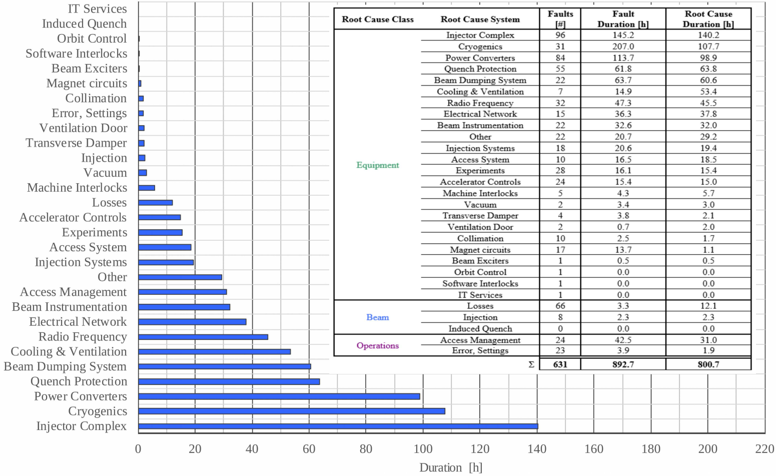

Root Cause Class	Root Cause System	Faults [#]	Fault Duration [h]	Root Cause Duration [h]
Equipment	Injector Complex	96	145.2	140.2
	Cryogenics	31	207.0	107.7
	Power Converters	84	113.7	98.9
	Quench Protection	55	61.8	63.8
	Beam Dumping System	22	63.7	60.6
	Cooling & Ventilation	7	14.9	53.4
	Radio Frequency	32	47.3	45.5
	Electrical Network	15	36.3	37.8
	Beam Instrumentation	22	32.6	32.0
	Other	22	20.7	29.2
	Injection Systems	18	20.6	19.4
	Access System	10	16.5	18.5
	Experiments	28	16.1	15.4
	Accelerator Controls	24	15.4	15.0
	Machine Interlocks	5	4.3	5.7
	Vacuum	2	3.4	3.0
	Transverse Damper	4	3.8	2.1
	Ventilation Door	2	0.7	2.0
	Collimation	10	2.5	1.7
	Magnet circuits	17	13.7	1.1
	Beam Exciters	1	0.5	0.5
	Orbit Control	1	0.0	0.0
	Software Interlocks	1	0.0	0.0
	IT Services	1	0.0	0.0
Beam	Losses	66	3.3	12.1
	Injection	8	2.3	2.3
	Induced Quench	0	0.0	0.0
Operations	Access Management	24	42.5	31.0
	Error, Settings	23	3.9	1.9
	Σ	631	892.7	800.7

LHC is an extremely complicated system

- Even small technical problems add up over 1 year
- Statistics for LHC availabitity/faults monitored by *availability working group*, e.g. 2017:

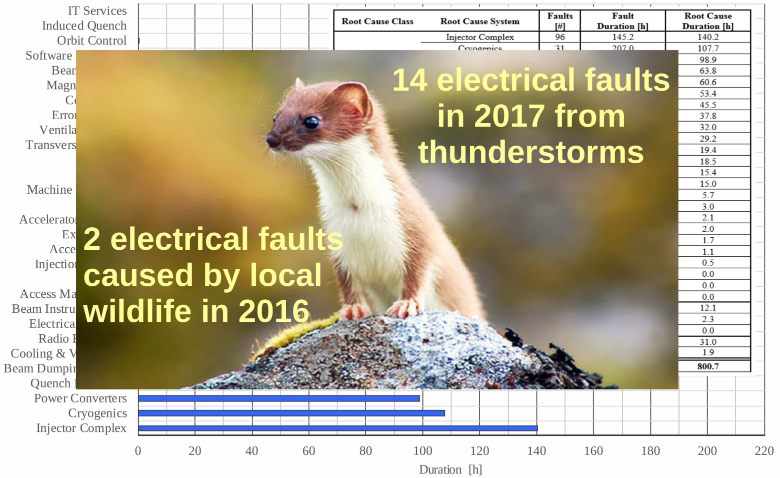

Not all time during operation spent colliding beams: **LHC cycle (2012)**

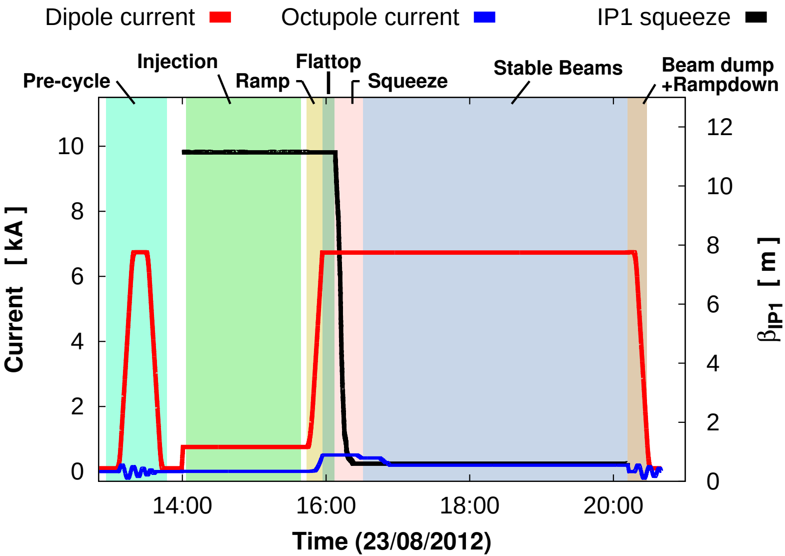

Reduced turn-around-time inceases integrated lumi: **LHC cycle (2018)**

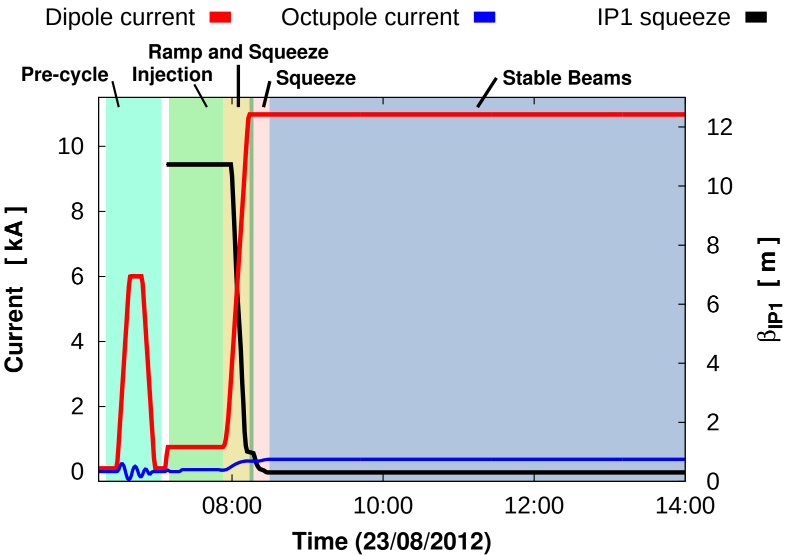

Gain 6 day/year from combined Ramp/Squeeze & precyle optimization

Key Points

- **Integrated luminosity is the key figure of merit for a collider like the LHC**
- **How much time is actually spent colliding beams together?**
- **What are we doing the rest of the time?**

Some useful resources for further study!

Proceedings of the CERN Accelerator School

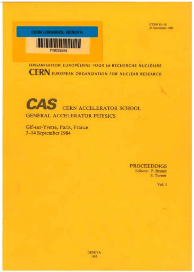

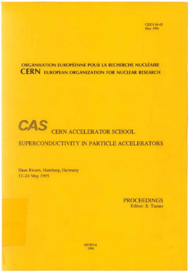

Wide range of general & specialized courses ranging from introductory to advanced from schools going back to 1983

Proceedings available at:
https://cas.web.cern.ch/previous-schools

Particle Physics Reference Library, Vol. 3, Accelerators and Colliders

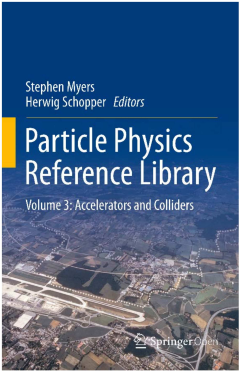

3 volume textbook on Accelerators, Detectors & HEP jointly produced by CERN & Springer

Available free as open-access ebook at:
https://www.springer.com/gp/book/9783030342449#aboutBook
https://cds.cern.ch/record/2702370

Many thanks for your attention!

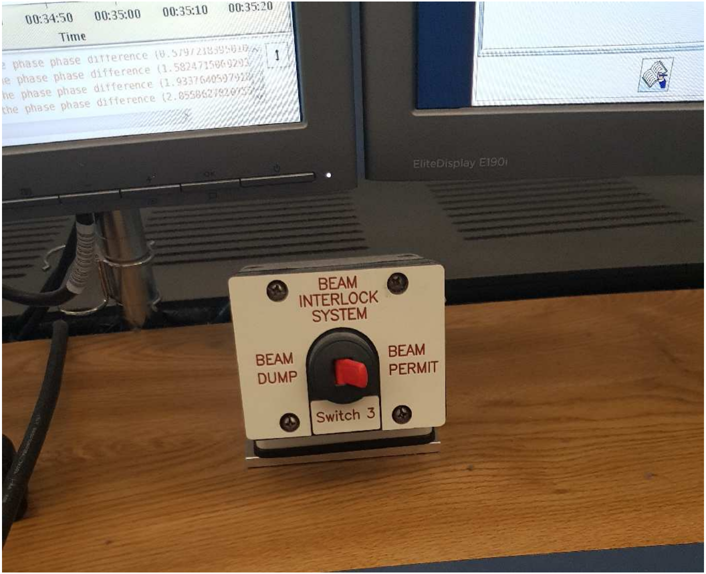

Reserve

Medicine

Center for proton therapy, Paul Scherrer Institute, Villigen, Switzerland

■ INDUSTRY

Science & Technology Facilities Council | UK Research and Innovation

Funding | Research | Innovation | Skills | Public engagement | News, events and publications | About us

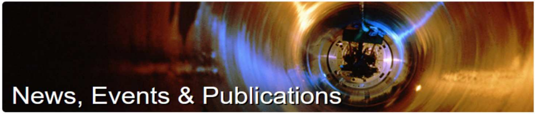

Home / News / STFC launches VELA – bringing a new imaging capability for UK industry

STFC launches VELA – bringing a new imaging capability for UK industry

13 March 2015

BBC Sign in | News | Sport | Weather | Shop | Reel | Travel

NEWS

Home | Video | World | UK | Business | Tech | Science | Stories | Entertainment & Arts

World | Africa | Asia | Australia | Europe | Latin America | Middle East | US & Canada

World's only particle accelerator for art is back at the Louvre

23 November 2017 Share

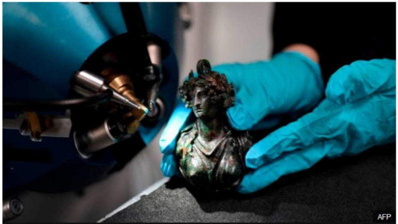

The machine bombards sculptures with helium and hydrogen atoms

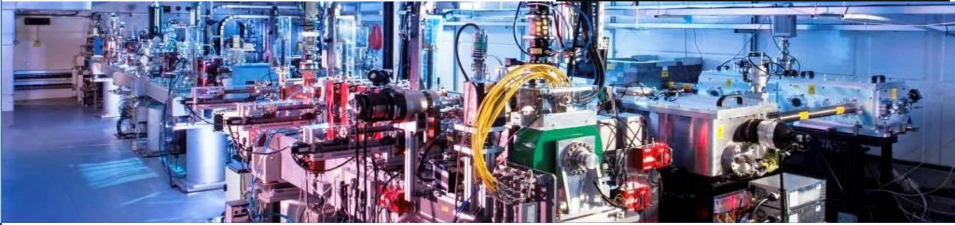

Arcs utilize superconducting $8.3\,\mathrm{T}$ dual bore dipoles

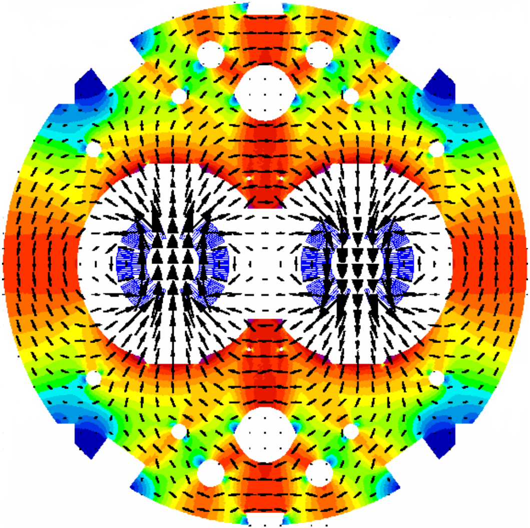

NbTi coils cooled to $1.9\,\mathrm{K}$ with superfluid helium

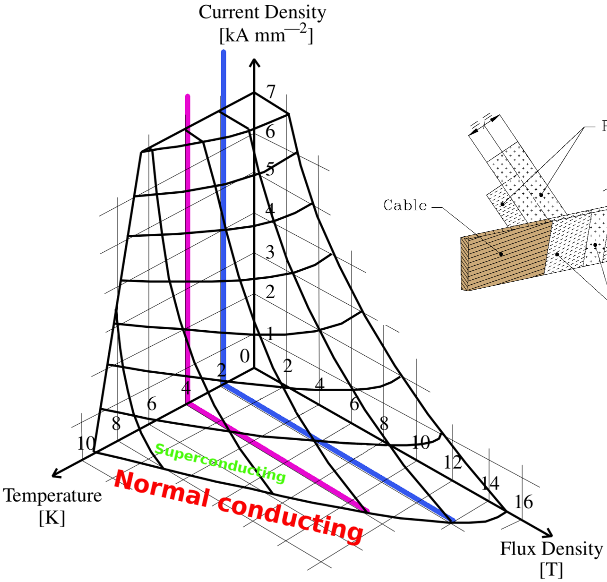

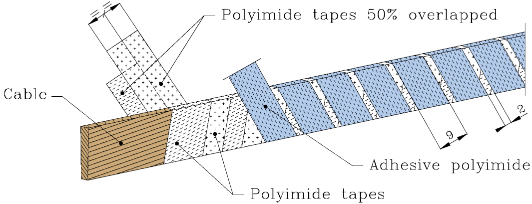

NbTi coils cooled to $1.9\,\mathrm{K}$ with superfluid helium

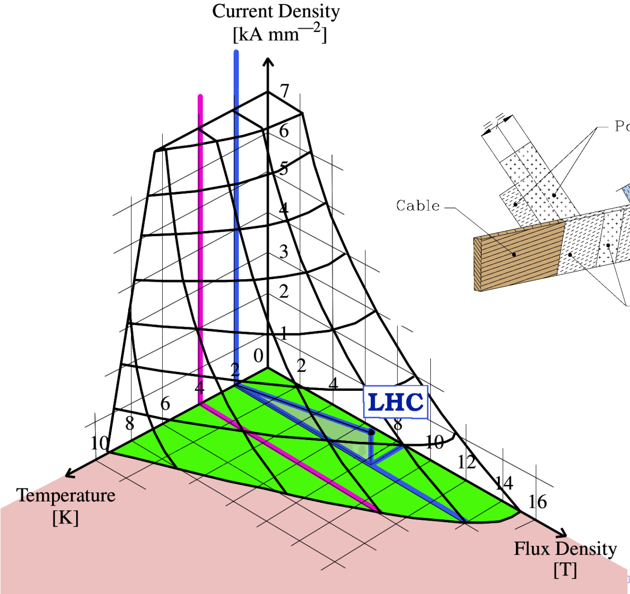

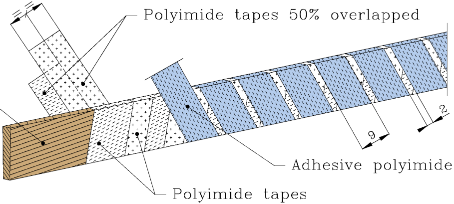

NbTi coils cooled to $1.9\,\mathrm{K}$ with superfluid helium

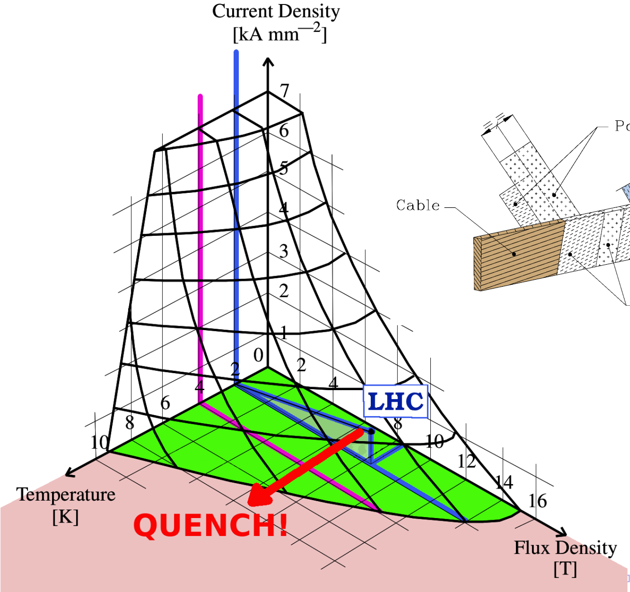

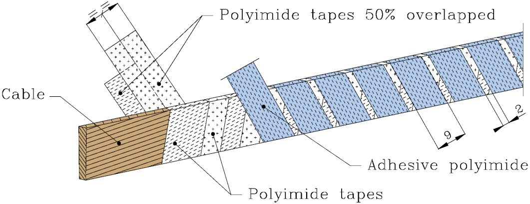

Limiting factor for circular hadron collider:

$\rightarrow$ **High Energy = high magnetic ridIdity**

$$F_{Lorentz} = F_{centrip}$$

$$F_{Lorentz} = q(\vec{E} + \vec{v} \times \vec{B})$$

- consider proton $(\mathrm{q/A} = 1)$
- assume pure dipole fields
- $(p_x, p_y) << p_s$

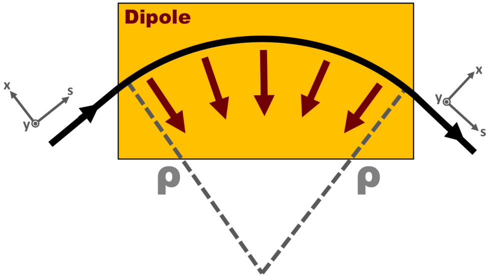

Limiting factor for circular hadron collider:

$\rightarrow$ **High Energy = high magnetic rididity**

$$F_{Lorentz} = F_{centrip}$$

$$F_{Lorentz} = q(\vec{E} + \vec{v} \times \vec{B}) = evB_{dipole}$$

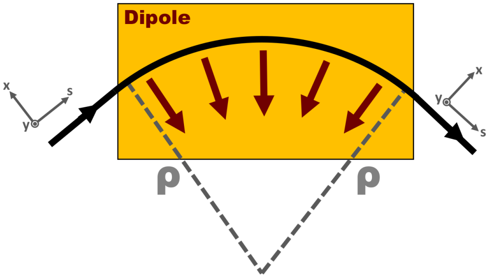

Limiting factor for circular hadron collider:

→ **High Energy = high magnetic rididity**

$$F_{centrip} = \frac{\mathrm{d}p}{\mathrm{d}t}$$

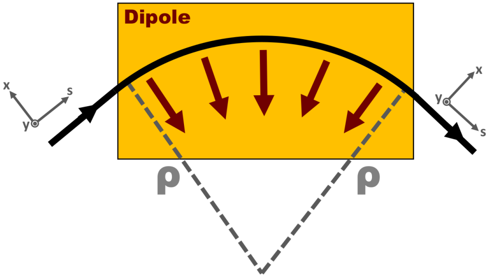

Limiting factor for circular hadron collider:

$\rightarrow$ **High Energy = high magnetic ridID̶ity**

$$\mathrm{d}p = p\mathrm{d}\theta$$

$$\mathrm{d}s = \rho\mathrm{d}\theta$$

$$p = \gamma_{rel} m_{rest} v$$

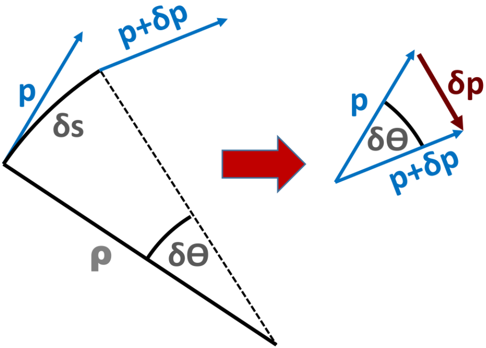

Limiting factor for circular hadron collider:

$\rightarrow$ **High Energy = high magnetic ridigity**

$$F_{centrip} = \frac{\mathrm{d}p}{\mathrm{d}t}$$

$$= p\frac{\mathrm{d}\theta}{\mathrm{d}t} = \frac{p}{\rho}\frac{\mathrm{d}s}{\mathrm{d}t}$$

$$= \frac{pv}{\rho} = \frac{\gamma m_0 v^2}{\rho}$$

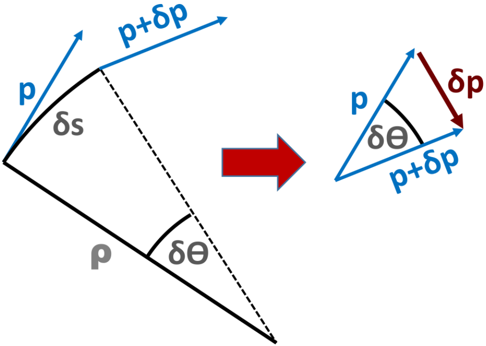

Limiting factor for circular hadron collider:

$\rightarrow$ **High Energy = high magnetic ridiDity**

$$F_{Lorentz} = F_{centrip}$$

$$evB = \frac{\gamma m_0 v^2}{\rho} = \frac{pv}{\rho}$$

$$B\rho = \frac{p}{e}$$

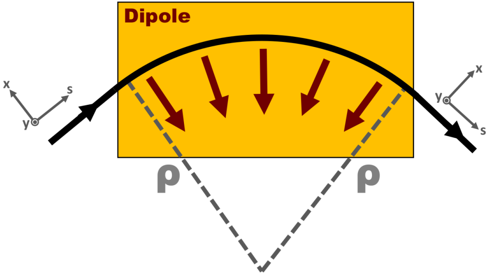

Limiting factor for circular hadron collider:

$\rightarrow$ **High Energy = high magnetic ridIdity**

$B\rho$ is *'Magnetic Rigidity'*

$$B\rho \ \ [\mathrm{Tm}] = \frac{p \ \ [\mathrm{kgms^{-1}}]}{e \ \ [\mathrm{C}]}$$

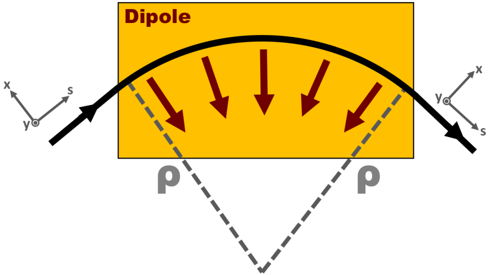

- Not so convenient units

Limiting factor for circular hadron collider:

→ **High Energy = high magnetic rididity**

$B\rho$ is *'Magnetic Rigidity'*

$$B\rho \ \ [\mathrm{Tm}] = \frac{10}{2.998} p \ \ [GeV/c]$$

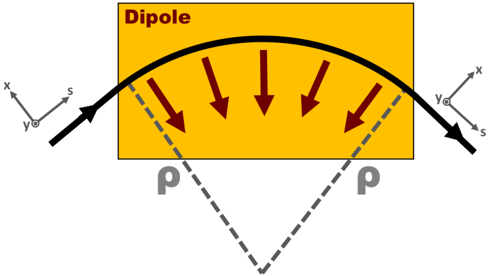

Magnetic rigidity defines the maximum energy you can reach for a given dipole field in a given tunnel geometry

Beams themselves can introduce large nonlinearities into the dynamics e.g.

Direct Space Charge

- Repulsive (defocusing) force on a particle due to the field of all other particles in the bunch
- **A big challenge at low energy in injector chain**

K.Schind, `Space Charge'
CERN Accelerator School

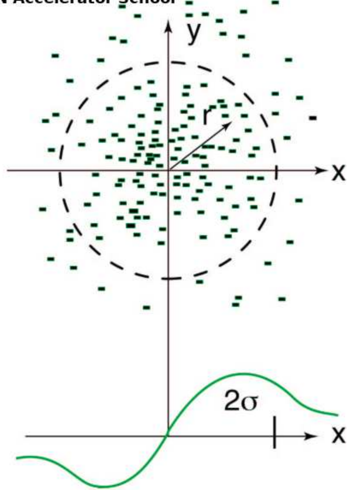

Similar problem at injection

IR8 (LHCb / beam2 injection)
Right side viewed from above

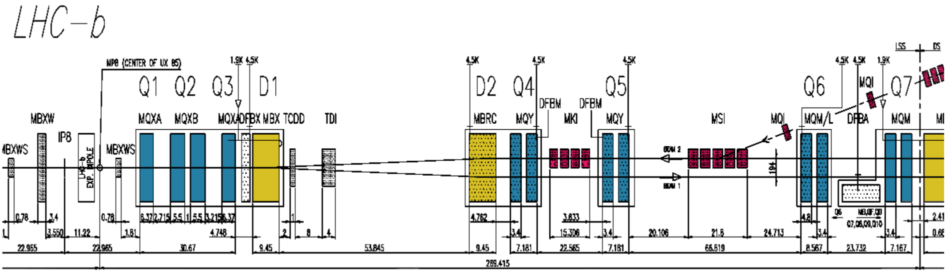

Injection kickers have rise time of ~1us

- **Optics errors can reduce data delivered to HEP experiments**
- **Create Luminosity imbalance between HEP experiments**

$\rightarrow$ **Aim for β^*-beat $\leq 1\,\%$**

- **MACHINE PROTECTION** $\rightarrow$ **require beta-beat $\leq 18\,\%$**

Ph.D thesis of F.Burkhart

CERN-THESIS-2016-148